

AMC PAMPHLET

AMCP 706-127

ENGINEERING DESIGN HANDBOOK

INFRARED MILITARY SYSTEMS

PART ONE

HEADQUARTERS, U.S. ARMY MATERIEL COMMAND

APRIL 1971

LIST OF ILLUSTRATIONS

<i>Figure No.</i>	<i>Title</i>	<i>Page</i>
2-1	Angle θ in Radians	2-4
2-2	Solid Angle Ω in Steradians	2-4
2-3	Blackbody Curves	2-7
2-4	Geometry of a Lambertian Source	2-10
2-5	The GE Radiation Calculator	2-15
2-6	The Near-infrared Spectra of Solar Irradiation and of CO, CH ₄ , N ₂ O, O ₃ , CO ₂ , and H ₂ O	2-19
2-7	Seasonal Variation of the Vertical Distribution of Ozone	2-20
2-8	Annual Variation of Total Ozone for Each 10° of N. Latitude	2-21
2-9	Water Vapor Profile in the Atmosphere	2-22
2-10	Lorentz Line Shape	2-24
2-11	The 6.3-micron Band of H ₂ O	2-26
2-12	Experimental Fit of Burch and Williams Data to Error Function Absorption at 2.7 Microns	2-45
2-13	Variation of Continuum Absorption Coefficient vs Wavelength	2-46
2-14	Geometrical Relation Between Observer A and Object B	2-48
2-15	IR Absorber Content Above a Given Altitude	2-49
2-16	Water Vapor Content Above a Given Altitude	2-50
2-17	Normalized Particle Density As a Function of Altitude	2-53
2-18	Scintillation vs Telescope Aperture	2-56
2-19	Frequency of Intensity Scintillation	2-57
2-20	Dependence of the Diameter d_o of the Collecting Optics, Upon Wavelength λ , and Altitude at a Zenith Angle of 70° for Both Nighttime and Daytime Conditions	2-57
2-21	The Electromagnetic Spectrum	2-58
2-22	Incident, Refracted, and Reflected Light Beams at the Interface of Two Media (drawn in the plane of incidence)	2-64
2-23	Transmission Curves for Representative IR Optical Materials	2-66
2-24	Comparisons of Material Properties	2-67
2-25	Idealized Background Spectrum	2-69
2-26	Comparison of Calculated Earth Radiance with Measurements for Downlooking System at 37 km Altitude	2-70
2-27	Radiance of 50° and 15°C Blackbodies	2-72
2-28	Hourly Variation in the 10-micron Radiance of Various Backgrounds	2-73
2-29	Daytime Spectral Radiance of Miscellaneous Targets	2-74
2-30	Relative Contrast of Deciduous Trees to Short Grass	2-77

LIST OF ILLUSTRATIONS (Cont)

<i>Figure No</i>	<i>Title</i>	<i>Page</i>
2-31	Relative Contrast of Wooden Catwalk Atop a Dam to the River Upstream from the Dam	2-78
2-32	Relative Contrast of a Small Asphalt-Surfaced Concrete Bridge to an Asphalt Roadway	2-79
2-33	Reflectivity of Solar Radiation vs Sun Angle for Various Sea-Surface Roughnesses	2-80
2-34	Reflectance of a Water Surface at 0°, 60°, and 80° Angle of Incidence	2-81
2-35	Typical 1.2- to 2.5-micron Cirrus Cloud Spectrum	2-84
2-36	Average Spectrum of Gladys I	2-85
2-37	Cloud Spectrum	2-86
2-38	Probability of Clear Lines-of-sight over Northern Hemisphere for All Seasons Combined	2-87
2-39	Probability of Clear Lines-of-sight Between Aircraft at ~30,000 ft and the Horizon	2-88
2-40	Probability of Clear Lines-of-sight Between Aircraft at ~30,000 ft and Space at an Angle of 30° Above the Horizon	2-89
2-41	Spectral Irradiance of the Brightest Visual and Red Stars As a Function of Wavelength	2-90
2-42	Major Planet Solar Reflection and Emission	2-91
2-43	Normalized Spectral Irradiance of R. Monocerotis As a Function of Wavelength	2-93
2-44	Normalized Spectral Irradiance of the Orion Infrared Star As a Function of Wavelength	2-94
2-45	Spectral Irradiance of the Cygnus Infrared Star As a Function of Wavelength	2-94
2-46	Stellar Irradiance As a Function of Visual Magnitude	2-95
2-47	Visual Fraction of Total Blackbody Irradiance As a Function of Temperature	2-96
2-48	Relative Spectral Distribution of Stellar Radiation As a Function of Star Class	2-98
2-49	Detector Response Fraction $F_d(T)$ for Ge:Hg Detectors As a Function of Spectral Band and Target Temperature	2-99
2-50	Number of K and M Stars in the 8- to 14-micron Band Exceeding a Given Irradiance	2-101
2-51	Lunar Temperature Measured by Surveyor I	2-102
2-52	Solar Spectral Irradiance As a Function of Wavelength	2-103
2-53	Infrared Map of the Galactic Center	2-104
2-54	Flow Chart for Plume Radiation Calculations	2-106
2-55	Low Altitude Plume Structure	2-109
2-56	Plume Structure As a Function of Altitude	2-110
2-57	Typical Line-of-sight Variations on the Saturn S-II Stage	2-111

LIST OF ILLUSTRATIONS (Cont)

<i>Figure No.</i>	<i>Title</i>	<i>Page</i>
2-58	Limiting Particle Streamlines in the Near Field	2-112
2-59	Trajectories of 0.79-micron Radius Particle External to the Gas Plume As a Function of Altitude	2-112
2-60	Near Field Isotherms for 0.79-micron Radius Particle	2-113
2-61	Far Field Temperature Profile, Vacuum Profile	2-114
2-62	Water Vapor and Carbon Dioxide Regions	2-116
2-63	Emission Spectrum of HF for 0.5 cm-atm at 2640° K	2-117
2-64	Theoretical Radiance Spectrum for a Solid Metallized Propellant Rocket Plume	2-117
2-65	Spectral Radiance of RP1/O ₂ Rocket Exhaust	2-118
2-66	Spectral Radiance of Solid Propellant Rocket	2-119
2-67	Flow Field Around Blunt and Slender Vehicles	2-120
2-68	Typical Radiant Signature of a Jet Aircraft	2-121
2-69	Idealized Reflectance Curve of a Uniform Fabric to Afford Camouflage Protection Over a Spectral Range from 0.4 to 1.2 Microns	2-123
2-70	Reflectance from Typical Uniform Cloth	2-123
2-71	Reflectance from Human Skins	2-124
3-1	Functional Relationship of the Major Disciplines and Associated Design Specialties	3-2
3-2	Refractive Index vs Wavelength for Several Optical Materials	3-12
3-3	Dispersion vs Wavelength for Several Optical Materials	3-13
3-4	Effects of Anti-reflection Coatings on Ge Transmission	3-17
3-5	Basic Lens Forms	3-19
3-6	Basic Mirror Forms	3-20
3-7	Typical Spectrophotometric Filter Curves	3-21
3-8	Prism Configurations and Functions	3-23
3-9	Conventional Geometry in First-order Optics	3-28
3-10	Cardinal Points for Single-surface Element	3-30
3-11	Cardinal Points for Double-surface Thick Lens Element	3-31
3-12	System Cardinal Points by Ray Tracing	3-32
3-13	Meridian Plane Section of a Refractive Optical System	3-33
3-14	Meridian Plane Section of a Reflective System	3-33
3-15	Virtual Image Formation by an Optical System	3-34
3-16	Application of Sine Condition	3-35
3-17	IR Optical System Showing Arrangement of Stops and Baffles	3-36
3-18	Display Pickup System	3-36
3-19	Relationship of Clear Aperture and Effective Focal Length	3-37

LIST OF ILLUSTRATIONS (Cont)

<i>Figure No.</i>	<i>Title</i>	<i>Page</i>
3-20	Geometrical Presentation of Refracted and Reflected Rays	3-38
3-21	Optical Diagram Illustrating Spherical Aberration	3-39
3-22	Optical Diagram Illustrating Coma Aberration	3-40
3-23	Optical Diagram Illustrating Astigmatism	3-41
3-24	Field Curvature	3-42
3-25	Examples of Pincushion and Barrel Distortion	3-43
3-26	Lens Bending for Minimum Spherical Aberration	3-44
3-27	Elementary Ray Trace Required for Computing Seidel Aberrations	3-45
3-28	Graphical Ray Trace	3-48
3-29	Graphical Ray Tracing. Surface May Be Convex, Flat, or Concave	3-49
3-30	Graphical Ray Tracing. Surface May Be Concave, Flat, or Convex	3-50
3-31	Afocal Systems	3-54
3-32	Optical Relay System	3-55
3-33	Example of Simple IR Radiometer	3-55
3-34	Geometry of an Aplanatic System	3-56
3-35	Symmetrical Relay System	3-57
3-36	Reduction of Spherical Aberration in Series Lens Combinations	3-58
3-37	Reflective Systems	3-59
3-38	Catadioptric Systems	3-60
3-39	Setup for Determining the Curvature of Concave Spherical Mirrors	3-67
3-40	Knife-edge Test Setup for Spherical and Paraboloidal Mirrors	3-68
3-41	Knife-edge Shadow Patterns	3-69
3-42	Knife-edge Test Setup for Complex and Hyperboloidal Systems	3-71
3-43	Ritchie Setup for Testing a Large Flat Mirror Using a Highly Accurate Spherical Mirror as Reference	3-72
3-44	Ronchi Grating for Determining Duration of Rays from Perfect Focus	3-72
3-45	Resolution Chart	3-74
3-46	Spectral Distribution of Xenon Discharge With Resolution of 0.1 Micron for Selected Input Powers	3-79
3-47	Spectral Distribution of 10-kilowatt Xenon Discharge With Resolution of 0.01 Micron	3-80
3-48	Spectral Radiant Power of Experimental dc Lamp (1.7- atm Xe; amp cm ⁻²) Normalized to Input Power. Spectral Resolution Equal to 0.01 Micron	3-81
3-49	Diagram of the Experimental 20-kw Lamp	3-82
3-50	Spectral Radiant Energy of FZ-47A Flashtube Normalized to Input Power. Spectral Resolution Equal to 0.01 Micron	3-83

LIST OF ILLUSTRATIONS (Cont)

<i>Figure No.</i>	<i>Title</i>	<i>Page</i>
3-51	Simplified Laser Energy-level Diagram	3-87
3-52	Outline of Solid-state Laser	3-91
3-53	Injection Laser	3-95
3-54	Frustrated-internal-reflection Modulator	3-96
3-55	Electro-optical Modulator	3-96
3-56	Digital Deflector	3-99
3-57	Schematic Diagram Showing Basic Types of Detectors	3-110
3-58	Electron Excited Into Vacuum by IR Radiation Impinging on Photocathode	3-111
3-59	Semiconductor Energy Levels at Absolute Zero	3-112
3-60	Semiconductor With Thermally Excited Electrons ...	3-112
3-61	Electron Excited by a Photon	3-113
3-62	Semiconductor (Intrinsic Detector) With Electric Field \vec{E}	3-113
3-63	Semiconductor (N-type Extrinsic Detector) With Donors	3-114
3-64	Semiconductor (P-type Extrinsic Detector) With Acceptors	3-114
3-65	P-n Junction (Photovoltaic Detector)	3-115
3-66	Photo-induced Hall Effect (Photoelectromagnetic Detector)	3-116
3-67	Spectral Range and Sensitivity of IR Photographic Material	3-118
3-68	Density vs Exposure for Various IR Film Sheets	3-122
3-69	Density vs Exposure for Various Types of 35-mm IR Film	3-123
3-70	Density vs Exposure for Various Types of High-speed IR Film	3-124
3-71	Block Diagram of D^* Measurement Apparatus	3-127
3-72	Modulation Factor for Sine and Square Wave Chopping	3-129
3-73	Idealized Spectral Response of Photon and Thermal Detectors	3-130
3-74	Detectivity of Long-wavelength Detectors	3-131
3-75	Detectivity of Short-wavelength Detectors	3-132
3-76	Equivalent Circuit Illustrating Detector- associated Capacitance	3-134
3-77	Typical Noise Voltage Spectrum and Signal Response of a Photoconductor	3-136
3-78	Detector Performance vs Temperature	3-142
3-79	Liquid Cryogen Cooling System	3-143
3-80	Vapor Pressure of Liquid Cryogens	3-145
3-81	Solid Cryogen Cooling System	3-146
3-82	Vapor Pressure of Solid Cryogens	3-147
3-83	Closed Cycle Joule-Thomson System	3-149
3-84	Joule-Thomson Closed Cycle System Temperature-entropy Diagram	5-150
3-85	Closed Cycle Stirling System	3-151

LIST OF ILLUSTRATIONS (Cont)

<i>Figure No.</i>	<i>Title</i>	<i>Page</i>
3-86	Refrigeration Efficiency vs Temperature	3-152
3-87	Closed Cycle Claude (Reversed Brayton) System	3-153
3-88	Closed Cycle Solvay (Gifford-McMahon) System	3-154
3-89	Vuilleumier Cycle Cooling System	3-155
3-90	Point Spread Function and Modulation Transfer Function of a Rectangular Slit	3-164
3-91	Spatial Filter Amplitude Response of Rectangular Detector	3-167
3-92	Spatial Frequency Amplitude Response (R) of a Plus-minus Detector Spaced One Detector Width Apart ($c = 2a$)	3-168
3-93	Spatial Amplitude Response of Circular Detector	3-170
3-94	Characterization of Thermal Noise from (A) Voltage Source, and (B) Current Source	3-171
3-95	Characterization of Shot-noise from (A) Current Source, and (B) Voltage Source	3-172
3-96	Classic Conventional Transistor Noise-equivalent Circuit	3-173
3-97	Low-frequency ($1/f$) Noise Characteristics	3-175
3-98	FET Noise Equivalent Circuit	3-176
3-99	\bar{e}_n, \bar{i}_n Noise Equivalent Circuit	3-177
3-100	\bar{e}_n, \bar{i}_n Approach Noise Figure Computational Model ..	3-178
3-101	Noise Figure As a Function of Frequency from (A) Transistor, and (B) FET	3-179
3-102	Gross Comparison of Transistor and FET Noise Figures vs Source Resistance	3-179
3-103	Transconductance and Drain Current As a Function of Temperature	3-181
3-104	Junction FET Noise As a Function of Temperature ..	3-182
3-105	FET Noise As a Function of Frequency	3-183
3-106	Model of Filter Relating Output Response $e_o(t)$ to Input $e_i(t)$ and output Noise n_o to Input Noise n_i	3-185
3-107	Rectangular Pulse Input and Simple RC Filter	3-186
3-108	Peak S/N for Various Filters, Compared With Matched Filter (Rectangular Pulse Input)	3-186
3-109	Input Sinusoidal Pulse Train and Second-order Filter	3-187
3-110	Signal-to-noise Performance for a Single Tuned Circuit of Quality Q-filtering a Train of n -sinusoidal Pulses	3-187
3-111	Detector Output for One Frame	3-189
3-112	Standard Luminosity Curve for the Average Human Eye	3-193
3-113	Two Basic Types of Cathode Ray Tubes	3-194

LIST OF ILLUSTRATIONS (Cont)

<i>Figure No.</i>	<i>Title</i>	<i>Page</i>
3-114	Change in Spot Size With V_{g_2} , Spot Size vs V_{g_1} ; Anode Voltage $V_B = 7000$ V	3-195
3-115	Spot Size for Several Beam Currents	3-196
3-116	Variation of Luminous Intensity With Anode Potential	3-197
3-117	Variation of Luminous Intensity With Electron Beam Current Density	3-198
3-118	Efficiency of (A) Aluminized, and (B) Unaluminized Screens	3-198
3-119	Display Storage Tube	3-202
3-120	Typical Scan-conversion Tube	3-204
3-121	Matricon Tube	3-205
3-122	Monoscope Tube	3-206
3-123	Shaped-beam Tube	3-207
3-124	Typical Image-converter Tube in Use	3-210
3-125	Screen Luminous Efficiency	3-210
3-126	Photocathode Sensitivities	3-211
3-127	Image Quality of Image Converter Tube in Terms of Distortion	3-212
3-128	Spectral Sensitivity of Various Types of Film	3-214
3-129	Typical Characteristic Curve of a Photographic Emulsion	3-215
3-130	Typical Variation of Gamma With Development Time	3-216
3-131	Typical Arrangement for Making Holograms	3-219
3-132	Reconstruction of a Hologram	3-220
3-133	Projection CRT Characteristics	3-221
3-134	Exploded View of All-glass EL Readout Panel and Sectional View of Metal-glass Unit	3-223
3-135	Example of Electroluminescent (EL) Panel	3-224
3-136	Brightness vs Voltage With 60% Transmission Glass for Both Metal-glass and All-glass EL Readout Panels at 115 and 250 V rms, Respectively	3-225
3-137	Voltage-current Curve for Nonlinear Resistor	3-226
3-138	CdSe Hysteresis Curve	3-227
3-139	Illuminating Panel Consisting of GaAs Photo-emitter Diode Array	3-228
3-140	Spectral Line Width for GaAsP Emitter Diode	3-229
3-141	Characteristic Curve for Typical GaAsP Emitter Diode	3-230
3-142	Forward Current vs Forward Bias Voltage of a Typical GaAsP Emitter Diode	3-231
3-143	Spatial Distribution of Radiation Emitted by GaAsP Diode	3-232
3-144	Beam-deviating Mirror Schematic Diagram	3-237
3-145	Lambertian Radiation	3-239
3-146	Density of Saturated Water Vapor (100% Relative Humidity) at 1 atm, 760 mm Hg	3-240

LIST OF ILLUSTRATIONS (Cont)

<i>Figure No.</i>	<i>Title</i>	<i>Page</i>
3-147	Section of Knife-edge Recording Characteristic Curve	3-244
3-148	Typical Knife-edge Record for Different Focus Positions	3-245
3-149	Conceptual Layout of Two-axis Gimbal Assembly . . .	3-251
3-150	Conceptual Layout of Three-axis Gimbal Assembly	3-252
3-151	Relationship of Gimbal and Target Coordinates	3-253
3-152	Servo Loop for Search or Measurement System	3-254
3-153	Servo Loop for Rate Search	3-255
3-154	Servo Loop for Tracker	3-255
3-155	Servo Loop Diagram	3-256
3-156	Error Constants and Responses of Type 0, I, and II Servos	3-257
3-157	Servo Response of $\frac{\omega_n^2}{s^2 + 2\xi\omega_n s + \omega_n^2}$ to Unit Step	
	Input for Various Damping Factors	3-258
3-158	Overshoot vs Damping Factor for Second-order System	3-260
3-159	Block Diagram of dc Torque Motor	3-262
3-160	Equivalent Circuit of Tachometer Generator	3-263
3-161	Block Diagram of Tachometer Generator	3-263
3-162	Block Diagram of System in Example Problem	3-264
3-163	Root Locus for Inner (Rate) Loop	3-266
3-164	Output Rate and Torque Response for Step-function Input to Rate Loop	3-268
3-165	Root Locus for Outer Loop	3-270
3-166	Output Angle and Torque Response for Step-function Input to Position Loop	3-272
3-167	Thermocouple Circuit Schematic	3-276
3-168	Resistance Thermometer Circuit	3-276
3-169	Block Diagram of Voltage and Current Monitors	3-278
3-170	Diagrams of Typical IR Calibration Systems	3-279
3-171	Mechanical Sun Shutter	3-280
3-172	Electrical Sun Shutter	3-282
3-173	Window-shade Type Protection for Focal Plane Shutter Camera	3-283
3-174	Hood-type Sun Shutter	3-284
3-175	Four-leaf Clover Sun Shutter	3-285
3-176	Rotary Damper Sun-shutter Mechanism	3-285
3-177	Classic Schmidt Sun-shutter System	3-286
3-178	Blocking Mechanism in Schmidt System	3-286
3-179	Schematic Illustrating Electromagnetic Coupling Parameters	3-288
4-1	Typical Imaging System Block Diagram	4-8
4-2	End of Scan Distortion	4-17

LIST OF ILLUSTRATIONS (Cont)

<i>Figure No.</i>	<i>Title</i>	<i>Page</i>
4-3	Typical Search System Block Diagram	4-20
4-4	Typical Tracker Block Diagram	4-23
4-5	Reticles	4-25
4-6	LWIR Radiometer	4-30
4-7	Typical Laser Rangefinder Block Diagram	4-34
5-1	Infrared Missile Seeker Block Diagram	5-12
5-2	Spectral Characteristics of Aircraft vs Viewing Aspect	5-13
5-3	Typical Sunlit Cloud Radiances vs Wavelength	5-15
5-4	Relative Target Energy and Transmission vs Wavelength for Plume Emission	5-16
5-5	Estimate of Probability of Cloud-free Line- of-sight from (or to) Surface Level (Washington, D. C.—Summer)	5-17
5-6	Example Spectral Background and Target Radiant Intensity	5-19
5-7	Sample Spectral Signature of Target and Background	5-20
5-8	Spectral Transmission Curves	5-20
5-9	Apparent Target and Background Signatures	5-21
5-10	Target and Background Cumulative Irradiance vs Upper Wavelength Cutoff	5-21
5-11	Signal-to-background Plus Noise Ratio for Various Upper and Lower Wavelength Cutoffs	5-22
5-12	Cumulative Signal-to-noise Ratios for Two Detector Types	5-23
5-13	Optical Diagram	5-26
5-14	Constraints on System Aperture Selection	5-27
5-15	Sensitivity of Detectors and Number Required vs Detector Aspect Ratio	5-29
5-16	Detector Overlap	5-30
5-17	Basic Scan Modes	5-31
5-18	Line Scanning Technique	5-32
5-19	Scanning Image System	5-32
5-20	Typical Missile Guidance Geometries	5-34
5-21	Seeker Servo Block Diagram	5-36
5-22	Apparent Target Intensity	5-37
5-23	Tracker Signal Processing	5-43
5-24	System Geometry	5-44
5-25	System Block Diagram	5-47
5-26	Relation Among Brightness Contrast, Brightness of Background, Exposure Time, and Visual Acuity	5-50
5-27	Critical Flicker Frequency As a Function of Brightness	5-51
5-28	Performance on a Visual, Auditory, and Combined Visual-auditory Vigilance Task	5-52

LIST OF TABLES

<i>Table No.</i>	<i>Title</i>	<i>Page</i>
2-1	Standard Symbols	2-2
2-2	Basic Radiometric Terms	2-3
2-3	Physical Constants	2-5
2-4	Experimental Values of Emissivity	2-6
2-5	Absorber Concentrations in the Atmosphere	2-23
2-6	Band Parameters S/d and $2\pi\gamma_o/d$ for CO_2	2-27
2-7	Band Model Parameters S/d and $S/(2\pi\gamma_o)$ for H_2O	2-32
2-8	Summary of Band-model Methods for Computing Atmospheric Absorption	2-39
2-9	Summary of Laboratory Measurements of Homogeneous-path Absorption Spectra	2-41
2-10	Wide-band Absorption of Carbon Dioxide	2-43
2-11	Wide-band Absorption of Water Vapor	2-44
2-12	Conversion Table of Physical Quantities	2-60
2-13	Reflectance ρ and Emissivity ϵ of Common Terrain Features	2-75
2-14	Total Emissivity of Snow and Ice Particles	2-76
2-15	Cloud Types and Characteristics	2-82
2-16	0.5- to 0.7-micron Albedos for Various Cloud Types	2-83
2-17	Calculated Thick Cloud Emissivities	2-83
2-18	Visual Magnitudes and Effective Temperatures of Planets and the Brightest Visual and Red Stars	2-92
2-19	Estimated Number of Stars Brighter Than a Given Magnitude	2-97
2-20	Calculations of Irradiance of K and M Spectral Class Stars	2-100
2-21	Number of Stars Per Square Degree Brighter Than Photographic Magnitude M , As a Function of Galactic Latitudes	2-105
2-22	Combustion Products for a Selection of Liquid Propellants	2-107
2-23	LOX/RP-1 Combustion Products in Mole Percent Calculated at Chamber Pressure 1000 psia, Exit Pressure 14.696 psia With Shifting Equilibrium	2-108
2-24	Combustion Products for Metallized Solid Propellant Polyurethane + 13% Al	2-108
2-25	Major Emission Bands for Common Molecular Combustion Products	2-115
3-1	Salient Characteristics of Optical IR Materials	3-4
3-2	Mirror Materials	3-14
3-3	Reflectivity Characteristics of Common Mirror Coatings	3-15
3-4	Standard Symbols for Par. 3-3	3-75

LIST OF TABLES (Cont)

<i>Table No.</i>	<i>Title</i>	<i>Page</i>
3-5	Spectral Emissivity of Tungsten at Temperatures Between 1600° and 2800° K	3-78
3-6	Selected Solid Lasers	3-92
3-7	Commonly Used Gas Lasers	3-93
3-8	IR Detector Terminology for Par. 3-4	3-105
3-9	Filters for Infrared Photography	3-119
3-10	Exposures of Infrared Photography Assuming Open Landscape, Summer Sun, Closeups, and Bright Sun	3-121
3-11	Comparative Performance of Infrared Detectors	3-139
3-12	Standard Symbols for Par. 3-5	3-144
3-13	Comparison of Cooling Techniques	3-156
3-14	Standard Symbols for Par. 3-7	3-191
3-15	Phosphor Data	3-197
3-16	Phosphor Screen Chart	3-199
3-17	Multi-gun Tubes	3-222
3-18	Standard Symbols for Par. 3-8	3-234
3-19	Window Regions in the Infrared	3-242
3-20	Methods of Protecting IR Detectors, Mirrors, and Lenses from Direct Solar Illumination	3-281
4-1	Infrared System Definitions	4-1
4-2	Comparison of 23-in. Xenon Arc, 30-in. Carbon Arc, and 30-in. Xenon Arc Searchlights	4-33
5-1	List of Symbols	5-2

PREFACE

This publication is one of a group of handbooks prepared for the U. S. Army Materiel Command under the auspices of the Engineering Handbook Office, Duke University, as part of the Engineering Design Handbook Series. Presented in this Handbook are the basic information and fundamental principles essential to the design and development of infrared systems for military applications.

A great deal of information has already been published describing time-proven IR systems and technology; whereas, little or no information has appeared in open literature, such as this, describing the significant recent advances in IR technology and systems development. Therefore, the approach to this topic departs from the time-honored treatment of the subject of infrared technology. No attempt is made to present a complete exposition of the overall infrared discipline, but rather, most of the material is devoted to the significant technological advances of recent years.

Recent requirements for tactical nighttime surveillance and detection capabilities have introduced new challenges. The result has been the successful development and application of multi-element arrays of IR detectors for reconnaissance and surveillance. This approach has considerably increased the effectiveness of IR systems in the field of combat as well as in global defense systems. Noteworthy advances have been made in the areas of low-light-level television and long-wavelength infrared. The implementation of IR searchlight and laser sources has further improved the range capability of IR systems, and has added a new capability to infrared technology—direct measurement of range or distance. It is in the light of these advances that the bulk of this book has been prepared. This handbook, therefore, is intended to complement the previously-published IR literature by bridging the gap between the historically-proven, well-documented technology and the advancing state of the art.

The material is presented in a form which will be most useful to the graduate engineer who must become informed about the technology and operational performance of present-day IR systems and who appreciates their attendant advantages and limitations. This handbook is also intended to aid the professional engineer concerned with the design and development of new systems.

The information contained in this handbook consists of contributions from many infrared specialists engaged in the design and development of IR systems and associated hardware at the Electronics Division of Aerojet-General Corporation, Azusa, California. Mr. I. M. Maine was the Program Director and Dr. K. Seyrafi, Technical Editor.

The material is organized in a logical structure which will result in maximum usefulness of the information. The reader is introduced to the fundamental elements of IR radiation, the basic laws governing the nature of infrared radiation and transmission. The target and background infrared signatures are then outlined, and the techniques for signal detection and background discrimination are described. Each discrete element of the conventional IR system is discussed including optics, detectors, signal-processing electronics, and associated support systems. Passive as well as active IR systems presently in existence are described. Design considerations and optimization techniques are presented.

The essential equations which describe systems operation are drawn from sound and proven sources, and are presented without proof. References are included at the end of each chapter. A selected additional Bibliography is presented at the end of this handbook.

Chapter 1 gives a short history of infrared technology and the significant military applications.

Chapter 2 introduces basic infrared terminology and describes the sources of IR radiation, laws governing this radiation, atmospheric transmission and absorption, radiation from targets of military interest, and background radiation.

Chapter 3 describes the basic tools needed for the transmission and detection of infrared signals. The optical elements are analyzed as are their characteristics and basic design parameters, thermal as well as mechanical. Sources of target illumination, including lasers and their applications, are noted. The characteristics of IR receiving systems, including various infrared detectors, are studied in terms of fabrication techniques, cooling requirements and, finally, performance. Signal-processing techniques (including spatial filtering, scanning aperture, temporal filtering, and display) are also discussed in this chapter.

Chapter 4 describes the operation of the most commonly-used passive and active infrared systems. The discussion includes the principles of imaging systems (including scanners), image tubes, viewers, and sights. Search equipment discussed includes trackers, radiometers, interferometers, spectrometers and hybrid systems. Active systems include illuminators, viewers and sights, rangefinders, communication, data transmission, and weapon applications.

Chapter 5 discusses system design approaches and operational requirements. System analyses entail target and background definition, baseline design concepts, and trade-off techniques. The design of a sample infrared system is analyzed at the end of this chapter.

A separate publication, AMCP 706-128, has been prepared in order to present classified information dealing with target signatures of military interest, IR technology, and classified military systems.

The Handbooks are readily available to all elements of AMC, including personnel and contractors having a need and/or requirement. The Army Materiel Command policy is to release these Engineering Design Handbooks to other DOD activities and their contractors and to other Government agencies in accordance with current Army Regulation 70-31, dated 9 September 1966. Procedures for acquiring these Handbooks follow:

- a. Activities within AMC and other DOD agencies order direct on an official form from:

Commanding Officer
Letterkenny Army Depot
ATTN: AMXLE-ATD
Chambersburg, Pennsylvania 17201

b. Contractors who have Department of Defense contracts should submit their requests through their contracting officer with proper justification to:

Commanding Officer
Letterkenny Army Depot
ATTN: AMXLE-ATD
Chambersburg, Pennsylvania 17201

c. Government agencies other than DOD having need for the Handbooks may submit their request directly to:

Commanding Officer
Letterkenny Army Depot
ATTN: AMXLE-ATD
Chambersburg, Pennsylvania 17201

or

Commanding General
U. S. Army Materiel Command
ATTN: AMCAM-ABS
Washington, D. C. 20315

d. Industries not having Government contracts (this includes colleges and Universities) must forward their requests to:

Commanding General
U. S. Army Materiel Command
ATTN: AMCRD-TV
Washington, D. C. 20315

e. All foreign requests must be submitted through the Washington, D. C. Embassy to:

Assistant Chief of Staff for Intelligence
Foreign Liaison Office
Department of the Army
Washington, D. C. 20310

f. All requests, other than those originating within DOD, must be accompanied by a *valid justification*.

Comments are invited and should be addressed to Commanding Officer, U. S. Army Research Office-Durham, Box CM, Duke Station, Durham, North Carolina 27706.

HEADQUARTERS
UNITED STATES ARMY MATERIEL COMMAND
WASHINGTON, D.C. 20315

AMC PAMPHLET
No. 706-127

21 April 1971

ENGINEERING DESIGN HANDBOOK
INFRARED MILITARY SYSTEMS
PART ONE

TABLE OF CONTENTS

<i>Paragraph</i>		<i>Page</i>
	List of Illustrations	xvi
	List of Tables	xxv
	Preface	xxvii

CHAPTER 1
INTRODUCTION

1-1	Definition of Infrared Spectrum	1-1
1-2	Milestones in the Development of Infrared Technology	1-1
1-3	Military Application	1-2
1-3.1	IR Imaging Systems	1-3
1-3.2	Infrared Missiles	1-3
1-3.3	Infrared Fire Controls	1-3
1-3.4	Tail-warning Systems	1-4
1-3.5	Space Applications	1-4
1-3.6	Spectroscopy	1-4
1-4	Advantages and Disadvantages of Infrared Systems	1-4
	References	1-5

CHAPTER 2
INFRARED PHYSICS

2-1	Basic IR Symbols and Definitions	2-1
2-2	Radiation Laws	2-1
2-2.1	Kirchhoff's Law	2-1
2-2.2	Planck's Law	2-5
2-2.3	Rayleigh-Jeans Law	2-5
2-2.4	Wien's Law	2-8

TABLE OF CONTENTS (Cont)

<i>Paragraph</i>		<i>Page</i>
2-2.5	Stefan-Boltzmann Law	2-8
2-2.6	Wien's Displacement Law	2-8
2-3	Radiant Energy Transmission	2-8
2-3.1	Radiant Intensity from a Point Source	2-8
2-3.1.1	Isotropic Point Source	2-8
2-3.1.2	Lambertian Point Source	2-8
2-3.2	Radiant Energy Density	2-9
2-3.2.1	Energy Density for Collimated Irradiance	2-9
2-3.2.2	Energy Density Within an Isothermal Enclosure	2-9
2-3.3	Transfer of Radiant Power	2-9
2-3.3.1	An Object in Space	2-9
2-3.3.2	Transfer Between Two Infinite Planes	2-11
2-3.4	Irradiance As a Function of Range	2-12
2-3.4.1	Point Source	2-12
2-3.4.2	Extended Source	2-12
2-3.5	Calculation Aids	2-13
2-3.5.1	Use of GE Radiation Calculator	2-14
2-3.5.2	Sample Calculations	2-16
2-4	Atmospheric Transmission	2-17
2-4.1	Extinction Coefficient	2-17
2-4.2	Molecular Absorption	2-18
2-4.2.1	Absorption Coefficient	2-18
2-4.2.2	Absorber Constituents	2-20
2-4.2.3	Absorption Models	2-23
2-4.2.3.1	Absorption Due to a Single Line	2-23
2-4.2.3.2	Absorption Due to an Assembly of Independent Lines	2-25
2-4.2.3.3	The Elsasser Band Model	2-25
2-4.2.3.4	The Goody Model	2-29
2-4.2.3.5	Other Less Frequently Used Models	2-30
2-4.2.3.6	Selective Absorption of Plume Radiation	2-30
2-4.2.4	Absorption Calculation	2-30
2-4.2.4.1	Narrow-band Absorption Data	2-31
2-4.2.4.2	Wide-band Absorption Data	2-31
2-4.2.4.3	Atmospheric Windows	2-31
2-4.2.4.4	Equivalent Sea-level Path	2-47
2-4.2.4.4.1	Equivalent-path Absorption Calculations	2-47
2-4.2.4.4.2	Equivalent-path Absorber Contents	2-47
2-4.2.4.5	Examples of Atmospheric Transmission Calculations	2-51
2-4.3	Scattering	2-51
2-4.3.1	Scattering Coefficient	2-52
2-4.3.2	Meteorological Range	2-55
2-4.3.3	Atmospheric Scintillation	2-55
2-5	Transmission of Infrared Radiation Through Optical Materials	2-58
2-5.1	Maxwell's Equations	2-59
2-5.2	Units	2-59

TABLE OF CONTENTS (Cont)

<i>Paragraph</i>		<i>Page</i>
2-5.3	Boundary Relations	2-60
2-5.4	Plane Waves	2-61
2-5.5	Poynting Vector	2-61
2-5.6	Refractive Index	2-61
2-5.7	Snell's Law	2-62
2-5.8	Reflection Coefficient	2-62
2-5.9	Brewster's Angle	2-63
2-5.10	Polarization	2-63
2-5.11	Anti-reflection Coatings	2-64
2-5.12	Dielectric Waveguides and Cavities	2-65
2-5.13	Spectral Transmission of Optical Materials	2-65
2-6	Sources of Natural Radiation	2-68
2-6.1	Background Radiation	2-68
2-6.1.1	Terrain	2-71
2-6.1.2	Sea	2-79
2-6.1.3	Clouds	2-81
2-6.1.4	Celestial Background	2-90
2-6.2	Target Radiation	2-106
2-6.2.1	Rockets and Missiles	2-107
2-6.2.2	Plume Radiation	2-107
2-6.2.2.1	Chemical Composition	2-107
2-6.2.2.2	Plume Structure	2-108
2-6.2.2.3	Infrared Emission	2-115
2-6.2.3	Re-entry Vehicles	2-119
2-6.2.4	Aircraft	2-121
2-6.2.5	Clear Air Turbulence	2-122
2-6.2.6	Ground Targets	2-122
	References	2-125

CHAPTER 3 IR SYSTEM COMPONENTS

3-1	Introduction	3-1
3-2	Optics	3-3
3-2.1	Optical Materials	3-3
3-2.1.1	Material Types	3-3
3-2.1.1.1	Refractive Materials	3-3
3-2.1.1.2	Reflective Materials	3-3
3-2.1.2	Material Properties	3-16
3-2.1.3	Anti-reflection Coatings	3-16
3-2.2	Optical Components	3-18
3-2.2.1	Types of Lenses and Principal Characteristics	3-18
3-2.2.2	Types of Mirrors	3-18
3-2.2.3	Filters	3-18
3-2.2.4	Prisms	3-22
3-2.3	Optical Design	3-27
3-2.3.1	Definition, Notations, and Sign Conventions	3-27
3-2.3.1.1	Optical Systems	3-27

TABLE OF CONTENTS (Cont)

<i>Paragraph</i>		<i>Page</i>
3-2.3.1.2	Object	3-27
3-2.3.1.3	Image	3-27
3-2.3.1.4	Object and Image Space	3-27
3-2.3.1.5	Point Image	3-27
3-2.3.1.6	Extended Image	3-27
3-2.3.1.7	First-order (Gaussian) Optical Theory—Paraxial Region	3-27
3-2.3.1.8	Ray—Slope of a Ray	3-28
3-2.3.1.9	Sign Conventions	3-28
3-2.3.1.10	Nomenclature	3-29
3-2.3.2	First-order Theory—Formulations	3-29
3-2.3.2.1	Cardinal Points of Optical Elements	3-29
3-2.3.2.2	Multiple Element Systems	3-31
3-2.3.2.3	Image Position, Magnification, and Virtual Image	3-32
3-2.3.2.4	Sine Condition—Lagrange Law of Invariance	3-34
3-2.3.3	Limitation of Rays	3-35
3-2.3.3.1	Entrance Pupil—Exit Pupil	3-35
3-2.3.3.2	Relative Aperture Speed, $f/\text{no.}$, and Numerical Aperture	3-35
3-2.3.4	Aberrations in Third-order Optics	3-38
3-2.3.4.1	Third-order Theory	3-38
3-2.3.4.2	Monochromatic Aberrations	3-39
3-2.3.4.3	Chromatic Aberration	3-43
3-2.3.4.4	Correction of Aberrations	3-43
3-2.3.4.5	Relation of Aberrations to Optical System Parameters	3-44
3-2.3.5	Ray Tracing	3-47
3-2.3.5.1	Use of Computers for Ray Tracing	3-47
3-2.3.5.2	Graphical Ray Tracing	3-47
3-2.3.6	Image Quality in Terms of Resolution, Spot Size, and Energy Distribution	3-51
3-2.3.6.1	The Diffraction Effect—Airy Disc	3-51
3-2.3.6.2	Geometrical Effects—Image Blur	3-51
3-2.3.6.3	Overall Effect	3-51
3-2.3.6.4	Resolution	3-51
3-2.3.6.5	Geometrical Energy Distribution—Spot Diagrams ...	3-52
3-2.3.6.6	Energy Distribution—Spread Function	3-52
3-2.3.6.7	Frequency Response	3-52
3-2.3.6.8	Image Evaluation	3-52
3-2.3.6.9	Depth of Focus	3-52
3-2.4	Optical System Descriptions and Engineering	3-53
3-2.4.1	Afocal Systems	3-53
3-2.4.2	Relay and Field Lenses	3-53
3-2.4.3	Aplanatic Systems	3-53
3-2.4.4	Symmetrical Combinations	3-53
3-2.4.5	Multiple-element Systems	3-57
3-2.4.6	Reflective IR Optical Systems	3-57

TABLE OF CONTENTS (Cont)

<i>Paragraph</i>		<i>Page</i>
3-2.4.6.1	Simple Mirror	3-57
3-2.4.6.2	Folded Systems	3-58
3-2.4.6.3	Off-axis Configuration	3-60
3-2.4.6.4	Compound Reflectors	3-60
3-2.4.6.5	Paired Conics	3-60
3-2.4.7	Catadioptric Systems	3-60
3-2.4.7.1	Mangin Mirror	3-61
3-2.4.7.2	Schmidt System	3-61
3-2.4.7.3	Maksutov—Bouwers System	3-61
3-2.4.7.4	Hybrid Configurations	3-61
3-2.4.8	Rapid Estimation of Blur Size	3-61
3-2.4.8.1	Spherical Mirror, On-axis	3-61
3-2.4.8.2	Spherical Mirror, Off-axis	3-62
3-2.4.8.3	Paraboloidal Mirror	3-62
3-2.4.8.4	Off-axis Paraboloidal Mirror	3-62
3-2.4.8.5	Schmidt System	3-62
3-2.4.8.6	Bouwers Concentric Design	3-62
3-2.4.8.7	Single Refractive Element	3-62
3-2.4.9	Mechanical Stability of Large Optical Systems	3-63
3-2.4.10	Thermal Stability	3-63
3-2.4.11	Establishing Optical Tolerances	3-63
3-2.4.11.1	Surface Quality	3-63
3-2.4.11.2	Thickness and Spacing	3-64
3-2.4.11.3	Optomechanical Centering	3-64
3-2.4.11.4	Prism Angles and Dimensions	3-64
3-2.4.11.5	Materials	3-64
3-2.4.11.5.1	Index of Refraction	3-65
3-2.4.11.5.2	Annealing	3-65
3-2.4.11.5.3	Transmission Range	3-65
3-2.4.11.5.4	Imperfections	3-65
3-2.4.11.6	Summation of Tolerances	3-65
3-2.5	Testing of Optical Systems	3-65
3-2.5.1	Material Inspection Tests	3-65
3-2.5.1.1	Index of Refraction	3-65
3-2.5.1.2	Stresses and Strains	3-66
3-2.5.1.3	Imperfections	3-66
3-2.5.2	Calibration	3-66
3-2.5.2.1	Focal Length Calibration	3-66
3-2.5.2.2	Curvature Measurements	3-66
3-2.5.2.3	Reflectance and Transmittance	3-67
3-2.5.3	Image Quality Measurements	3-67
3-2.5.3.1	Knife-edge Autocollimation	3-67
3-2.5.3.2	Knife-edge Testing of Complex System	3-70
3-2.5.3.3	Knife-edge Testing of Hyperbola	3-70
3-2.5.3.4	Knife-edge Testing of Large, Flat Mirrors	3-70
3-2.5.3.5	Ronchi Grating	3-70
3-2.5.4	Resolution Targets	3-73
3-3	Emitters and Illuminators	3-73

TABLE OF CONTENTS (Cont)

<i>Paragraph</i>		<i>Page</i>
3-3.1	Sources of Illumination	3-73
3-3.1.1	Flares	3-73
3-3.1.2	Lamps	3-76
3-3.1.2.1	Tungsten Filament	3-76
3-3.1.2.2	Carbon Arc	3-77
3-3.1.2.3	Gaseous Arc	3-77
3-3.1.2.4	Flashlamps	3-83
3-3.1.3	Lasers	3-84
3-3.1.3.1	Introduction	3-84
3-3.1.3.2	Laser Theory	3-84
3-3.1.3.2.1	Pumping	3-86
3-3.1.3.2.2	Optical Cavities	3-87
3-3.1.3.2.3	Condition for Threshold of Oscillation	3-89
3-3.1.3.2.4	Heat Dissipation	3-89
3-3.1.3.2.5	Cavity <i>Q</i> and Width of Resonance	3-89
3-3.1.3.2.6	<i>Q</i> -switching	3-90
3-3.1.3.3	Laser Types	3-90
3-3.1.3.3.1	Solid-state Lasers	3-90
3-3.1.3.3.1.1	Ruby Lasers	3-91
3-3.1.3.3.1.2	Neodymium Ion Lasers	3-91
3-3.1.3.3.1.3	Other Ions and Hosts	3-92
3-3.1.3.3.2	Gas Lasers	3-92
3-3.1.3.3.2.1	Neutral Atom Laser (He-Ne)	3-93
3-3.1.3.3.2.2	Ion Laser (Ionized Argon)	3-93
3-3.1.3.3.2.3	Molecular Laser (Carbon Dioxide)	3-94
3-3.1.3.3.3	Injection Lasers	3-94
3-3.1.3.4	Beam Control Devices	3-95
3-3.1.3.4.1	Modulators	3-95
3-3.1.3.4.1.1	Mechanical Modulator	3-95
3-3.1.3.4.1.2	Frustrated-internal-reflection Modulator	3-95
3-3.1.3.4.1.3	Acoustic Modulator	3-96
3-3.1.3.4.1.4	Electro-optical Modulator	3-97
3-3.1.3.4.1.5	Magneto-optical Modulator	3-97
3-3.1.3.4.1.6	Cavity Length Modulator	3-97
3-3.1.3.4.2	<i>Q</i> -switches	3-97
3-3.1.3.4.2.1	Mechanical Shutter <i>Q</i> -switch	3-97
3-3.1.3.4.2.2	Rotating Reflector <i>Q</i> -switch	3-97
3-3.1.3.4.2.3	Electro-optical and Magneto-optical Shutter <i>Q</i> -switch	3-97
3-3.1.3.4.2.4	Passive <i>Q</i> -switching	3-98
3-3.1.3.4.3	Beam Deflection	3-98
3-3.1.3.5	Nonlinear Optics	3-100
3-3.1.3.5.1	Harmonic Conversion	3-100
3-3.1.3.5.2	Raman Conversion	3-100
3-3.2	Design Considerations	3-100
3-3.2.1	Coherence	3-100
3-3.2.2	Optical Design for Incoherent and Coherent Sources	3-103

TABLE OF CONTENTS (Cont)

<i>Paragraph</i>		<i>Page</i>
3-4	Detectors	3-104
3-4.1	Detector Terminology	3-104
3-4.2	Detector Classifications	3-109
3-4.2.1	Quantum Detectors	3-109
3-4.2.1.1	Photoemissive Detectors	3-109
3-4.2.1.2	Photoconductive Detectors	3-109
3-4.2.1.3	Photovoltaic Detectors	3-115
3-4.2.1.4	Photoelectromagnetic Detectors	3-116
3-4.2.2	Thermal Detectors	3-116
3-4.2.2.1	Liquid Thermometer	3-116
3-4.2.2.2	Golay Cell	3-116
3-4.2.2.3	Calorimeter	3-117
3-4.2.2.4	Thermocouple	3-117
3-4.2.2.5	Thermopile	3-117
3-4.2.2.6	Bolometer	3-117
3-4.2.3	Imaging Devices	3-118
3-4.2.3.1	Photographic Film	3-118
3-4.2.3.2	IR Vidicon	3-125
3-4.2.3.3	Image Converter	3-125
3-4.3	Detector Performance and Test Procedures	3-125
3-4.3.1	Detector Figures of Merit	3-125
3-4.3.1.1	Noise Equivalent Power (<i>NEP</i>)	3-125
3-4.3.1.2	Detectivity (<i>D</i>)	3-125
3-4.3.1.3	Specific Detectivity (<i>D</i> [*])	3-125
3-4.3.2	Theoretical Background Limited Detectors	3-126
3-4.3.3	Measurement of <i>D</i> [*]	3-127
3-4.3.4	Spectral Responsivity	3-129
3-4.3.5	Input-output Relationship	3-133
3-4.3.5.1	Frequency Response	3-133
3-4.3.5.2	Time Response	3-133
3-4.3.6	Detector Noise	3-135
3-4.3.6.1	Johnson Noise (also Nyquist or Thermal)	3-135
3-4.3.6.2	Temperature Noise	3-135
3-4.3.6.3	Generation-recombination Noise	3-135
3-4.3.6.4	Shot Noise	3-135
3-4.3.6.5	Current Noise	3-137
3-4.4	Detector Fabrication	3-137
3-4.4.1	General	3-137
3-4.4.2	Photon Detectors	3-137
3-4.4.3	Thermal Detectors	3-137
3-4.5	Comparative Performance of Infrared Detectors	3-138
3-5	Cooling Systems	3-141
3-5.1	Requirements	3-141
3-5.1.1	Detector Cooling	3-141
3-5.1.2	Cooling of IR Optics	3-141
3-5.2	Types of Cooling Systems	3-141
3-5.2.1	Direct Contact	3-141
3-5.2.1.1	Liquid Coolant Systems	3-141

TABLE OF CONTENTS (Cont)

<i>Paragraph</i>		<i>Page</i>
3-5.2.1.2	Solid Coolant Systems	3-146
3-5.2.1.3	Passive Cooling	3-148
3-5.2.2	Joule-Thomson	3-148
3-5.2.2.1	Closed Cycle	3-148
3-5.2.2.2	Open Cycle	3-150
3-5.2.3	Expansion Engine	3-150
3-5.2.3.1	Stirling Cycle	3-150
3-5.2.3.2	Claude Cycle (Reversed Brayton)	3-150
3-5.2.3.3	Solvay Cycle (Gifford-McMahon)	3-150
3-5.2.3.4	Vuilleumier Cycle	3-154
3-5.2.4	Thermoelectric	3-155
3-5.2.5	Other Cooling Systems	3-155
3-5.2.5.1	Pulse Tube	3-155
3-5.2.5.2	Vortex Tube	3-157
3-5.2.5.3	Adsorption	3-157
3-5.2.6	Comparison of Cooling Systems	3-157
3-5.3	Cooling System Selection	3-157
3-5.3.1	Design Criteria	3-160
3-5.3.1.1	Weight	3-160
3-5.3.1.2	Volume	3-160
3-5.3.1.3	Durability	3-160
3-5.3.1.4	Logistics	3-160
3-5.3.2	Reliability	3-160
3-5.3.2.1	Mechanical Design	3-160
3-5.3.2.2	Structural	3-161
3-5.3.2.3	Vibrational	3-161
3-5.4	Insulation	3-161
3-5.4.1	Vacuum Insulation	3-161
3-5.4.2	Radiation Shields	3-161
3-5.4.3	Superinsulation Materials	3-161
3-5.4.4	Support of Insulating Materials	3-161
3-6	Signal Processing	3-162
3-6.1	Introduction	3-162
3-6.2	Spatial Filtering	3-162
3-6.2.1	Optical Transfer Function (OTF)	3-163
3-6.2.1.1	Point Spread Function (PSF)	3-163
3-6.2.1.1.1	Modulation Transfer Function (MTF)	3-163
3-6.2.1.1.2	One-dimensional Image Analysis	3-165
3-6.2.1.2	Line Spread Function (LSF)	3-165
3-6.2.1.3	Resolution Criteria and MTF	3-165
3-6.2.2	Detector Spatial Filtering	3-165
3-6.2.2.1	Analyses	3-165
3-6.2.2.2	Analysis in the Time Domain	3-165
3-6.2.2.3	Analysis in the Frequency Domain	3-166
3-6.2.2.4	Spatial Filtering Neglecting the Time-effect	3-166
3-6.2.2.5	Spatial Filter of a Detector Scanning in One Dimension Only	3-167
3-6.2.2.6	Rectangular Detector of Width a and Length b . . .	3-167

TABLE OF CONTENTS (Cont)

<i>Paragraph</i>		<i>Page</i>
3-6.2.2.7	Plus-minus Detectors	3-169
3-6.2.2.8	Circular Detectors	3-169
3-6.3	Electronic Signal Processing	3-170
3-6.3.1	Low-noise Amplification	3-170
3-6.3.1.1	Thermal Noise	3-171
3-6.3.1.2	Shot Noise	3-171
3-6.3.1.3	1/f Noise	3-173
3-6.3.1.4	Performance Characterization	3-173
3-6.3.1.4.1	Classic Approach for Conventional Transistors	3-173
3-6.3.1.4.2	Classic Approach for Field-effect Transistors	3-175
3-6.3.1.4.3	e_n, \bar{i}_n Approach for Conventional Transistors	3-176
3-6.3.1.5	IR Application Problems	3-178
3-6.3.1.5.1	Field-effect vs Conventional Transistor Characteristics	3-178
3-6.3.1.5.2	True Noise-figure	3-180
3-6.3.1.6	Cryogenic Amplifiers	3-180
3-6.3.2	Electronic Filtering	3-184
3-6.3.2.1	Application and Response Analysis	3-184
3-6.3.2.2	Detection Filters	3-185
3-6.3.3	Electronic Multiplexers	3-188
3-7	Data Display and Recording	3-189
3-7.1	Introduction	3-189
3-7.2	Terminology	3-189
3-7.3	Types of Displays	3-193
3-7.3.1	Cathode Ray Tube (CRT)	3-193
3-7.3.1.1	Resolution	3-195
3-7.3.1.2	Brightness	3-196
3-7.3.1.3	Contrast	3-200
3-7.3.1.4	Deflections	3-200
3-7.3.1.5	Focus	3-201
3-7.3.1.6	Bandwidth	3-201
3-7.3.2	Storage Type Cathode Ray Tubes	3-201
3-7.3.3	Electrical-readout Storage Tubes	3-203
3-7.3.4	Character Generation Tubes	3-204
3-7.3.4.1	Matricon	3-204
3-7.3.4.2	Monoscope	3-205
3-7.3.4.3	Shaped-beam Tube	3-206
3-7.3.4.4	Stroke Technique	3-207
3-7.3.4.5	Lissajous Techniques	3-207
3-7.3.4.6	Alphanumeric Indicator Tubes	3-208
3-7.3.4.7	Comparison of Character Generating Devices	3-208
3-7.3.5	Image-converter Tubes	3-208
3-7.3.6	Tape Recording	3-212
3-7.3.6.1	Magnetic Tape	3-212
3-7.3.6.2	Thermoplastic Film	3-213
3-7.3.7	Photography	3-213
3-7.3.8	Holography	3-217
3-7.3.9	Special Purpose Displays	3-220

TABLE OF CONTENTS (Cont)

<i>Paragraph</i>		<i>Page</i>
3-7.3.9.1	Projection CRT	3-220
3-7.3.9.2	Multi-gun CRT	3-222
3-7.3.9.3	Electroluminescent (EL) Panels	3-224
3-7.3.9.4	Photo-emitter Diodes	3-227
3-7.4	Display Equipment Design Parameters	3-232
3-8	Testing IR and Associated Equipment	3-233
3-8.1	Test Categories	3-235
3-8.2	Laboratory Instruments and Techniques	3-235
3-8.2.1	IR Collimator	3-235
3-8.2.2	Blackbody	3-238
3-8.2.3	Chopper-modulator	3-241
3-8.2.4	Blackbody Usage	3-241
3-8.2.5	Modulation Transfer Function (MTF) Measurements	3-243
3-8.2.5.1	Method 1	3-244
3-8.2.5.2	Method 2	3-246
3-8.2.5.3	Method 3	3-246
3-8.3	On-board Calibration	3-247
3-8.3.1	Radiometric Source	3-247
3-8.3.1.1	Quantitative Calibration	3-247
3-8.3.1.2	Qualitative Calibration	3-247
3-8.3.2	Simulated Electronic Signal	3-247
3-8.3.3	Type of BITS	3-248
3-8.3.3.1	Lamps	3-248
3-8.3.3.2	Emitters	3-248
3-8.3.3.3	Blackbody Sources	3-249
3-8.3.3.4	Modulation of Blackbody Radiation	3-249
3-8.3.4	Calibration of BITS	3-250
3-9	Ancillary IR Components and EMI Rejection Techniques	3-251
3-9.1	Gimbals	3-252
3-9.1.1	Coordinate System	3-254
3-9.1.2	Servo Loop	3-254
3-9.1.3	Specifications	3-256
3-9.1.3.1	Steady-state Errors	3-256
3-9.1.3.2	Transient Response	3-259
3-9.1.4	Design Considerations	3-260
3-9.1.4.1	Example Design Problem	3-261
3-9.1.4.1.1	Moment of Inertia	3-261
3-9.1.4.1.2	Acceleration	3-261
3-9.1.4.1.3	Component Selection	3-261
3-9.1.4.1.4	Analysis	3-264
3-9.1.4.1.4.1	Rate Loop	3-264
3-9.1.4.1.4.2	Position Loop	3-267
3-9.1.4.1.4.3	Response to Torque Disturbance	3-269
3-9.1.5	Components	3-273

TABLE OF CONTENTS (Cont)

<i>Paragraph</i>		<i>Page</i>
3-9.1.5.1	Bearings	3-273
3-9.1.5.2	Motors	3-273
3-9.1.5.3	Gears	3-274
3-9.1.5.4	Amplifiers	3-274
3-9.1.6	Gimbal Associated Measurements	3-274
3-9.1.6.1	Angle Measurement	3-274
3-9.1.6.2	Rate Measurement	3-275
3-9.2	IR System Monitors	3-275
3-9.2.1	Requirements for Monitor Devices	3-275
3-9.2.2	Thermocouples	3-275
3-9.2.3	Thermistors and Resistance Thermometers	3-277
3-9.2.4	Voltage and Current Monitors	3-277
3-9.2.5	Calibration of IR Sensors	3-277
3-9.3	Sun Shutters	3-278
3-9.4	Electromagnetic Interference	3-287
3-9.4.1	Sources of Electromagnetic Radiation	3-287
3-9.4.2	Elimination and Rejection	3-287
3-9.4.2.1	Methods	3-288
3-9.4.2.1.1	Bonding	3-288
3-9.4.2.1.2	Grounding	3-288
3-9.4.2.1.3	Shielding	3-289
	References	3-290

CHAPTER 4 IR SYSTEMS DESCRIPTION

4-1	Passive Systems	4-7
4-1.1	Imaging Systems	4-7
4-1.1.1	Mechanical Scanners	4-9
4-1.1.1.1	Scanner Parameters	4-9
4-1.1.1.1.1	Noise Equivalent Temperature (Sensitivity)	4-9
4-1.1.1.1.2	Optical Gain and Resolution	4-13
4-1.1.1.1.3	Scan Rate and Bandwidth	4-13
4-1.1.1.1.4	Performance Requirements and Instrumentation Parameters	4-14
4-1.1.1.2	Thermographs	4-16
4-1.1.1.3	Down-looking Line Scanners	4-16
4-1.1.1.4	Forward-looking Infrared Systems	4-18
4-1.1.2	Image Tubes	4-18
4-1.2	Search Equipment	4-19
4-1.2.1	Spectral Filtering	4-21
4-1.2.2	Spatial Filtering	4-21
4-1.2.3	Temporal Filtering	4-21
4-1.3	Trackers	4-22
4-1.3.1	The IR Scanner As an Optical Angle Transducer	4-24
4-1.3.1.1	Small Instantaneous Field-of-view Scanning	4-24

TABLE OF CONTENTS (Cont)

<i>Paragraph</i>		<i>Page</i>
4-1.3.1.2	Large Instantaneous Field-of-view	
	Reticle Scanning	4-26
4-1.3.2	Tracking Scanner Sensitivity	4-27
4-1.3.3	Tracking Loop Servo Parameters	4-28
4-1.4	Radiometers	4-29
4-1.5	Spectrometers	4-30
4-1.6	Interferometers	4-31
4-1.7	Hybrid Systems	4-31
4-1.7.1	Track-while-scan	4-31
4-1.7.2	Scanning Radiometer/Spectrometers	4-31
4-2	Active Systems	4-32
4-2.1	Illuminators	4-32
4-2.1.1	Searchlights	4-32
4-2.1.2	Lasers	4-32
4-2.2	Rangefinders	4-33
4-2.3	Communications and Data Transmission	4-35
	References	4-37

CHAPTER 5 IR SYSTEM DESIGN

5-1	System Approach to Infrared Design	5-1
5-2	Requirements	5-1
5-2.1	System Analysis	5-2
5-2.1.1	Operational Environment	5-2
5-2.1.2	Functions	5-8
5-2.1.3	Requirement Analysis	5-8
5-2.1.4	Block Diagrams	5-12
5-2.2	Target Definition	5-13
5-2.2.1	Spectral Radiant Intensity Bounds	5-13
5-2.2.2	Radiance Gradients	5-14
5-2.3	Background Definition	5-14
5-2.3.1	Terrain, Sea	5-14
5-2.3.2	Clouds	5-14
5-2.3.3	Stellar Backgrounds	5-15
5-2.4	Transmission	5-15
5-2.4.1	Absorption	5-15
5-2.4.2	Obscuration	5-16
5-2.5	Countermeasures	5-17
5-2.5.1	Passive Countermeasures	5-17
5-2.5.2	Active Countermeasures	5-17
5-3	Baseline Design Concept	5-18
5-3.1	Spectral Optimization	5-18
5-3.1.1	Trade-offs	5-18
5-3.1.2	Detector Selection	5-22
5-3.2	Frame-time Optimization	5-24

TABLE OF CONTENTS (Cont)

<i>Paragraph</i>		<i>Page</i>
5-3.3	Parametric Design	5-25
5-3.3.1	Collecting Aperture Diameter	5-25
5-3.3.2	Number of Detectors	5-27
5-3.3.3	Cooling Requirements	5-30
5-3.3.4	Scanning Systems	5-31
5-4	Sample IR System Designs	5-32
5-4.1	Missile Seeker	5-32
5-4.1.1	Missile Seeker Requirements	5-33
5-4.1.1.1	Operational Environment	5-33
5-4.1.1.2	Seeker Functions	5-33
5-4.1.1.3	Functional Description	5-35
5-4.1.1.4	Apparent Radiant Intensity of Targets and Backgrounds	5-35
5-4.1.2	Baseline Design Concept	5-35
5-4.1.3	Seeker Design	5-39
5-4.1.3.1	Optical and Mechanical	5-39
5-4.1.3.2	Detector	5-40
5-4.1.3.3	Acquisition-mode Programmer	5-40
5-4.1.3.4	Track-loop-mode Servo	5-40
5-4.1.3.5	Sensitivity	5-41
5-4.1.3.6	Signal Processing	5-42
5-4.2	Active Imaging Systems	5-42
5-4.2.1	Sample Design of Active IR Imaging Systems	5-42
5-4.2.1.1	Spatial Resolution and Field of View	5-42
5-4.2.1.2	Data Rate and System Bandwidth	5-44
5-4.2.1.3	Laser Power and Signal-to-noise Characteristics	5-45
5-5	Trade-off Analyses	5-46
5-5.1	General Principles	5-46
5-5.2	Use of Advanced Components and Concepts	5-47
5-5.3	Cost, Space, Weight, and Power Trade-offs	5-47
5-5.4	Human Factors	5-48
5-5.4.1	Visible Spectrum	5-48
5-5.4.2	Visual Acuity	5-48
5-5.4.3	Other Factors Affecting Acuity	5-49
5-5.4.4	Flicker	5-49
5-5.4.5	Supplementary Auditory Displays	5-50
5-5.4.6	Human Reaction Time	5-50
5-5.4.7	Human Engineering	5-52
5-5.5	Reliability	5-53
5-5.5.1	The Importance of Reliability	5-53
5-5.5.2	Reliability Program	5-53
5-5.5.3	Definitions	5-53
5-5.5.4	Reliability Prediction	5-53
5-5.5.5	What the IR Design Engineer Should Know About Reliability	5-54

TABLE OF CONTENTS (Cont)

<i>Paragraph</i>		<i>Page</i>
5-5.5.6	Design Practices for Achieving	
	High Reliability	5-54
5-5.5.6.1	Borrowing and Buying	5-54
5-5.5.6.2	Simplification	5-54
5-5.5.6.3	Selection of Reliable Part Types	5-54
5-5.5.6.4	Derating	5-55
5-5.5.6.5	Redundancy	5-55
5-5.5.6.6	Providing for Satisfactory	
	Heat-transfer Properties	5-55
5-5.5.6.7	Mechanical Strength and Stability	5-56
5-5.5.6.8	Formulating Alternative Designs	5-56
5-5.5.6.9	Miscellaneous Considerations	5-56
5-5.6	Maintainability	5-57
5-5.6.1	The Importance of Maintainability	5-57
5-5.6.2	Maintainability Program	5-57
5-5.6.3	Definitions	5-58
5-5.6.4	Maintainability Predictions	5-58
5-5.6.5	What the IR Design Engineer Should Know	
	About Maintainability	5-58
5-5.7	Producibility	5-59
5-5.7.1	Definition and Importance	5-59
5-5.7.2	Producibility Program	5-60
5-5.7.3	What the IR Design Engineer Should Know	
	About Producibility	5-60
5-5.8	Mobility	5-61
5-5.8.1	Definitions and Importance	5-61
5-5.8.2	Transportability Design Program	5-61
5-5.8.3	What the IR Design Engineer Should Know	
	About Mobility	5-61
5-5.9	Integrated Logistic Support	5-62
5-5.10	Ground Support Equipment	5-63
5-5.10.1	The Importance of Ground Support Equipment	5-63
5-5.10.2	Ground Support Equipment Functions	5-63
5-5.10.3	Ground Support Equipment Design Factors	5-63
5-5.10.4	Selection of Aerospace Ground Equipment	5-63
5-5.10.5	Applicability of Government Equipment	5-64
5-5.10.6	Multi-function Concept	5-64
5-5.10.6.1	General	5-64
5-5.10.6.2	Advantages	5-64
5-5.10.6.3	Disadvantages	5-64
5-5.10.6.4	Unitized Multi-purpose Equipment	5-64
5-5.10.7	Quality	5-65
5-5.10.7.1	Criteria	5-65
5-5.10.7.2	Evaluation Factors	5-65
5-5.10.8	Commercial Counterparts	5-65
5-5.10.9	System Safety	5-65

TABLE OF CONTENTS (Cont)

<i>Paragraph</i>		<i>Page</i>
5-5.10.10	General Military Documents	5-66
5-5.10.11	What the IR Engineer Should Know About	
	Ground Support Equipment	5-66
5-6	Test Requirements	5-67
5-6.1	Quality Control and Inspection	5-67
5-6.2	Inspection and Testing	5-67
5-6.2.1	Test and Inspection Planning	5-68
5-6.2.2	Inspection and Testing of Infrared	
	Components and Systems	5-68
5-6.2.2.1	Optical Elements, Lenses, Prisms,	
	and Mirrors	5-68
5-6.2.2.2	Optical Materials	5-68
5-6.2.2.3	Optical Coatings and Filters	5-69
	References	5-70
	Appendix	5-72
	Bibliography	B-1

CHAPTER 1

INTRODUCTION*

1-1 DEFINITION OF INFRARED SPECTRUM

The infrared (IR) region of electromagnetic radiation consists of that portion of the spectrum located between the longest visible wavelengths and the shortest microwave wavelengths. The IR spectral band is many times as broad as the visible optical spectrum which ranges from about 0.3 to 0.72 micron. The IR band is, therefore, divided somewhat arbitrarily into the following three regions for convenience:

1. The near IR between 0.72 - 1.2 microns
2. The intermediate IR between 1.2 - 7.0 microns
3. The far IR between 7.0 - 1000 microns

Recently, many IR systems have been developed for operation in the 8- to 30-micron region. This region, which is a subclass of the far IR region, is conventionally referred to as the Long-wavelength (LWL) Infrared Region.

1-2 MILESTONES IN THE DEVELOPMENT OF INFRARED TECHNOLOGY

This chapter contains a cursory survey of the significant milestones in the advancement of infrared technology and its application. A more detailed account of the development and applications of IR technology is given by Smith, Jones, and Chasmer¹† and by Arnquist².

The actual discovery of infrared radiation was the result of Sir William Herschel's pioneering experiments in 1800¹. While investigating the distribution of thermal energy among various colors of solar radiation, Herschel found that thermal energy increased toward the red end of the visible spectrum and continued beyond the visible region. He concluded that radiant energy exists beyond the visible region. He called this radiation "invisible radiation". Further experiments by Herschel indicated that IR radiation obeys the same laws as does visible light.

Herschel's discovery opened a new frontier in optical science. It did not lead to any further advancement for almost twenty years, however, due primarily to the lack of detectors more sensitive than the thermometer. Although progress during the nineteenth and early twentieth centuries was not dramatic, significant advancement has been made during the past 30 years.

In 1830, L. Nobili developed the thermocouple which detects IR radiation with a higher degree of sensitivity than does the thermometer. Within five years, M. Melloni developed an even more sensitive sensor by integrating a large number of thermocouples and called it a "thermopile". The development of the thermocouple and thermopile are considered to be the first important steps in the advancement of IR technology.

During 1830-1840, Sir John Herschel, the son of Sir William Herschel, continued his father's work and supported his father's conclusion regarding the nature of IR radiation. He maintained that IR radiation and visible light are similar in many basic respects. This opinion was the cause of considerable controversy until 1847 when Fizeau, Foucault, and Knoblauch illustrated that IR radiation exhibits interference effects in exactly the same way as does visible light.

In 1843, E. Becquerel discovered the photographic and phosphorescent effects of IR radiation. In 1880, S. P. Langley invented the first bolometer which is considerably more sensitive than the thermopile. A bolometer consists of a thin wire whose ohmic resistance changes as the result of the heat generated by the incident radiation.

In 1920, T. W. Case³ developed the photoconductive "Thalofide Cell" detector which is more sensitive and has faster response characteristics than thermocouples and bolometers. Although the principles of photoconductivity were discovered by Willoughby Smith⁴ in 1873 using selenium, Case should be credited for actually developing and implementing the photoconductor detector for use as an active IR infrared

* Written by K. Seyrafi.

† Superscript numbers refer to References at the end of each chapter.

transmitter and receiver system having an operating range of over 18 miles². His device stimulated widespread interest in IR in this country and abroad.

In 1876, Adams and Day discovered the photovoltaic detector (selenium) and in 1934, Kikoin and Noskov developed the first photoelectromagnetic detector (cuprous oxide).

In 1904, Bose* discovered the photosensitive property of lead sulfide (galena). Later on, in 1917, during a routine investigation of 162 materials, Case⁵ reported the photoconductor properties of lead sulfide (PbS).

In 1944, Cashman developed the first practical PbS detectors in this country⁶. Lead sulfide detectors had been previously developed by Gudden⁷ in Germany during the 1930's and were used in some of their IR systems during World War II. Cashman's development marked the beginning of a rapid expansion in IR technology and systems application in this country.

Later on during the late 1940's and early 1950's, Cashman, McFee, and Levinstein extended PbS technology into lead selenide (PbSe), lead telluride (PbTe), and indium antimonide (InSb) detectors.

Another significant technological advance was the development of a pneumatic IR detector by Marcel Golay in 1946. The Golay detector is still considered the best detector for long-wavelength IR applications because of its *uniform* spectral sensitivity.

During the late 1940's, the first extrinsic photoconductor detectors were discovered by Burstein⁸. The spectral response of detectors such as gold-doped germanium (Ge:Au), zinc-doped germanium (Ge:Zn), and copper-doped germanium (Ge:Cu) was found to extend to about 40 microns. Later on, the discovery of a mercury-doped germanium detector (Ge:Hg), having a high-sensitivity response up to 14 microns, was reported by Borrello and Levinstein⁹. Most of these detectors required cooling to temperatures ranging from 4° to 40°K.

In 1959, Lawson¹⁰ described the first pseudobinary detector (mercury-cadmium telluride) as having a spectral response that could be extended to 40 microns. This detector, in contrast to other LWLIR detectors, required cooling only to about 77°K (liquid nitrogen).

Today, because of the availability of highly-sensitive detectors in the range of about 0.7 to 40 microns, the most useful part of the IR spectrum can be detected with almost the same sensitivity as visible light.

1-3 MILITARY APPLICATION

Although IR has been part of the scientific world for over 150 years, its application for military purposes has only taken place within the last 40 years. Secure signaling, detection of objects in the dark, and detection of and homing on military targets by their natural IR radiation are a few of the many military applications of IR systems. During World War I, the Americans, British, and Germans produced IR devices which were, for the most part, experimental.

In 1920, S. Hoffman¹¹ described a passive imaging system which utilized a thermopile and galvanometer. This system could detect a man at 600 feet and an airplane at nearly 1 mile.

During the 1930's, IR systems found their way slowly into the military arsenals. The advent of World War II, however, accelerated the tempo of activity in this area. During 1940-1941, the Optics and Camouflage Branch of the National Defense Research Committee and Office of Scientific Research and Development was assigned the responsibility for developing the military potential of optics and IR systems.

During 1947-1955, the growing military demand for IR systems necessitated close technical coordination between the military and contract groups of the rapidly developing Southern California infrared community. Consequently the Office of Naval Research (ONR) Branch Office, Pasadena, California, sponsored a series of meetings under the leadership of W. N. Arnquist¹². Initially these gatherings were called "The Conference on IR Instrumentation", and then, as the emphasis shifted to systems, the "Guided Missile Infrared Conference". An effective information exchange and discussion forum were thus provided for the relatively new work-

* Patent — 755,840. "Detector For Electrical Disturbances," Jagadis C. Bose, Calcutta, India, assignor of one-half to Sara Chapman Bull, Cambridge, Mass., filed Sept. 30, 1901, Serial No. 77,028 (No model).

ing groups in the area. The attendance at these conferences grew at such a rapid rate that by the mid-1950's it was no longer possible to continue on such an informal basis. Instead, formal meetings, called "Symposiums", replaced the informal conferences within the necessary security regulations. In November 1955, the name "Infrared Information Symposium" (IRIS), was formally adopted. IRIS symposiums have been convened regularly at least once a year ever since. IRIS has provided an effective means for exchanging information and stimulating new ideas for the advancement of IR research and technology. Other activities of ONR that stimulated developments in IR, especially during 1950-55, were Project Metcalf, a comprehensive review of the Navy's IR program and special liaison with the British through ONR's London Branch Office¹².

Today, various basic types of IR systems are used in conjunction with tactical weapons in military arsenals throughout the world. The brief summary which follows is a description of some of the more notable applications of IR systems.

1-3.1 IR IMAGING SYSTEMS

Development of the RCA infrared image tube by Morton, Ramberg, and Zyorykin² is considered to be the most significant IR development in the United States during the 1930's. The device converts IR radiation into visible light.

The first and most notable military application of near-IR technology during World War II involved use of the IR imaging tube mounted on small arms for use by foot soldiers¹³. Named the Sniperscope, it was used successfully during night operations. Infrared illuminators and receiving devices were used for night driving and battlefield surveillance by all the major powers.

1-3.2 INFRARED MISSILES

Chronologically, the next step in the advancement of IR occurred as a result of its successful application for air-to-air and air-to-surface missile guidance. The Germans developed an IR antiaircraft missile detection system during the early 1930's, to the point where piston-engine bombers could be observed at distances up to five km. However, they were not successful in

implementing this latter capability in an operational system.

In this country, the use of IR in the missile field reached its peak after World War II. The most successful developments in the 1950's were the Navy SIDEWINDER air-to-air missile and the Air Force FALCON homing missile¹⁴. The SIDEWINDER missile is 5 in. in diameter, 9 ft long, and weighs 150 lb. It can be carried by a variety of aircraft, including the F84, F-104, and FJ-4.

The FALCON missile was developed by the Air Force to complement a radar-guided missile. These missiles are about 6-1/2 in. in diameter, about 6-1/2 ft long, and weigh slightly more than 120 lb. Used in F102A and F-89H interceptors, the missile's tracking capability is such that it can be launched many miles from the target.

Beginning about 1958 and extending to the early 1960's, the REDEYE missile was developed for the Army, to provide the foot soldier with a defense against low-flying aircraft. The 20-lb missile, which is less than 3 in. in diameter and 4 ft long, is aimed and fired from a shoulder-mounted launch tube.

1-3.3 INFRARED FIRE CONTROLS

The first IR fire control system for search, acquisition, and tracking became operational in the mid-1950's. A gunsight was developed at this time for the F-104 aircraft, and the AAA-4 IR fire control system was developed in the early 1960's by the Navy.

An early version of a down-looking (3 to 5 microns) IR reconnaissance system was developed by the Air Force in the early 1960's.

Recent breakthroughs in the fabricating of large arrays (consisting of LWIR sensors, cryogenic cooling, and LWL optics) have further increased the potential capability of IR high-resolution fire-control systems, unmatched by any other system at this time^{15,16}. Forward-looking IR Reconnaissance (FLIR) systems, designed for mounting on airborne platforms, provide armament system operators with IR target detection, acquisition, recognition, and angle information. The FLIR systems, developed specially for nighttime use, provide real-time display of the

terrestrial scene within the field of view of the sensors.

1-3.4 TAIL-WARNING SYSTEMS

Infrared systems are also used for detecting missile plumes. An IR search system for use in the detection of attacking missiles was developed by the Air Force as a tail-warning system for a fighter aircraft and became operational in the mid-to-late 1960's.

1-3.5 SPACE APPLICATIONS

The first spaceborne high-resolution IR temperature mapping system was launched aboard the Nimbus 1 satellite into an earth orbit in 1964¹⁷. The Nimbus infrared detector, sensing in the 3.4- to 4.2-micron region, provided the first nighttime cloud pictures with a ground resolution of about two nmi.

Nimbus 1 performed temperature measurements with a resolution of about 1°K making it possible to map gradients in ocean currents, ice caps, land masses, and cloud formations. Furthermore, because of the correlation between cloud temperature and cloud altitude (a 1°K temperature change is comparable to a 1000-ft change in altitude), the IR picture provided a simple and effective method of determining cloud altitude.

1-3.6 SPECTROSCOPY

Infrared spectroscopy plays a key role in detection systems for military applications. Evaluation of targets and background in terms of spectral intensity has provided considerable information for use in the design of effective detection and homing systems. It has also provided an enormous amount of information about the sun, planets, and stars. New low-temperature stars have been discovered¹⁸. Terrestrial atmospheric phenomena and the atmospheres of other planets are being investigated.

In biology and medicine, infrared techniques are continually finding new uses and applications. Spectroscopy has made possible the study of plant diseases as well as the characterization and identification of fossils.

1-4 ADVANTAGES AND DISADVANTAGES OF INFRARED SYSTEMS

Infrared systems offer a distinct advantage over other detection devices, such as radar or visible optics, by being able to operate in the passive mode. This makes IR systems impervious to detection and countermeasures by methods which are effective against active systems such as radar. In addition, the passive IR systems are less complex by the absence of transmitter hardware. The fact that most natural objects radiate in the IR region makes IR wavelengths most attractive for passive systems.

A summary of the advantages of IR systems includes:

1. Small size and lightweight compared to comparable active systems
2. Low cost compared to active systems
3. Capable of passive or active operation
4. Effective against targets camouflaged in the visible region of the optical spectrum
5. Day or night operation
6. Greater angular accuracy than radar
7. No minimum range limitation
8. Minimum requirement for auxiliary equipment.

The performance limitations of IR systems are imposed mostly by atmospheric conditions. Humid atmosphere, fog, and clouds present serious limitations. The problems can be briefly summarized as follows:

1. Lack of all-weather capability (in operation within the atmosphere)
2. Line-of-sight detection capability *only*
3. Requirements for cryogenic cooling during LWL operation.

Notwithstanding these inherent limitations, IR technology faces an ever-expanding future made possible by the recent dynamic advances in the development of components such as solid-state detectors and detector arrays, cooled optics, cryogenic electronics, and IR lasers.

REFERENCES

1. R. A. Smith, et al., *The Detection and Measurement of Infrared Radiation*, Oxford at the Clarendon Press, 1957.
2. W. N. Arnquist, "Survey of Early Infrared Developments", *Proc IRE* 47, No. 9, 1420-1431 (1959).
3. T. W. Case, "Thalofide Cell—A New Photo-Electric Substance", *Phys. Rev.* 15, 289 (1920).
4. W. Smith, "Effect of Light on Selenium", *Nature* 7, 303 (1873).
5. T. W. Case, "Notes on the Change of Resistance of Certain Substances in Light", *Phys. Rev.* 9, 305 (1917).
6. R. J. Cashman, "New Photo-Conductive Cells", *J.D.S.A.* 36, 356 (1946).
7. J. A. Jamieson, et al., *Infrared Physics and Engineering*, McGraw-Hill Book Co., New York, 1963.
8. E. Burstein, J. J. Oberly, J. W. Davisson, and B. W. Hennis, "The Optical Properties of Donor and Acceptor Impurities in Silicon", *Phys. Rev.* 82, 764 (1951).
9. S. R. Borrello and H. Levinstein, "Preparation and Properties of Mercury-doped Germanium", *J. Appl. Phys.* 33, No. 10, (1962).
10. W. D. Lawson, S. Neilson, E. H. Putley, and A. S. Young, "Preparation and Properties of HgTe and Mixed Crystals of HgTe-CdTe", *J. Phys. Chem. Solids* 9, 325 (1959).
11. S. D. Hoffman, "The Detection of Invisible Objects by Heat Radiation", *Phys. Rev.* 14, 163-166 (1919).
12. W. N. Arnquist, *Proc. IRIS* 1, 5 (June 1956).
13. R. S. Wiseman and M. W. Klein, "Infrared Viewing Systems", *Proc. IRE* 47, 1617 (1959).
14. L. W. Nichols, "Missile Seekers and Homers", *Proc. IRE* 47, No. 2, 1611-1614 (1959).
15. G. J. Hoover, *Fabrication and Statistical Evaluation of High Density Ge:Hg Linear Arrays*, presented at 16th National Meeting of IRIS, 1968.
16. Hodges, et al., *System Optimization of Long-Wavelength Infrared Detection Systems*, Aerojet Report No. 3009, Azusa, Calif., March 1965.
17. *TRW Space Log*, 4-23-24 (Winter 1964-65).
18. R. C. Ramsey, "Spectral Irradiance from Stars and Planets Above the Atmosphere from 0.1 to 100 μ ", *Appl. Opt.* 6, No. 4, 465 (1962).

CHAPTER 2

INFRARED PHYSICS*

2-1 BASIC IR SYMBOLS AND DEFINITIONS

During the advance of IR technology, various symbols have evolved as "standard" symbols while others have been used at the whim of the authors. The system of symbols used in this handbook is based on the recommendations of the Office of Naval Research¹. Special care has been given to distinguish *intrinsic* material properties such as absorptivity α from total sample properties such as absorptance a . Some symbols occasionally have two functions. For instance, t can mean either time or total transmittance. Where confusion might possibly occur, the terms are carefully explained in the accompanying text. The standard symbols are given in Table 2-1.

Table 2-2 is a dictionary of the basic radiometric terms used in infrared physics. *Spectral* radiometric terms are the same as the corresponding radiometric terms but are defined per unit wavelength, per unit frequency or per unit wavenumber. They are evaluated at a specific wavelength, frequency or wavenumber. Symbols for spectral radiometric quantities are formed by adding subscripts λ , ν , or $\bar{\nu}$, respectively, referring to where the quantities are to be evaluated. For example, H_λ is the irradiance per unit wavelength evaluated at wavelength λ . Typical units would be $\text{W cm}^{-2} \mu^{-1}$. The relation between H and H_λ is

$$H = H_\lambda \Delta\lambda \quad \text{or} \quad H_\lambda = \frac{\partial H}{\partial \lambda}$$

where $\Delta\lambda$ is a small wavelength interval about λ .

Table 2-3 is a list of the most commonly used physical constants for infrared physics. The standard symbols for the constants is also given. A complete list and discussion are given in Ref. 2.

2-2 RADIATION LAWS

2-2.1 KIRCHHOFF'S LAW

Kirchhoff's Law states that, for any temperature and any wavelength, the emissance of an opaque body in an isothermal enclosure is equal to its absorptance. Thus

$$e(\lambda, T) = a(\lambda, T) \quad (2-1)$$

This law is a consequence of the Conservation of Energy which requires that the energy emitted by the body be equal to the energy absorbed by it under isothermal conditions. Thus

$$W_{\text{emitted}} = eW_{BB} = aW_{BB} = W_{\text{absorbed}} \quad (2-2)$$

For a blackbody, $e = a = 1$ by definition. For real materials emissance depends on the material and the finish (see Table 2-4).

More generally, the Conservation of Energy says that light incident on a surface is either reflected, transmitted, or absorbed. Thus

$$r + t + a = 1 \quad (2-3)$$

For an opaque object, $t = 0$. Therefore

$$r + a = 1 \quad (2-4)$$

Using Kirchhoff's Law, Eq. 2-1 gives

$$r = 1 - e \quad (2-5)$$

for an opaque object.

*Written by M. L. Bhaumik and M. A. Levine

TABLE 2-1. STANDARD SYMBOLS

SYMBOL	NAME	TYPICAL UNITS
<i>a</i>	absorptance	%
<i>A</i>	area	cm ²
<i>BB</i>	blackbody	—
<i>BG</i>	background	—
<i>e</i>	emittance	%
<i>E</i>	photon energy	erg
<i>GB</i>	graybody	—
<i>H</i>	irradiance	w cm ⁻²
<i>J</i>	radiant intensity	w sr ⁻¹
<i>N</i>	radiance	w sr ⁻¹ cm ⁻²
<i>P</i>	power	w
<i>r</i>	reflectance	%
<i>S</i>	line intensity	(absorber content) ⁻¹ cm ⁻¹
<i>T</i>	absolute temperature	°K
<i>t</i>	transmittance	%
<i>U</i>	energy	J
<i>u</i>	energy density	J cm ⁻³
<i>V</i>	volume	cm ³
<i>W</i>	radiant emittance (flux density)	w cm ⁻² , (J sec ⁻¹ cm ⁻²)
<i>w</i>	absorber content	“atm-cm”, “pr-cm”
<i>α</i>	absorbtivity	cm ⁻¹
<i>ε</i>	emissivity	%
<i>λ</i>	wavelength	cm
<i>ν</i>	frequency	Hz, (sec ⁻¹)
<i>$\bar{\nu}$</i>	wavenumber	cm ⁻¹
<i>ρ</i>	density	g cm ⁻³
<i>τ</i>	transmissivity	cm ⁻¹
<i>Ω</i>	solid angle	sr (steradian)

TABLE 2-2. BASIC RADIOMETRIC TERMS

TERM	DEFINITION
Absorber content	The equivalent pathlength through a gaseous absorber (par. 2-4)
Absorptance	The fraction of irradiance that is absorbed by a sample placed in the path of the incident light
Absorptivity	The absorptance per unit pathlength through a material
Blackbody	An ideal radiator or absorber with unit emissivity
Emissance	The fraction of radiant emittance of a real surface relative to a blackbody surface
Emissivity	The fraction of radiant emittance of an ideal surface (opaque, optically smooth, flat) relative to a blackbody surface
Energy density	The energy per unit volume contained in the electromagnetic fields
Graybody	A radiator or absorber with constant emissivity less than one; i.e., $\epsilon_{GB} < 1$ for all λ
Irradiance	The power per unit area incident upon a surface
Point source	A radiating surface both characteristic dimensions of which are small compared with the source-to-observer distance
Power	Energy per unit time
Radian	The unit of angular measure, which is the angle for which the subtended arc length of a circle is equal to the radius of the circle (Fig. 2-1)
Radiance	Radiant power per unit solid angle per unit area of source projected normal to the solid angle
Radiant emittance	The power per unit area, or the energy per unit time per unit area, radiated from a surface. Radiant emittance is an energy flux.
Radiant intensity	Radiant power per unit solid angle from a point source
Reflectance	The fraction of irradiance that is reflected from a real surface
Reflectivity	The fraction of irradiance that is reflected from an ideal surface (perfectly smooth and flat)
Steradian	The unit of solid angular measure, being the subtended surface area divided by the radius squared for a solid angle at the center of a sphere (Fig. 2-2)
Transmittance	The fraction of irradiance that is transmitted through a sample placed in the path of the incident light
Wavelength	The distance between two successive crests in the electromagnetic field of light traveling through a vacuum
Wavenumber	Reciprocal of wavelength in centimeters. Wavenumbers are proportional to the photon energy of the light ($E = hc\bar{\nu}$) where $\bar{\nu} = 1/\lambda$.

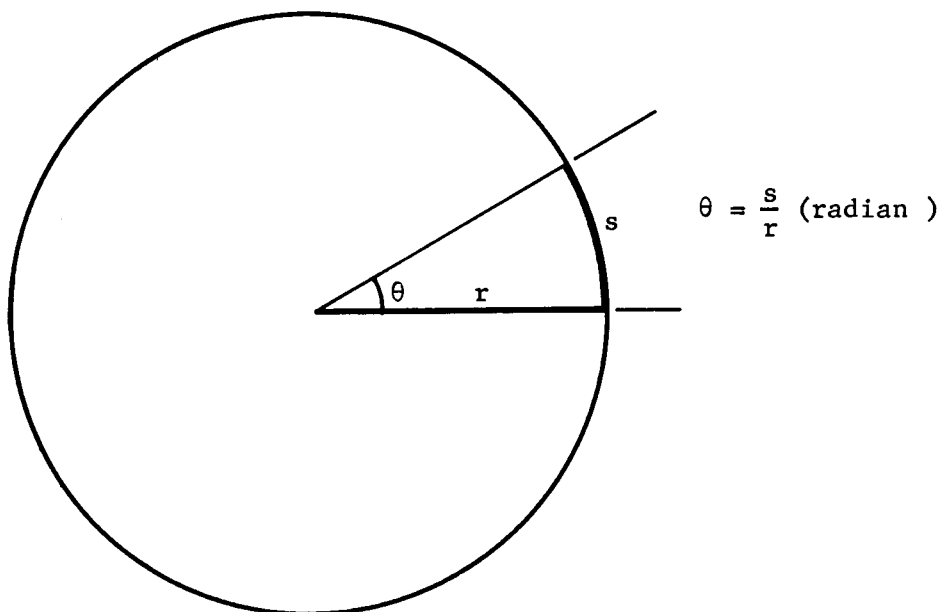


FIGURE 2-1. Angle θ in Radians

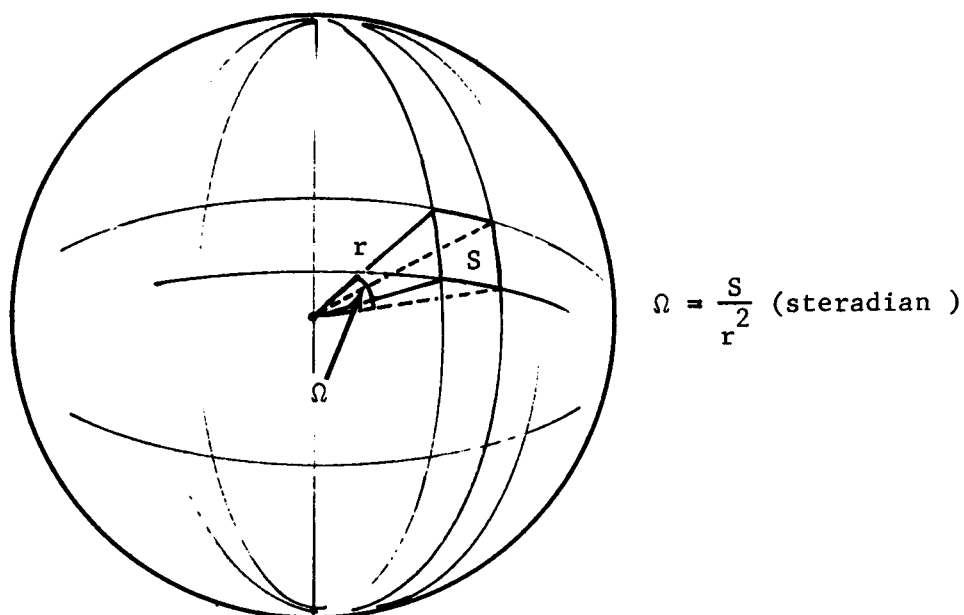


FIGURE 2-2. Solid Angle Ω in Steradians

TABLE 2-3. PHYSICAL CONSTANTS

Planck's constant	h	$6.6256 \times 10^{-34} \text{ w sec}^2$
Speed of light	c	$2.9979 \times 10^{10} \text{ cm sec}^{-1}$
Boltzmann's constant	k	$1.3805 \times 10^{-23} \text{ w sec } ^\circ\text{K}^{-1}$ $8.617 \times 10^{-5} \text{ eV) } ^\circ\text{K}^{-1}$
Stefan-Boltzmann constant	σ	$5.6697 \times 10^{-12} \text{ w cm}^{-2} \text{ } ^\circ\text{K}^{-4}$ $1.354 \times 10^{-12} \text{ cal sec}^{-1} \text{ cm}^{-2} \text{ } ^\circ\text{K}^{-4}$ $3.658 \times 10^{-11} \text{ w in.}^{-2} \text{ } ^\circ\text{K}^{-4}$
Wein's constant	a	$0.28978 \text{ cm } ^\circ\text{K}$
Electronic charge	e	$1.6021 \times 10^{-19} \text{ C}$
Capacivity of vacuum	ϵ_o	$8.8543 \times 10^{-12} \text{ F m}^{-1}$
Permeability of vacuum	μ_o	$4\pi \times 10^{-7} \text{ H m}^{-1}$
Electron mass	m_e	$9.109 \times 10^{-28} \text{ g}$
Proton mass	m_p	$1.673 \times 10^{-24} \text{ g}$
Avogadro's number	N_A	$6.023 \times 10^{23} \text{ per g mole}$
<hr/>		
1 electron volt	=	$1.602 \times 10^{-19} \text{ w sec}$
Energy of 1°K	=	$8.617 \times 10^{-5} \text{ eV)$
λ (1 eV)	=	1.24μ

2-2.2 PLANCK'S LAW

The spectral energy flux, or spectral radiant emittance W_λ from a blackbody was derived empirically by Planck⁸ who had to postulate that radiation consisted of discrete quanta of energy hc/λ in order to fit a smooth curve to the experimentally measured spectral distributions of radiant emittance from blackbodies. The expression he derived was

$$W_\lambda = \frac{C_1}{\lambda^5} \left[\frac{1}{e^{C_2/(\lambda T)} - 1} \right], \text{ w cm}^{-3} \quad (2-6)$$

The constants are

$$C_1 = 2\pi c^2 h = 3.7415 \times 10^{-12} \text{ w cm}^2$$

$$C_2 = hc/k = 1.4388 \text{ cm } ^\circ\text{K}$$

c = speed of light

h = Planck's constant

k = Boltzmann's constant

λ = wavelength, cm

A plot of W_λ vs λ will result in the familiar blackbody radiation curves for various temperatures (Fig. 2-3).

2-2.3 RAYLEIGH-JEANS LAW

For long wavelengths (far IR) at not too low a temperature,

$$hc/\lambda kT \ll 1 \quad (2-7)$$

which permits the exponential to be expanded in a power series. Thus

$$W_\lambda = 2\pi ckT/\lambda^4 \quad (2-8)$$

which is the Rayleigh-Jeans Law. Notice that it does not depend on h and therefore is not of quantum mechanical origin.

TABLE 2-4. EXPERIMENTAL VALUES OF EMISSIVITY*

MATERIAL	300°K RADN. ON 78°K SURFACE ³	ROOM TEMP. ⁴	14 μ RADN. ON 2°K POLISHED SURFACE ⁵	293°K RADN. ON 90°K SURFACE ⁶	273°K RADN. ON 77°K SURFACE ⁷
Al-clean polished foil	0.02	0.04	0.011	0.055	0.043
Al-plate	0.03				
Al-highly oxidized		0.31			
Brass-clean polished	0.029	0.03	0.018	0.046	0.10
Brass-highly oxidized		0.6			
Cu-clean polished	0.015-0.019	0.02	0.0062-0.015	0.019-0.035	
Cu-highly oxidized		0.6			
Cr-plate	0.08	0.08		0.065	0.084
Au-foil	0.010-0.023	0.02-0.03		0.026	
Au-plate	0.026				
Monel		0.2			0.11
Ni-polished		0.045			
Rh-plate	0.078				
Ag-plate	0.008	0.02-0.03		0.023-0.036	
Stainless steel	0.048	0.074			
Sn-clean foil	0.013	0.06	0.013	0.038	
Soft solder	0.03				0.047
Glass		0.9		0.87	
Wood's metal					0.16

* Note: Reference is made in column heads to references listed at end of Chapter 2.

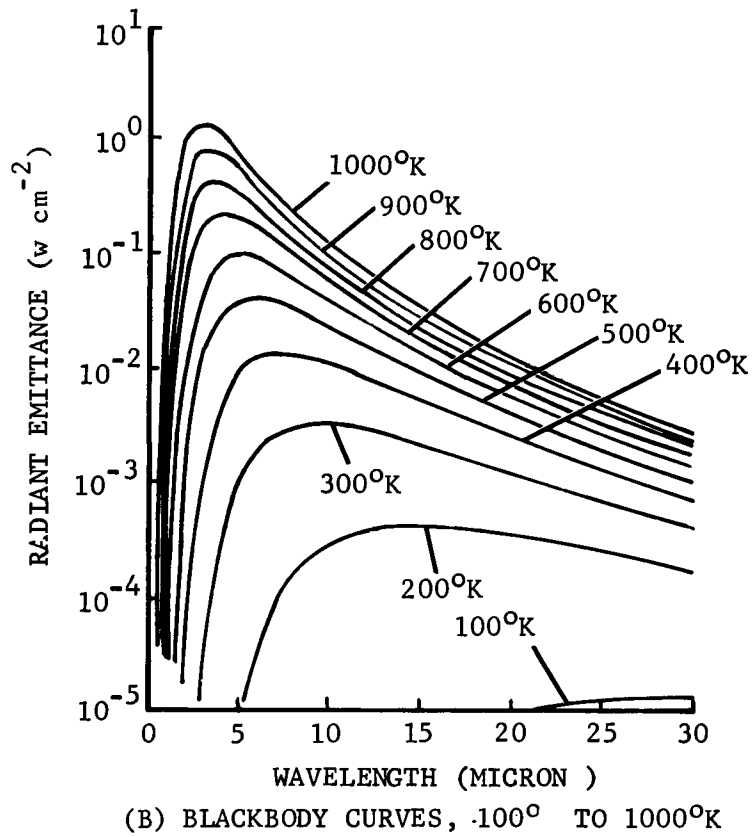
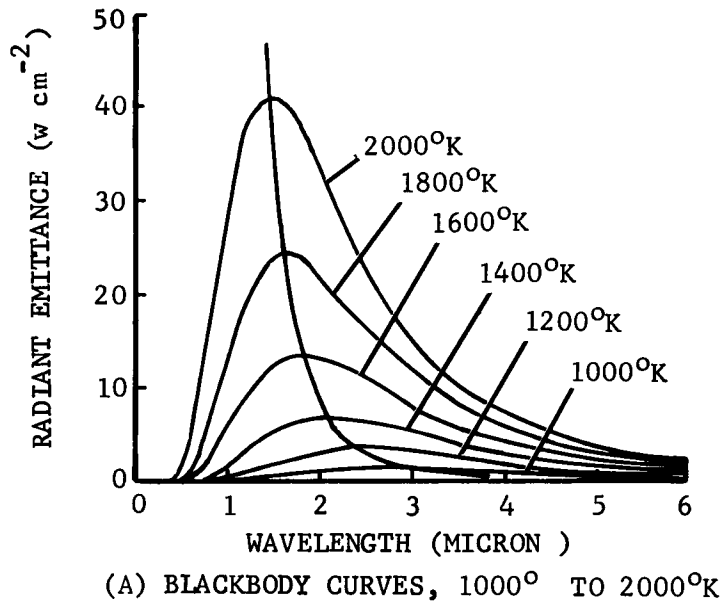


FIGURE 2-3. Blackbody Curves

2-2.4 WIEN'S LAW

For short wavelengths,

$$hc/\lambda kT \gg 1, \quad (2-9)$$

hence Planck's Law reduces to

$$W_\lambda = \frac{2\pi c^2 h}{\lambda^5} \exp \left[-hc/(\lambda kT) \right] \quad (2-10)$$

which is known as Wien's Law.

2-2.5 STEFAN-BOLTZMANN LAW

The radiant emittance from a blackbody W_{BB} can be obtained by integrating Eq. 2-6 over all wavelengths. Thus

$$W_{BB} = \int_0^\infty W_\lambda d\lambda = \left(\frac{2\pi^5 k^4}{15 h^3 c^2} \right) T^4 = \sigma T^4 \quad (2-11)$$

which is the Stefan-Boltzmann Law. The Stefan-Boltzmann constant σ for various units is listed in Table 2-3.

2-2.6 WIEN'S DISPLACEMENT LAW

The maximum value of W_λ occurs at some λ called λ_{max} . W_λ in Eq. 2-6 is of the form

$$W_\lambda = \lambda^{-5} f(\lambda T). \quad (2-12)$$

Setting

$$\left. \frac{d W_\lambda}{d \lambda} \right|_{\lambda = \lambda_{max}} = 0 \quad (2-13)$$

gives

$$\lambda_{max} T = \frac{5}{\left. \frac{d [\ln f(\lambda T)]}{d (\lambda T)} \right|_{\lambda = \lambda_{max}}} \quad (2-14)$$

For a given temperature T , evaluating λ at λ_{max} is equivalent to evaluating λT at $\lambda_{max} T$. Hence

$$\lambda_{max} T = \frac{5}{\left. \frac{d [\ln f(\lambda T)]}{d (\lambda T)} \right|_{\lambda_{max} T}} = a \quad (2-15)$$

where a is a constant. Eq. 2-15 is Wien's Displacement Law. Solving the transcendental equation numerically for $\lambda_{max} T$ gives $a = 0.2898 \text{ cm } ^\circ\text{K}$.

2-3 RADIANT ENERGY TRANSMISSION

2-3.1 RADIANT INTENSITY FROM A POINT SOURCE

A point source is a radiator all the dimensions of which are small compared to the source-to-observer distance. There are two basic types, the isotropic point source and the Lambertian point source.

2-3.1.1 Isotropic Point Source

The isotropic point source radiates uniformly in all directions, thus the radiant intensity J is

$$J = \frac{P}{4\pi}, \text{ w sr}^{-1} \quad (2-16)$$

where P is the total power radiated by the source.

Geometrically, the importance of an isotropic point source is that it presents the same radiating area to the viewer when looked at from any direction. It is assumed, of course, that the source, being small, has a uniform temperature.

2-3.1.2 Lambertian Point Source

A Lambertian "point" source is flat and does not present the same area to the viewer from all directions. Since the color does not change with the position of the viewer, he must assume that the radiant emittance is proportional to the apparent, or projected, area of the source. Thus

$$J = \frac{dP}{d\Omega} = kWA \cos \theta \quad (2-17)$$

where A is the area of the source, θ is the angle of the viewer with respect to the normal, and k is a proportionality constant (Fig. 2-4(A)). Integrating Eq. 2-17 over a hemisphere above the plane of dA (Fig. 2-4(B)) one gets the total radiated power

$$P = \int_{\text{hemisphere}} kWA \cos \theta \, d\Omega \quad (2-18)$$

$$= kWA \int_0^{\frac{\pi}{2}} \cos \theta (2\pi \sin \theta \, d\theta) = (\pi k)WA$$

Since $P = WA$, therefore $k = \pi^{-1}$. Thus

$$J = \frac{WA \cos \theta}{\pi}, \text{ w sr}^{-1} \quad (2-19)$$

This is called Lambert's Law.

2.3.2 RADIANT ENERGY DENSITY

Radiant energy density is the quantity of radiant energy per unit volume.

2.3.2.1 Energy Density for Collimated Irradiance

Collimated irradiance means that the flow of radiant energy is neither divergent nor convergent. Hence the energy flow down a tube of cross section dA is uniform and the energy density is constant. Therefore, for a tube of length ct , where t is the length of time during which energy entered the tube, and c is the speed of light,

$$u = \frac{U}{V} = \frac{HtdA}{ctdA} = \frac{H}{c} \quad (2-20)$$

Thus the irradiance on any cross section of the tube is

$$H = uc \quad (2-21)$$

This is also the radiant emittance from the same cross section.

2.3.2.2 Energy Density Within an Isothermal Enclosure

The temperature within an isothermal enclosure is a constant. Therefore the energy flux uc is a constant regardless of direction. Otherwise, there would be a net transfer of energy along some direction indicating a temperature difference somewhere. Therefore a calculation of the energy density next to a wall of the enclosure is sufficient.

The radiant emittance is given by

$$dW = \left(\frac{1}{2}u\right)c \frac{d\Omega}{4\pi} \quad (2-22)$$

The factor $1/2$ is because half the energy density is from irradiance and half from emittance as noted above. Integrating Eq. 2-22 over the hemisphere of Fig. 2-4(B) gives

$$W = \frac{uc}{4} \quad (2-23)$$

Thus the energy density within an isothermal enclosure is

$$u = \frac{4W}{c} \quad (2-24)$$

As an example, consider a 300°K isothermal enclosure.

$$\begin{aligned} u &= \frac{4W}{c} = \frac{4\sigma T^4}{c} = \frac{4 \times 5.67 \times 10^{-12} \times (300)^4}{3 \times 10^{10}} \\ &= 6.1 \times 10^{-12} \text{ J cm}^{-3} \end{aligned}$$

As a second example, consider the energy density above the earth's atmosphere due to the sun. The solar irradiance is about 0.13 w cm^{-2} and is nearly collimated. Therefore

$$u = \frac{H}{c} = \frac{0.13}{3 \times 10^{10}} = 4.3 \times 10^{-12} \text{ J cm}^{-3}$$

2.3.3 TRANSFER OF RADIANT POWER

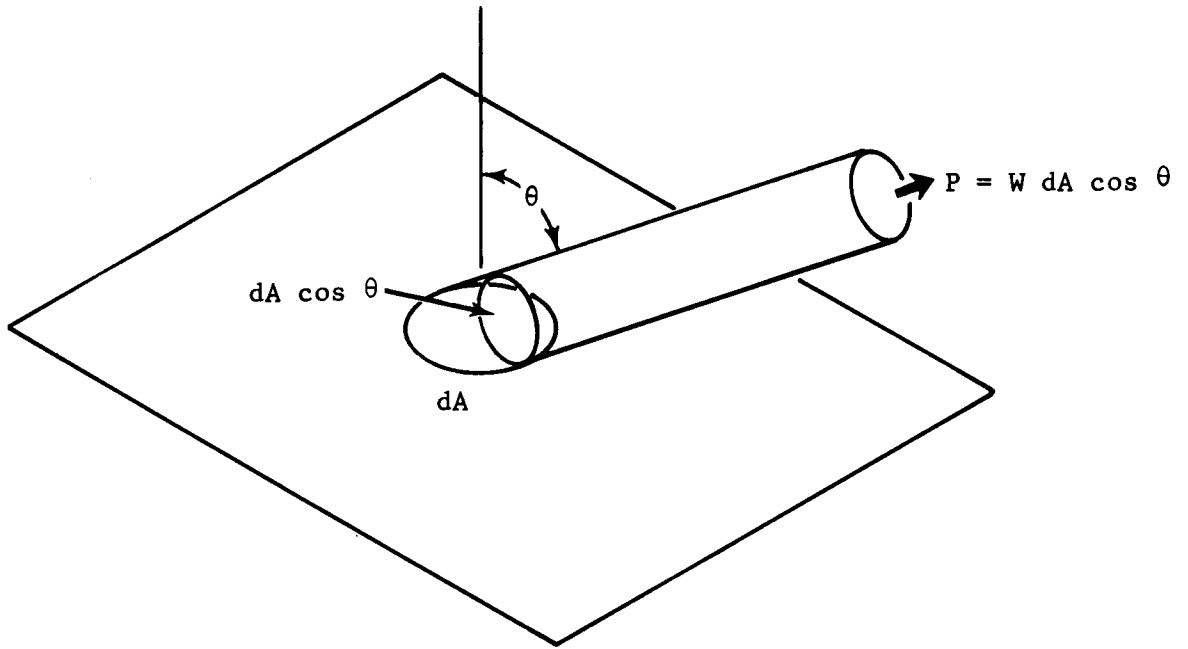
2.3.3.1 An Object in Space

An object in space receives energy from warm celestial bodies and radiates energy into space. Space can be considered a perfect absorber with no emittance, i.e., space is cold. Therefore, for a uniformly painted metal plate suspended in space near the earth and normal to the sun, the incident energy is $eA \times 0.13 \text{ w cm}^{-2}$, neglecting radiation from other sources. The emitted energy is $2eA\sigma T^4$, where the 2 occurs because both sides of the plate emit. Thus, at equilibrium,

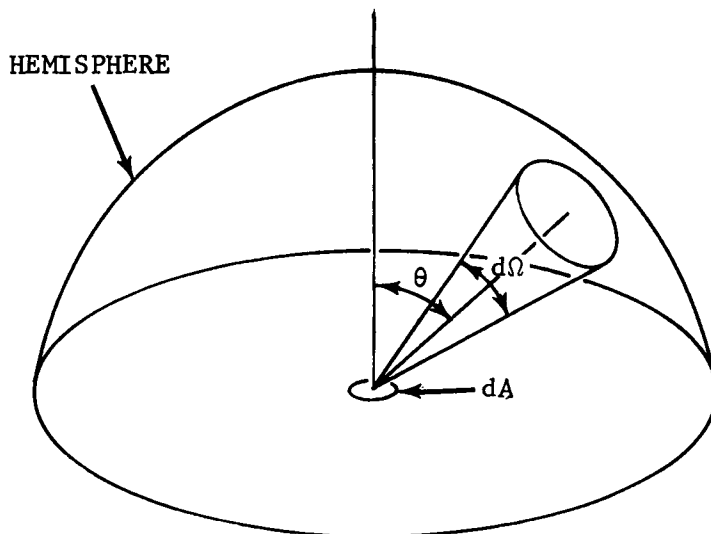
$$\begin{aligned} eA \times 0.13 &= 2eA\sigma T^4 \\ 0.13 &= 2 \times 5.67 \times 10^{-12} \times T^4 \\ T &= 327^\circ\text{K} \end{aligned}$$

If one side of the plate is black ($e = 1$) and the other is unpainted ($e = 0.1$) then, with the black side facing the sun,

$$\begin{aligned} 1 \times A \times 0.13 &= (1 + 0.1) A\sigma T^4 \\ 0.13 &= 1.1 \times 5.67 \times 10^{-12} \times T^4 \\ T &= 380^\circ\text{K} \end{aligned}$$



(A)



(B)

FIGURE 2-4. Geometry of a Lambertian Source

With the shiny side facing the sun,

$$\begin{aligned} 0.1 \times A \times 0.13 &= (1 + 0.1) A \sigma T^4 \\ 0.013 &= 1.1 \times 5.67 \times 10^{-12} \times T^4 \\ T &= 213^\circ \text{K} \end{aligned}$$

2-3.3.2 Transfer Between Two Infinite Planes

For two opaque plane-parallel infinite surfaces with emissances e_1 and e_2 and temperatures $T_2 > T_1$, one can calculate the *net* radiant emittance $W_{2 \rightarrow 1}$ from surface 2 to surface 1. Surface 2 has a radiant emittance $e_2 \sigma T_2^4$. Of that emittance $e_1 e_2 \sigma T_2^4$ is absorbed by surface 1 and $(1 - e_1) e_2 \sigma T_2^4$ is reflected. Then $(1 - e_2)(1 - e_1) e_2 \sigma T_2^4$ is reflected back toward surface 1. Of that radiant emittance, $e_1(1 - e_2)(1 - e_1) e_2 \sigma T_2^4$ is absorbed, etc. Thus

$$W_{2 \rightarrow 1} = \sigma T_2^4 \left[e_1 e_2 + e_1(1 - e_2)(1 - e_1) e_2 + e_1(1 - e_2)^2(1 - e_1)^2 e_2 + \dots \right] \quad (2-25)$$

Summing the series gives

$$W_{1 \rightarrow 2} = \sigma T_2^4 \left[\frac{e_1 e_2}{1 - (1 - e_1)(1 - e_2)} \right] \quad (2-26)$$

Similarly,

$$W_{1 \rightarrow 2} = \sigma T_1^4 \left[\frac{e_1 e_2}{1 - (1 - e_1)(1 - e_2)} \right] \quad (2-27)$$

Therefore $W_{2 \rightarrow 1}$ is given by

$$W_{2 \rightarrow 1} = W_{2 \rightarrow 1} - W_{1 \rightarrow 2} = \sigma(T_2^4 - T_1^4) \left[\frac{e_1 e_2}{1 - (1 - e_1)(1 - e_2)} \right] \quad (2-28)$$

A more extensive study of the transfer of radiant power is given in Ref. 4.

As an example, consider a black plate ($e_1 = 1$) at 2°K facing an electropolished copper plate ($e_2 = 0.01$) at 4°K . The net radiant emittance from the warmer copper plate to the cooler black plate is

$$W_{2 \rightarrow 1} = \frac{5.67 \times 10^{-12} (4^4 - 2^4) \times 1 \times 0.01}{1 - (0)(0.99)} = 1.36 \times 10^{-11} \text{ w cm}^{-2}$$

Note that the commonly accepted formula,

$$W_{2 \rightarrow 1} = \sigma(e_2 T_2^4 - e_2 T_1^4), \text{ yields}$$

$$W_{2 \rightarrow 1} = -7.6 \times 10^{-11} \text{ w cm}^{-2} \quad \text{indicating that the cooler plate is heating up the warmer one.}$$

2-3.4 IRRADIANCE AS A FUNCTION OF RANGE

2-3.4.1 Point Source

A small receiving area dA is oriented normal to the line of sight at a distance R from a point source. It subtends a solid angle $d\Omega = dA/R^2$. From the definition of radiant intensity J as the power radiated per unit solid angle from a point source, the power incident on the receiving area is

$$dP = Jd\Omega = J \left(\frac{dA}{R^2} \right) \quad (2-29)$$

and the power per unit area is the irradiance H given by

$$H = \frac{dP}{dA} = \frac{J}{R^2} \quad (2-30)$$

As an example, consider the irradiance at 400 cm from a 2 cm radius sphere with emittance $W = 3 \text{ w cm}^{-2}$ if the receiving area is slanted 60° to the line-of-sight.

$$H = \frac{J dA/R^2}{dA/\cos \theta} = \frac{J \cos \theta}{R^2} = \frac{WA_{\text{source}} \cos \theta}{4\pi R^2}$$

Thus,

$$H = \frac{3 \times 4\pi \cdot 2^2 \times \frac{1}{2}}{4\pi(400)^2} = 3.75 \times 10^{-5} \text{ w cm}^{-2}$$

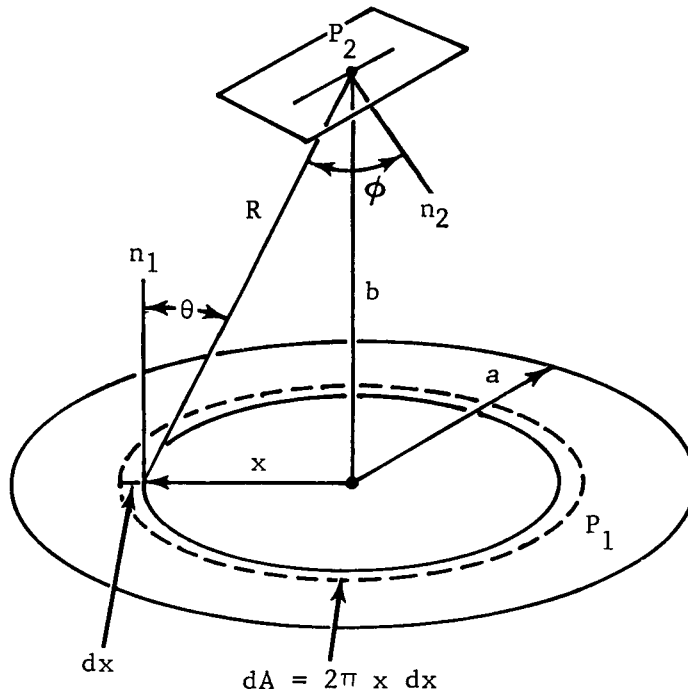
2-3.4.2 Extended Source

The concept of radiant intensity cannot be usefully applied to an extended source (one that subtends a finite solid angle to the viewer). However, in calculating irradiance H the extended source is divided into elemental areas dA and an expression is obtained for the radiant intensity of each. Contributions from each elemental source area to the irradiance are then integrated to obtain the total irradiance.

If θ is the angle between the line of sight and the normal n_1 to one of these small areas, and ϕ is the angle between the line of sight and the normal n_2 to the surface at which the irradiance is being determined, the irradiance is calculated as

$$H = \int_A \frac{dJ}{R^2} \cos \phi = \int_A \frac{W dA \cos \theta}{\pi R^2} \cos \phi \quad (2-31)$$

For example, assume that a plane circular area P_1 of radius a has an emittance W . What is the irradiance at a point located on the axis of the circle at a distance b , in the plane P_2 parallel to the source:



Since the receiving surface is parallel to the emitting surface, $\theta = \phi$. The elemental area consisting of an annular ring of diameter x and width dx has an area $dA = 2\pi x dx$ therefore

$$H = \int_0^a \frac{W}{\pi} \cos^2 \theta \frac{2\pi x dx}{x^2 + b^2}$$

$$= W \int_0^a \left[\frac{b^2}{(x^2 + b^2)} \right] \frac{2x dx}{(x^2 + b^2)} \quad (2-32)$$

Let $y = x^2 + b^2$; then $dy = 2x dx$. When $x = 0$, $y = b^2$; when $x = a$, $y = a^2 + b^2$. The integral becomes

$$H = W \int_{b^2}^{a^2 + b^2} \frac{b^2 dy}{y^2} = \left[-\frac{Wb^2}{y} \right]_{b^2}^{a^2 + b^2}$$

$$= W \left(1 - \frac{b^2}{a^2 + b^2} \right) = W \left(\frac{a^2}{a^2 + b^2} \right) \quad (2-33)$$

In the case where the receiving surface is very close to the emitting surface ($b \ll a$), $H = W$ which simply illustrates that all the radiation emitted by unit area of the source passes through unit area of the receiver. At the opposite extreme, where $b \gg a$

$$H = \frac{Wa^2}{b^2} = \frac{WA}{\pi R^2} \quad (2-34)$$

Using Eq. 2-19 with $\theta = 0$ gives

$$H = \frac{J}{R^2} \quad (2-35)$$

which is the same as Eq. 2-30 as expected.

2-3.5 CALCULATION AIDS

Since equations such as Planck's are difficult to use directly in actual calculations, several devices have been specifically devised. These include, in order of increasing accuracy, nomographs, radiation slide rules, blackbody tables, or computer storage data.

Nomographs are multi-scaled graphs designed so that a straight line drawn through a known point on each of two scales will provide an unknown's value on a third scale (Ref. 9, p. 20). Nomographs are not used extensively because of their inherent inaccuracy.

The General Electric Radiation Calculator (Ref. 1, pp. 11-17) is the most commonly used of various radiation slide rules. Radiation slide rules are sufficiently accurate for preliminary design calculations.

Blackbody data (Ref. 1, p. 21) are available for use in calculating more precise values than are possible with slide rules, but these data tables are more difficult to use.

Precise radiometric calculations require the use of highly accurate computerized data and direct, conventional calculation methods.

2-3.5.1 Use of GE Radiation Calculator

Many of the blackbody expressions given in

pars. 2-2 and 2-3 can be calculated by means of a special slide rule such as the General Electric Radiation Calculator shown in Fig. 2-5. At a single setting, the following data can be read:

INDEX TEMPERATURE

- (1) CENTIGRADE
- (2) KELVIN
- (3) FAHRENHEIT
- (4) RANKINE

$$\begin{aligned} &^{\circ}\text{C} \\ &^{\circ}\text{K} = ^{\circ}\text{C} + 273 \\ &^{\circ}\text{F} = (^{\circ}\text{C} + 40) \frac{9}{5} - 40 \\ &^{\circ}\text{R} = ^{\circ}\text{F} + 460 \end{aligned}$$

RADIANT EMITTANCE

- (5) w = WATTS/SQ CM
- (6) WATTS/SQ IN.
- (7) BTU/SQ FT/HR

Total emittance, $W_{0-\infty}$ for various emissivities (emissances) and in various units

SPECTRAL EMITTANCE

- (8) $W_{\lambda_{max}} = \text{WATTS/SQ CM/MICRON}$
 $\Delta\lambda$ AT MAXIMUM
- (9) $\frac{W_{\lambda}}{W_{\lambda_{max}}}$ vs λ
- (10) $\frac{W_{0-\lambda}}{W_{0-\infty}}$ vs λ
- (11) MAX vs λ

Spectral emittance at λ_{max} with $e = 1$.

Multiplying (8) by (9) gives spectral emittance at λ with $e = 1$.

Multiplying (5), (6) or (7) by (10) gives $\int_0^{\lambda} W_{\lambda} d\lambda$ for any given emissivity used in (5), (6) or (7). Wavelength λ_{max} at which W_{λ} is a maximum. (Note: This is maximum energy flux per unit wavelength interval. It is *not* maximum photon flux per unit wavelength interval.)

This scale converts λ_{max} to $\bar{\nu}_{max} = \lambda_{max}^{-1}$.

- (12) WAVES/CENTIMETER

IRRADIANCE

- (13) INCIDENT ENERGY IN WATTS/CM²
FOR 1 CM² SOURCE AT INDEX
TEMPERATURE
vs
RANGE (CENTIMETERS)
(NAUTICAL MILES)
- (14) TRANSMISSION SPECTRA OF THE
ATMOSPHERE 2000 YD (1 SEA MILE)
OF 17 MM PRECIPITABLE WATER

Multiply (11) by source area (cm²) to find irradiance H at ranges from 1 meter to 1000 nautical miles.

Transmission coefficient t vs wavelength λ over 1 nautical mile horizontally at approximately 80% relative humidity, 80°F. This graph is independent of index temperature setting.

PHOTON EMITTANCE

- (15) PHOTONS/SEC/CM²
- (16) PHOTON ENERGY AT λ_{max} IN
ELECTRON VOLTS

Total photon flux for a blackbody at index temperature.

$$E = \frac{hc}{\lambda_{max}} \text{ in electron-volts.}$$

There is also a C, D scale slide rule for simple calculations.

RADIATION CALCULATOR

courtesy of
LIGHT MILITARY ELECTRONICS
DEPARTMENT
GENERAL ELECTRIC
UTICA, N. Y.

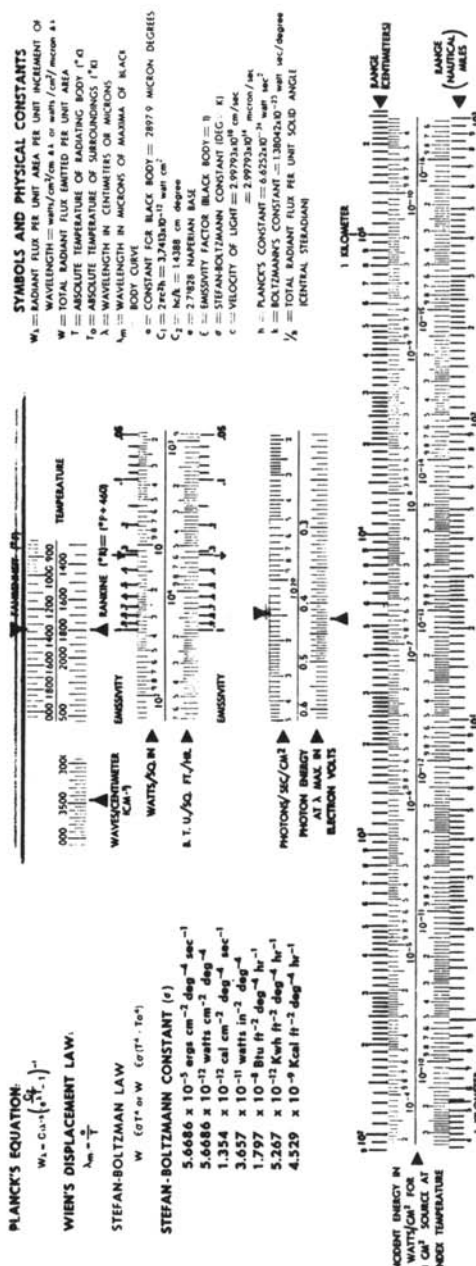
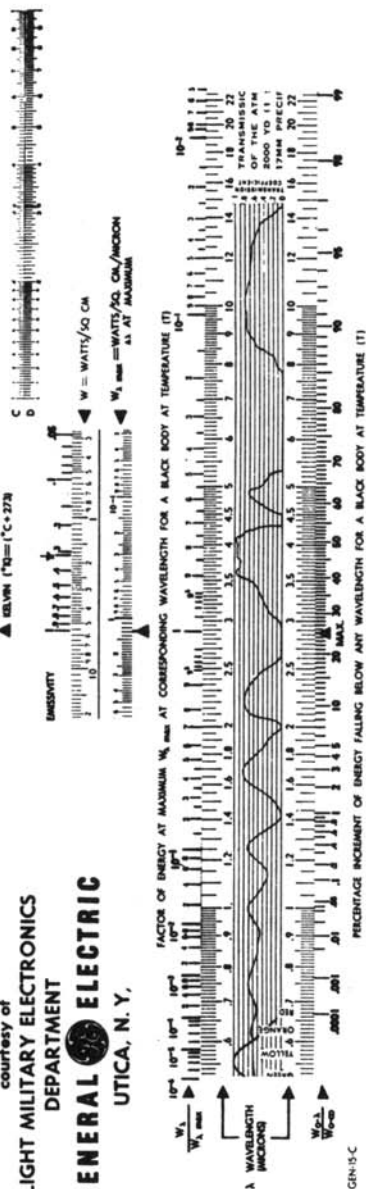


FIGURE 2-5. The GE Radiation Calculator

2-3.5.2 Sample Calculations

The following sample problems are stated and solved by direct calculation or by using the GE Radiation Calculator.

Example 1

Setup: A blackbody being used for testing is set to a temperature of 1000°C. (A blackbody aperture of 0.6 in. dia (approx. $2/\pi$ in. dia) is assumed.)

Problem A: Calculate the radiant emittance of the blackbody.

1. Solution (by direct calculation):

a. Convert °C to °K:

$$1000^{\circ}\text{C} = 1000 + 273 \\ = 1273^{\circ}\text{K}$$

b. Using the formula for the Stefan-Boltzmann Law:

$$W = \sigma T^4 \\ = 5.67 \times 10^{-12} \times (1273)^4$$

Answer: $W = 14.9 \text{ w cm}^{-2}$

2. Solution (using the GE Radiation Calculator):

Align CENTIGRADE pointer of TEMPERATURE scale with 1000 scale indicating $W = \text{WATTS/SQ CM}$. Since the radiation source is a blackbody, read the indication at 1 on the EMISSIVITY scale.

Answer: $W = 14.9 \text{ w cm}^{-2}$

Problem B: Calculate the radiant power of the source.

Solution (by direct calculation):

a. Convert aperture size in inches to area in cm^2 .

$$A = \pi r^2 \\ = \pi \left(\frac{1}{\pi}\right)^2 \\ A = \frac{1}{\pi} \text{ sq in.}$$

$$\text{Since } 1 \text{ sq in.} = 6.45 \text{ cm}^2$$

$$A = 2.05 \text{ cm}^2$$

b. Using the formula for radiant power as a function of radiant emittance:

$$P = WA \text{ (all other factors remaining constant)} \\ = 14.9 \text{ w cm}^{-2} \times 2.05 \text{ cm}^2$$

Answer: $P = 30.6 \text{ w}$

Problem C: Calculate the spectral radiant emittance W_{λ} in the wavelength interval between 2.5 and 3 μ .

1. Solution (by direct calculation):

Determine the total amount of radiant energy falling below each wavelength by integrating Planck's equation over the interval $\lambda = 0$ to each given wavelength ($\lambda = 2.5$ or $\lambda = 3.0$). The answer is the difference between the two radiant quantities.

2. Solution (using the GE Radiation Calculator):

Set the CENTIGRADE pointer of the TEMPERATURE scale to 1000°C position. Observing the $\frac{W_{0-\lambda}}{W_{0-\infty}}$ scale which

indicates the "Percentage increment, of energy falling below any wavelength for a blackbody at temperature T ", note that 45 percent falls below 3 μ and 31.5 percent falls below 2.5 μ .

Since the total energy = 14.9 w cm^{-2}

$$W_{\lambda} = 14.9 \times (0.450 - 0.315) \\ = 14.9 \times 0.135$$

Answer: $W_{\lambda} = 2.00 \text{ w cm}^{-2}$ (approx.)

Problem D: Determine the wavelength at the point of peak radiation of the 1000°C source.

1. Solution (by direct calculation):

Using Wien's Displacement Law:

$$\lambda_{max} = \frac{2897}{T(^{\circ}\text{K})} \\ = \frac{2897}{1273}$$

Answer: $\lambda_{max} = 2.27 \mu$

2. Solution (using the radiation calculator):

Retain TEMPERATURE at the same setting. Read MAX point on $\frac{W_{0-\lambda}}{W_{0-\infty}}$ scale.

$$\lambda_{max} = 2.27 \mu$$

Example 2

Setup: An oxidized steel graybody is heated to 2000°K.

Problem: Calculate the radiant emittance of the object.

1. Solution 1 (by direct calculation):

a. Calculate the blackbody emittance of 2000°K using the Stefan-Boltzmann Law.

$$W = \sigma T^4 \\ W = 90.8 \text{ w cm}^{-2}$$

- b. Using emissance tables, determine the emissance of oxidized steel. (e of oxidized steel ≈ 0.8).

- c. Transpose the formula for emissance:

$$e = \frac{W}{W_{BB}} \text{ to } W = e W_{BB}$$

$$= 0.8 \times 90.8$$

$$W = 72.6 \text{ w cm}^{-2}$$

Solution 2 (using the radiation calculator):

Set the KELVIN pointer to the 2000° position. The radiant emittance at the 0.8 position of the EMISSIVITY (emissance) scale is approximately 72 w cm⁻².

Example 3

Setup: The irradiance H at a point 5 ft from a radiation source is 20 w cm⁻².

Problem: Determine the irradiance at a point 20 ft from the source (disregarding atmospheric attenuation).

Solution (using the Inverse Square Law):

$$H_2 = H_1 \left(\frac{D_1}{D_2} \right)^2$$

$$= 20 \left(\frac{5}{20} \right)^2$$

$$= 20 \left(\frac{1}{16} \right)$$

$$H_2 = 1.25 \text{ w cm}^{-2}$$

2-4 ATMOSPHERIC TRANSMISSION

In passing through the atmosphere, infrared energy is attenuated before it is detected and measured. The two main causes of attenuation are molecular absorption by several minor constituents of the atmosphere and scattering due to the presence of particles of matter in the atmosphere (aerosols). Molecular absorption occurs mainly in several more or less narrow absorption bands, and is due to the ability of certain molecules to go from one state of vibration-rotation to another, thereby absorbing (or emitting) a photon. In addition, scattering causes attenuation of an incident beam of radiation because in the scattering process the energy is redistributed into all directions of propagation and lost to the observer.

2-4.1 EXTINCTION COEFFICIENT

The spectral transmittance $t(\lambda)$ through a path x of uniform atmosphere is

$$t(\lambda) = \exp [-K(\lambda)x] \quad (2-36)$$

where $K(\lambda)$ is the extinction coefficient at the discrete wavelength λ . $K(\lambda)$ is the sum of the molecular absorption coefficient $\alpha(\lambda)$ and the scattering coefficient $\beta(\lambda)$. Thus Eq. 2-36 can be written as

$$t(\lambda) = \exp \left\{ - [\alpha(\lambda) + \beta(\lambda)]x \right\}$$

$$= \exp [-\alpha(\lambda)x] + \exp [-\beta(\lambda)x] \quad (2-37)$$

The scattering and absorption coefficients, and therefore the extinction coefficient, depend on wavelength, atmospheric density, and the atmospheric composition. Care must be used when applying Eqs. 2-36 or 2-37 since the properties of the atmosphere, and hence its absorption, may change over the path x . To account for these changes, Eq. 2-36 can be written in integral form as

$$t(\lambda) = \exp \left[- \int_{x_1}^{x_2} K_x(\lambda) dx \right] \quad (2-38)$$

If a finite wavelength interval, $\Delta\lambda = \lambda_2 - \lambda_1$, is considered, then the average transmittance t in the interval $\Delta\lambda$ is

$$t = \frac{1}{\lambda_2 - \lambda_1} \int_{\lambda_1}^{\lambda_2} t(\lambda) d\lambda \quad (2-39)$$

Eq. 2-39 implicitly contains Eq. 2-38 and is hard to evaluate exactly. Therefore, various approximations to Eq. 2-39 are used, depending on the wavelength region and attenuating medium considered. In certain cases, either scattering or molecular absorption is negligible, and one need only consider one attenuation process. Since the transmittance due to scattering is a slowly varying function of wavelength, it will often be justified to take that part of the transmittance due to scattering out of the integral and replace it by an average value, especially if the interval $\lambda_1 - \lambda_2$ is small.

2-4.2 MOLECULAR ABSORPTION

2-4.2.1 Absorption Coefficient

Radiation traveling through the atmosphere undergoes attenuation, defined here by absorption coefficient α , which is a function of the wavenumber $\bar{\nu}$ (or wavelength $\lambda = 1/\bar{\nu}$). The transmittance of a beam of light passing through a given amount of absorber w in the atmospheric path is given by

$$t(\bar{\nu}) = \exp [- \alpha(\bar{\nu})w] \quad (2-40)$$

For gases, the units of $\alpha(\bar{\nu})$ and w are unusual. The generic term for the units of w is "absorber content", a unit of length. The simplest absorber content unit is the "atmosphere-kilometer". An atm-km is one kilometer of pathlength through the atmosphere at standard temperature and pressure with the "normal" amount of absorber present—such as O_3 , CO_2 , H_2O , etc. Since "normal" is difficult to ascertain, the atm-km is usually normalized to the "atmosphere-centimeter". The atm-cm is one centimeter of pathlength at standard temperature and pressure (STP) through the absorber alone. For example, "normal" atmospheres contain 3×10^{-4} parts by volume of CO_2 . Thus 1 atm-km of air with the normal amount of CO_2 is equivalent to 30 atm-cm of CO_2 alone.

Water vapor is still further normalized to "precipitable-centimeters". Water vapor in units of precipitable centimeters is the thickness in centimeters of the water along the path if it were condensed to liquid. Thus

$$w(\text{pr-cm}) = (\text{pathlength in cm}) \times [\rho(H_2O \text{ vapor}) \text{ in g cm}^{-3}] \quad (2-41)$$

Water vapor concentration is also found in units of $\text{g}(H_2O)/\text{kg}(\text{air})$ at STP, called mixing ratio. The conversion from g/kg to $\text{pr-cm}(H_2O)/\text{km}(\text{pathlength})$ is

$$\frac{\text{g}(H_2O)}{\text{kg}(\text{air})} = 35.2 \left[\frac{P(\text{atm})}{T(^{\circ}\text{K})} \right] \left[\frac{\text{pr-cm}(H_2O)}{\text{km}(\text{pathlength})} \right] \quad (2-42)$$

The dimensions of α are $(\text{absorber content})^{-1}$ such as $(\text{atm-km})^{-1}$, $(\text{atm-cm})^{-1}$, $(\text{pr-cm})^{-1}$. Note that these are actually units of reciprocal length.

The wavenumber dependence of the absorption coefficient α is extremely complex in the IR. IR absorption bands consist of many narrow

absorption lines each corresponding to a particular transition of the absorbing molecule from one vibration-rotation state to another. Transmission calculations will usually rely on band models which take into account the band structure parameters such as line width, spacing between lines, and line intensities.

There are three basic methods of calculating atmospheric absorption values. The first requires high-resolution spectral data or theoretical calcu-

lations of exact line positions on a high-speed computer^{10,11,12}. Computers are programmed to perform high-resolution transmission calculations which can then be averaged to provide transmission curves for lower resolution. A detailed discussion of this method is contained in Ref. 10. The application of this method to H₂O and CO₂ transmission is described in Refs. 11 and 12. The second method entails estimating, from a theoretical standpoint, the

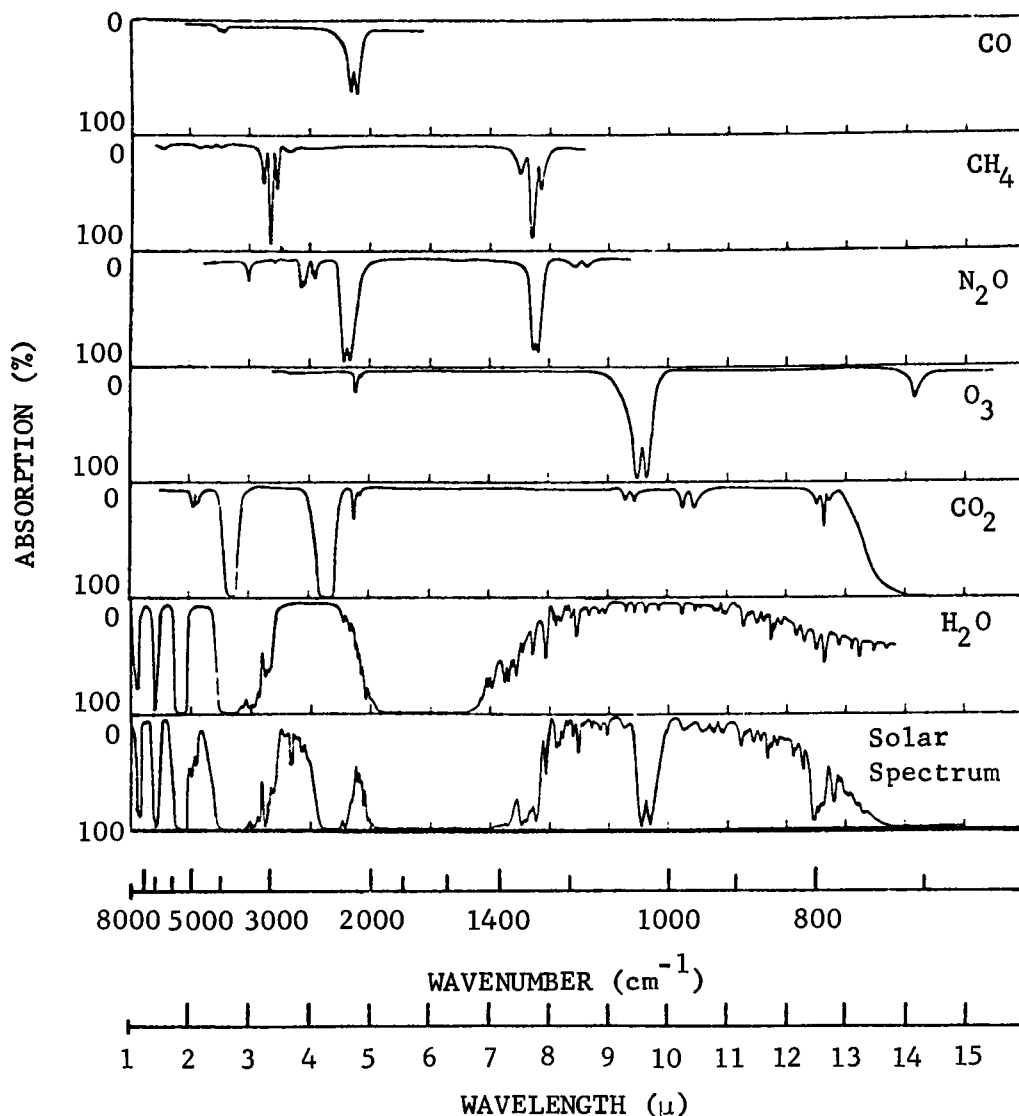


FIGURE 2-6. The Near-infrared Spectra of Solar Irradiation and of CO, CH₄, N₂O, O₃, CO₂, and H₂O

average transmission in a small wavelength interval containing many absorption lines as a function of certain band parameters¹³. The numerical values of the band structure parameters can be determined from experimental observations, and the resultant absorption effects then determined for any path length. This method is particularly useful for estimating medium-resolution ($\Delta\bar{\nu} \times 10$ to 50 cm^{-4}) transmission curves and provides the envelope of the absorption bands rather than their fine structure. The theory behind this method is discussed in par. 2-4.2.3, while the data and its application are considered in par. 2-4.2.4. The third method involves the use of formulas which are derived empirically to fit available data. It is applicable to low resolution systems for which the spectral bandpass completely encompasses one or more molecular bands. These formulas, which can be used to predict transmissions for a wide range of conditions, are also presented in par. 2-4.2.4.

2-4.2.2 Absorber Constituents

Molecular absorption in the atmosphere is primarily due to carbon dioxide (CO_2), water vapor (H_2O), and ozone (O_3). Other minor constituents which also contribute to the absorption include nitrous oxide (N_2O), carbon

monoxide (CO), and methane (CH_4). Fig. 2-6 illustrates the IR transmission characteristics of the atmosphere due to these constituents. Between 14 microns and the microwave region of the spectrum, water vapor is a strong absorber and practically no transmission would be apparent in this region. Ref. 14 surveys the measurements of concentration of the minor absorbing constituents in the atmosphere.

For most problems of practical interest, atmospheric concentrations of CH_4 , CO , N_2O , and CO_2 are assumed to be constant. Small variations of a few percent occur for CO_2 , especially near the ground¹⁵. Concentrations of N_2O , CO , and CH_4 are found to be the most variable (deviations ranging from 50 to 100% are not unusual). However, because of the relatively low density of these minor constituents, the variation does not significantly affect transmission calculations. The concentration of ozone, which is variable, peaks between the altitudes of 20 and 30 km where it is produced through the photodissociation of oxygen by ultraviolet radiation¹⁶. Ozone diffuses and is convected downward by atmospheric turbulence and winds¹⁷. Upon reaching the ground, it reacts upon organic materials. Ozone can also be created near the ground due to various chemical

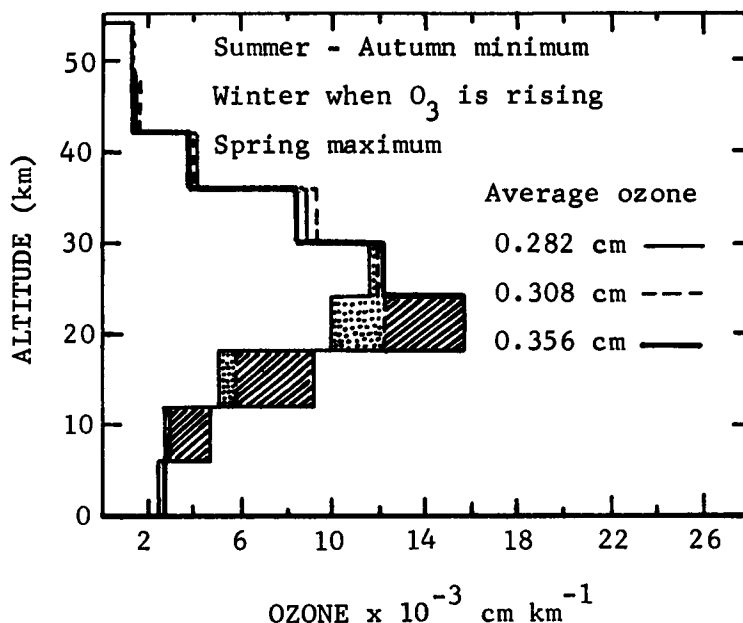


FIGURE 2-7. Seasonal Variation of the Vertical Distribution of Ozone

agents. Typical ozone profiles are shown in Fig. 2-7. Total ozone content depends on latitude and season (Fig. 2-8).

The water vapor concentration is highly variable, especially near the ground. The water vapor profile is closely related to the temperature profile of the atmosphere. These two profiles (temperature and mean H_2O) for the Gutnick¹⁸ standard atmosphere are presented in Fig. 2-9. The third profile included in Fig. 2-9 corresponds to a saturated atmosphere. The water vapor content decreases rapidly with altitude up to the tropopause (≈ 12 km) above which both the temperature and the water vapor

content cease to decrease. Good measurements of water vapor content above the tropopause are difficult to make because this content is so small. It therefore is not surprising that the measurements above the tropopause seldom agree. It is assumed that the volume mixing ratio of water vapor above the tropopause is either constant (dry stratosphere) or increases as the temperature rises (wet stratosphere).

Table 2-5 lists the mean values of absorber concentrations in the atmosphere and the absorber content along a 1 km pathlength at sea level.

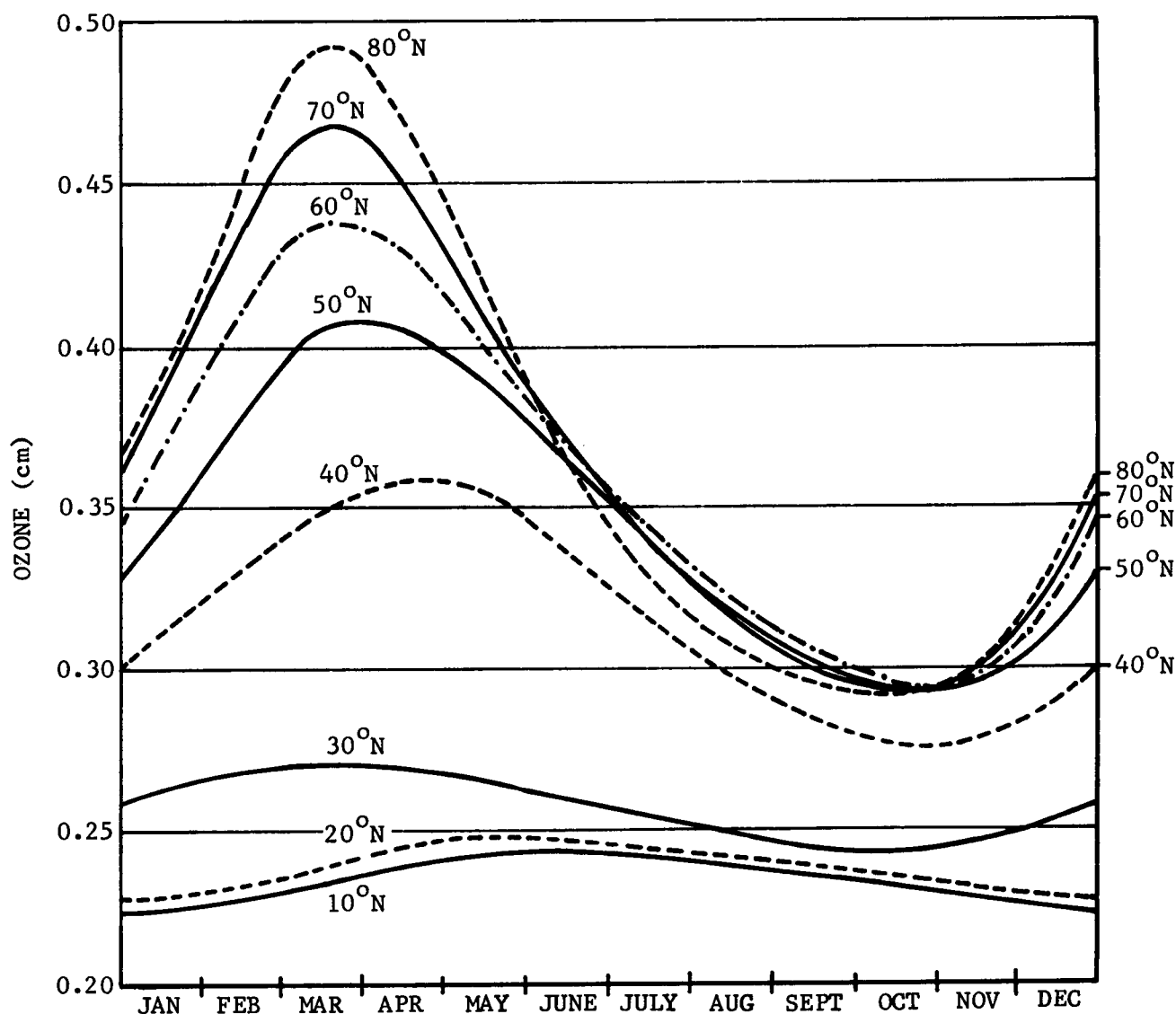


FIGURE 2-8. Annual Variation of Total Ozone for Each 10° of N. Latitude

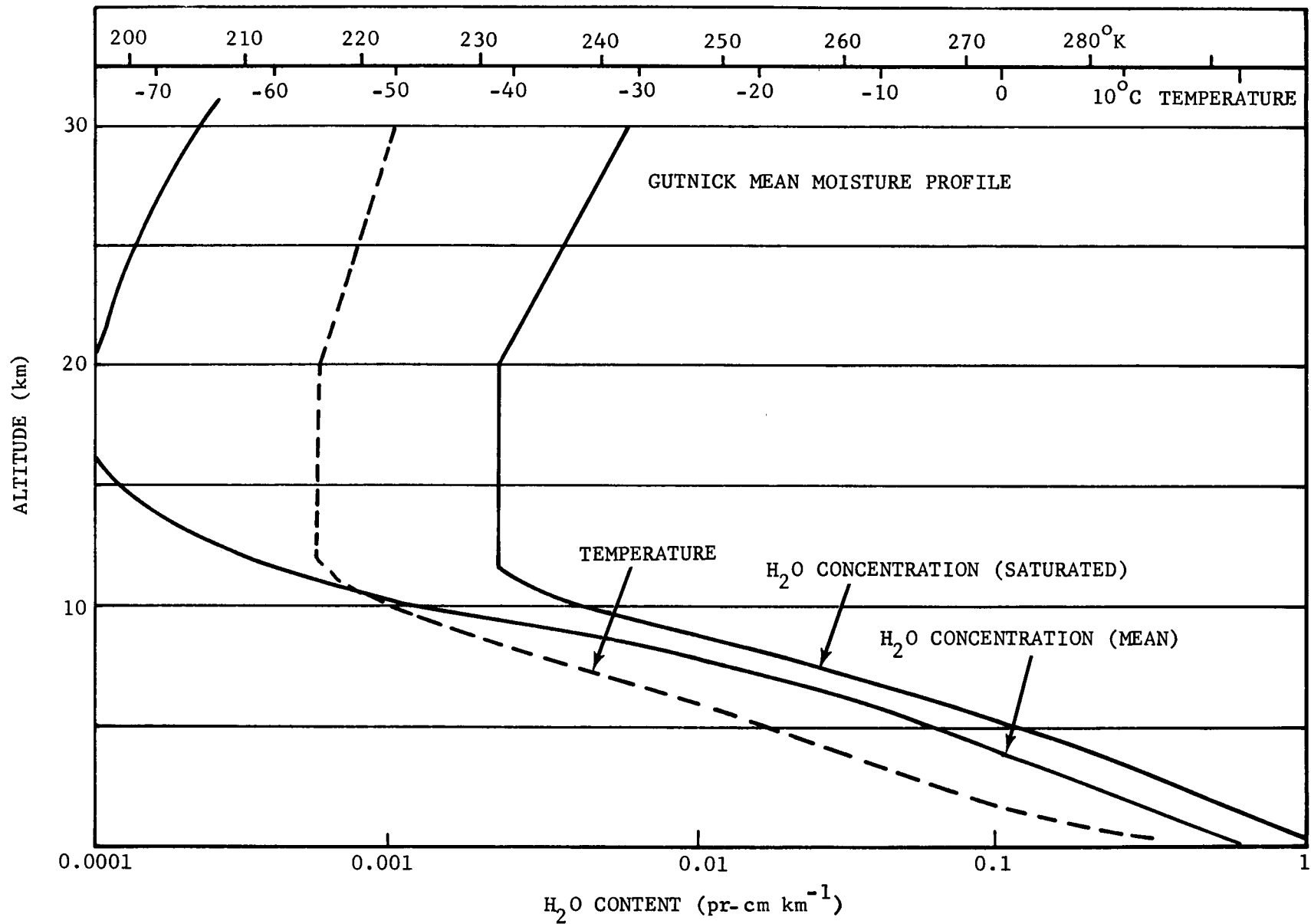


FIGURE 2-9. Water Vapor Profile in the Atmosphere

TABLE 2-5. ABSORBER CONCENTRATIONS IN THE ATMOSPHERE

REF.	CONSTITUENT	MOLECULAR MASS, G/MOLE	CONCENTRATION, % BY VOLUME	CONTENT IN 1 KM PATH AT SEA LEVEL
15	O ₃	48	Variable (10 ⁻⁶)	1 - 5 × 10 ⁻³ atm-cm
14	CO ₂	44	3.2 × 10 ⁻²	32 atm-cm
14	H ₂ O	18	Variable (1 - 10 ⁻³)	0.1 - 2 pr-cm
14	CH ₄	16	1.7 × 10 ⁻⁴	1.6 × 10 ⁻¹ atm-cm
14	CO	28	1.2 × 10 ⁻⁵	1.2 × 10 ⁻² atm-cm
15	N ₂ O	44	5 × 10 ⁻⁵	5 × 10 ⁻² atm-cm

2-4.2.3 Absorption Models

The theoretical models used for the computation of medium resolution transmission ($\Delta\bar{\nu} = 10$ to 50 cm⁻¹) are discussed in the following paragraphs:

- 2-4.2.3.1 — Absorption Due to a Single Line
- 2-4.2.3.2 — Absorption Due to an Assembly of Independent Lines
- 2-4.2.3.3 — The Elsasser Band Model
- 2-4.2.3.4 — The Goody Model
- 2-4.2.3.5 — Other Less Frequently Used Models
- 2-4.2.3.6 — Selective Absorption of Plume Radiation

2-4.2.3.1 Absorption Due to a Single Line

In the lower atmosphere, all lines constituting an IR band are assumed to have the Lorentz line shape for which the absorption coefficient is given by

$$\alpha(\bar{\nu}) = \frac{S}{\pi} \left[\frac{\gamma}{(\bar{\nu} - \bar{\nu}_0)^2 + \gamma^2} \right] \quad (2-43)$$

where

S = line intensity, (absorber units)⁻¹ · cm⁻¹
 γ = half-width at half maximum, cm⁻¹
 $\bar{\nu}_0$ = position of centerline, cm⁻¹

The Lorentz line shape is shown in Fig. 2-10. The integral of $\alpha(\bar{\nu})$ over all wavenumbers is equal to the line intensity S . The line half-width γ depends on the pressure P and the absolute temperature T as¹³

$$\gamma = \gamma_0 \left(\frac{P}{P_0} \right) \left(\frac{T_0}{T} \right)^{1/2} \quad (2-44)$$

For most H₂O and CO₂ lines at STP, γ_0 ranges from 0.03 to 0.15 cm⁻¹.

The Lorentz line shape, arising from molecular collisions, is valid only for low altitudes. Above 30 km, the line shape for CO₂ and H₂O become Gaussian¹⁹. For CO₂ it is questionable whether the wings of Eq. 2-43 are valid even at low altitudes, i.e., when $(\bar{\nu} - \bar{\nu}_0)^2 \gg \gamma$.

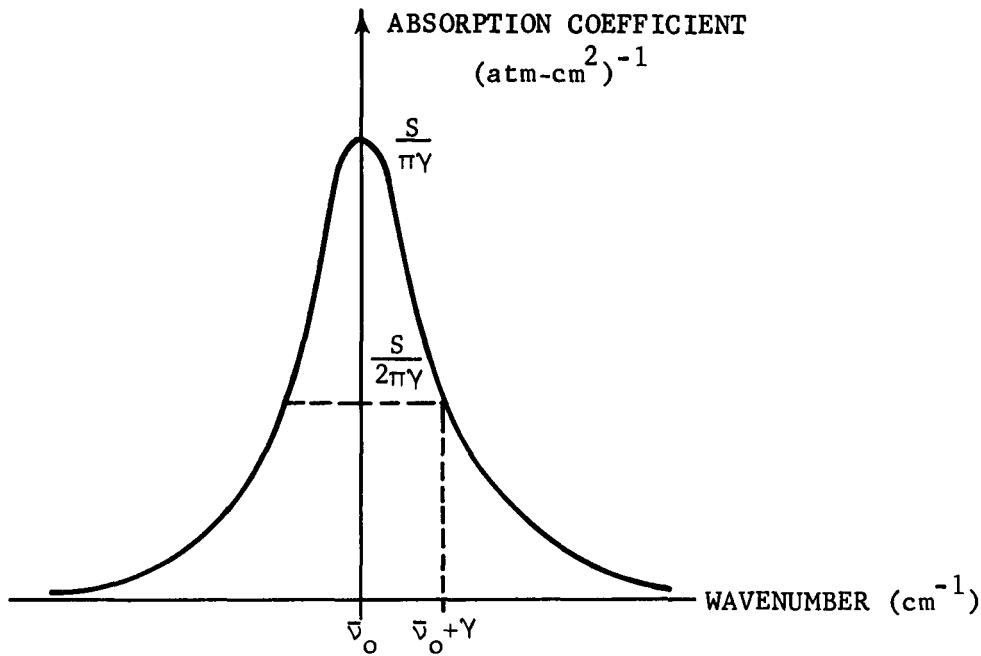


FIGURE 2-10. Lorentz Line Shape

The total absorption $\alpha \Delta \bar{\nu}$ in a band $\Delta \bar{\nu}$ centered at $\bar{\nu}_0$ —and due to a single Lorentz line viewed through a constant temperature, constant pressure pathlength containing an amount w of absorber—is

$$\alpha \Delta \bar{\nu} = \int_{\bar{\nu}_0 - \frac{\Delta \bar{\nu}}{2}}^{\bar{\nu}_0 + \frac{\Delta \bar{\nu}}{2}} \left\{ 1 - \exp \left[\frac{-Sw\gamma/\pi}{(\bar{\nu} - \bar{\nu}_0)^2 + \gamma^2} \right] \right\} d\bar{\nu}, \text{ cm}^{-1} \quad (2-45)$$

where α represents the average absorption over the interval $\Delta \bar{\nu}$. If $\Delta \bar{\nu} \gg \gamma$, then Eq. 2-45 can be approximated by

$$\alpha \Delta \bar{\nu} = \int_{-\infty}^{+\infty} \left\{ 1 - \exp \left[\frac{-Sw\gamma/\pi}{(\bar{\nu} - \bar{\nu}_0)^2 + \gamma^2} \right] \right\} d\bar{\nu}, \text{ cm}^{-1} \quad (2-46)$$

Although Eqs. 2-45 and 2-46 can be evaluated in terms of Bessel's functions²⁰, it is more usual to make weak and strong line approximations.

The weak line approximation corresponds to pathlengths and line intensities such that the exponent at the center line $Sw/\pi\gamma$ is much less than one. In that case, the exponential can be expanded in a power series. Keeping only the first two terms, the integral then easily yields

$$\alpha\Delta\bar{\nu} = Sw, \text{ cm}^{-1} \quad (2-47)$$

Thus, for the weak line approximation, the total absorption depends linearly on pathlength w .

In the strong line approximation $Sw/\pi\gamma \gg 1$, the line saturates for several half-widths about its center. The absorption is so great that only on the wings of the line can any shape be seen. Since $(\bar{\nu} - \bar{\nu}_0)^2 \gg \gamma^2$ before the exponential becomes important, the γ^2 in the denominator of the exponent can be dropped. Eq. 2-46 is then integrated to give*

$$\alpha\Delta\bar{\nu} = 2(S\gamma w)^{1/2}, \text{ cm}^{-1} \quad (2-48)$$

Thus, for the strong line approximation, the total absorption depends on the square root of pathlength w .

For pressures less than 1 atmosphere, and for most IR absorption bands of interest, the lines constituting the bands may be considered as strong under path conditions resulting in any appreciable absorptance (20% or more). The noted exception is ozone whose lines cannot be assumed to be strong even at 25 km altitude except for very long pathlengths.

2-4.2.3.2 Absorption Due to an Assembly of Independent Lines

If the total absorption of a band is due to the sum of the total absorptions of the lines in the band, then the lines are considered independent²¹. Thus independent means

$$\alpha\Delta\bar{\nu} = \sum_{i=1}^n (A\Delta\bar{\nu})_i = \sum_{i=1}^n \alpha_i\Delta\bar{\nu} \quad (2-49)$$

Summed over all n lines in the band. The individual lines themselves may be either strong or weak and still may be independent. Thus

$$\alpha\Delta\bar{\nu} = \begin{cases} \sum_{i=1}^n S_i w & \text{(weak lines)} \\ \sum_{i=1}^n (S_i \gamma_i w)^{1/2} & \text{(strong lines)} \end{cases} \quad (2-50)$$

If the lines have an average line strength S and an average spacing d in cm^{-1} , then the average absorptance is

$$\alpha = \begin{cases} \frac{wS}{d} & \text{(weak lines)} \\ \left(\frac{S\gamma w}{d^2}\right)^{1/2} & \text{(strong lines)} \end{cases} \quad (2-51)$$

2-4.2.3.3 The Elsasser Band Model

The Elsasser absorption band model²² is comprised of a series of regularly spaced, identical Lorentz lines. It is applicable to the IR bands of symmetric top molecules²³; i.e., CO, CO₂, N₂, CH₄. The lines comprising the IR bands of these molecules are evenly spaced. Their intensities, however, vary²⁰. Hence only portions of the bands can be represented accurately by the Elsasser model. The absorption coefficient of an Elsasser band is obtained from Eq. 2-43 by summing over all the lines. The average absorptance in an interval containing many lines, in the strong line approximation $\left(\frac{Sw}{\pi\gamma} \gg 1\right)$ is found²² to be

$$\alpha = \text{erf}\left(\frac{\sqrt{\pi S\gamma w}}{d}\right) \quad (2-52)$$

where the error function (erf) is defined as

$$\text{erf}(x) = \frac{2}{\sqrt{\pi}} \int_0^x e^{-t^2} dt$$

where d is the spacing between lines. Eq. 2-52 is valid only if the overlap parameter[†] $\frac{2\pi\gamma}{d}$ is much smaller than 1. The error function is tabulated in many standard mathematical tables^{24,25}. A fit of H₂O transmission measurements to the error function is shown in Fig. 2-11. If the argument

* The integration is done by: (1) letting $x = \bar{\nu} - \nu_0$; (2) changing to $y = \frac{1}{x}$; (3) inserting an integrating factor α in exponent; (4) differentiating with respect to α ; (5) integrating with respect to y ; and, (6) integrating with respect to α over the range 0 to 1.

† $\frac{2\pi\gamma}{d}$ is referred to as the overlap parameter because it contains the ratio of the line half width γ to the (average) spacing between lines d and expresses the extent of "overlap" between lines.

of the error function is much smaller than 1, there is little overlap between lines and Eq. 2-52 reduces to

$$\alpha = 2 \left(\frac{\sqrt{S \gamma w}}{d} \right) \tag{2-53}$$

Thus, the absorptance varies proportionately with the square root of the path length. The condition $\frac{2\pi\gamma}{d} \ll 1$ holds for the IR bands of CO, CO₂, N₂O, CH₄ if the pressure is less than 1 atmosphere. The condition $\frac{Sw}{\pi\gamma} \gg 1$ will hold for

any appreciable absorption ($\alpha \approx 20\%$ or greater for most bands at sea level). Therefore, Eq. 2-52 is valid in most cases of interest. When the condition $\frac{Sw}{\pi\gamma} \gg 1$ does not apply, the transmittance will be a function of the two parameters $\frac{2\pi\gamma}{d}$ and $\frac{S}{d}$ (Ref. 22). Table 2-6 lists these band parameters for CO₂ transmission. The coefficient γ_0 that appears in Table 2-6 is defined by Eq. 2-44 and corresponds to a pressure $P_0 = 1$ mm of Hg and to a temperature $T_0 = 300^\circ\text{K}$.

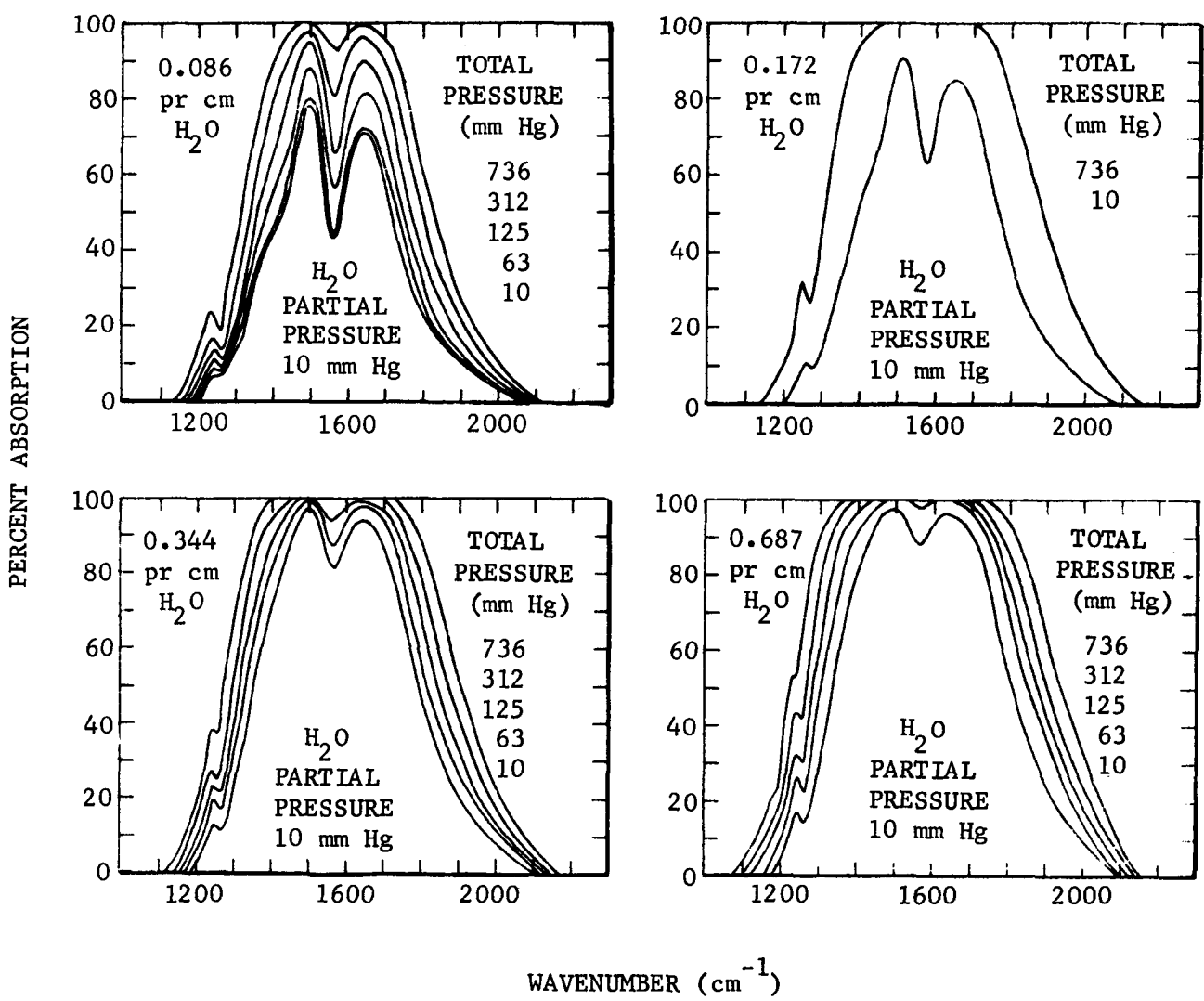


FIGURE 2-11. The 6.3-micron Band of H₂O

TABLE 2-6. BAND PARAMETERS S/d AND $2\pi\gamma_0/d$ FOR CO₂

WAVELENGTH, μ	S/d	$\frac{2\pi\gamma_0^*}{d}$
2.6434	0.3300E-03 **	0.4550E-05
2.6504	.1600E-02	.3750E-04
2.6674	.3700E+00	.1351E-03
2.6724	.5000E+00	.5000E-03
2.6738	.5000E+00	.6300E-03
2.6802	.5500E+00	.1000E-02
2.6831	.8800E+00	.6136E-03
2.6882	.8600E+00	.3256E-03
2.6911	.5400E+00	.3611E-03
2.6940	.8800E+00	.2955E-03
2.6969	.5200E+00	.6250E-03
2.7027	.7000E+00	.4929E-03
2.7086	.7400E+00	.3784E-03
2.7137	.6200E+00	.7177E-03
2.7211	.4400E+00	.8864E-04
2.7322	.1500E+00	.6667E-04
2.7397	.2500E-01	.6000E-03
2.7473	.7600E-01	.9868E-03
2.7548	.3600E+00	.7222E-03
2.7579	.5500E+00	.5455E-03
2.7609	.5800E+00	.4397E-03
2.7663	.5300E+00	.2453E-03
2.7685	.3300E+00	.2455E-03
2.7739	.2600E+00	.9231E-03
2.7778	.4200E+00	.6667E-03
2.7801	.4700E+00	.5745E-03
2.7855	.4400E+00	.3750E-03
2.7917	.2900E+00	.2414E-03
2.7941	.1600E+00	.3500E-03
2.8027	.1300E+00	.2692E-03
2.8129	.7000E-01	.1200E-03
2.8153	.3700E-01	.1568E-03
2.8177	.2700E-01	.1444E-03
2.8241	.1700E-01	.1176E-03
2.8281	.5000E-02	.3300E-03
2.8345	.3000E-02	.5167E-03
2.8433	.3900E-02	.5041E-03
2.8514	.3300E-02	.5000E-03
2.8555	.2400E-02	.5417E-03
2.8620	.1000E-02	.4500E-03
2.8686	.3000E-04	.3233E-02
2.8752	.0000E+00	.0000E+00
2.8810	.0000E+00	.0000E+00
4.1490	.0000E+00	.0000E+00
4.1580	.2600E-03	.1000E-05
4.1670	.5900E-02	.5000E-05
4.1750	.2400E+00	.8000E-04

* The values in this column correspond to a pressure of 1 mm Hg.

For sea level conditions the values in this column should be multiplied by 760.

** 0.3300E-03 = 0.3300×10^{-3} .

TABLE 2-6 (Continued)

WAVELENGTH, μ	S/d	$\frac{2\pi\gamma_0^*}{d}$
4.1840	0.9940E-01	0.1815E-02
4.1930	.9800E+00	.7368E-03
4.2020	.5046E+01	.7632E-03
4.2110	.1464E+02	.8026E-03
4.2190	.2728E+02	.1158E-02
4.2280	.3363E+02	.1500E-02
4.2370	.3363E+02	.1553E-02
4.2460	.2562E+02	.1605E-02
4.2550	.1344E+02	.1684E-02
4.2640	.2316E+02	.1576E-02
4.2740	.2592E+02	.1421E-02
4.2830	.2472E+02	.1355E-02
4.2920	.2070E+02	.1211E-02
4.3010	.1698E+02	.1435E-02
4.3100	.1219E+02	.1263E-02
4.3190	.7300E+01	.1316E-02
4.3290	.5000E+01	.1316E-02
4.3380	.2915E+01	.1448E-02
4.3480	.2020E+01	.1342E-02
4.3570	.1298E+01	.1448E-02
4.3670	.6860E+00	.1290E-02
4.3760	.3762E+00	.1302E-02
4.3860	.4599E+00	.8289E-03
4.3960	.6090E+00	.5527E-03
4.4050	.5890E+00	.5000E-03
4.4150	.5610E+00	.4342E-03
4.4250	.3833E+00	.4800E-03
4.4350	.2496E+00	.6851E-03
4.4440	.1855E+00	.9218E-03
4.4540	.8624E-01	.1013E-02

* The values in this column correspond to a pressure of 1 mm Hg.
For sea level conditions the values must be divided by 760.

2-4.2.3.4 The Goody Model

The statistical, or Goody, absorption band model^{26, 27} is best suited for asymmetric top molecules²³, such as ozone and water vapor, whose line positions appear randomly distributed within a band, and whose line intensities vary widely. This model assumes that both absorption line positions and intensities must be specified by probability functions. The absorption in an interval $\Delta\bar{\nu}$ is then calculated by a statistical averaging process. The selected interval $\Delta\bar{\nu}$ must be sufficiently large to give validity to statistical averaging. However, since the statistical properties of an absorption band will usually vary from one absorption region of the band to another, the $\Delta\bar{\nu}$ interval selected must not be too large. It is assumed that there is equal probability of finding a line centered at any wavelength inside the interval $\Delta\bar{\nu}$; that all lines have the same half width γ ; and that the normalized probability of a line having intensity S is $p(S)$.

If the line intensities have an exponential distribution with average value S_0 , then $p(S) = \frac{1}{S_0} \exp \left[-\frac{S}{S_0} \right]$ and the average absorptance in the interval $\Delta\bar{\nu}$ is found to be²⁶

$$\alpha = 1 - \exp \left[- \frac{wS_0}{d \left(1 + \frac{wS_0}{\pi\gamma} \right)^{1/2}} \right] \quad (2-54)$$

where d is the average space between lines.

If the line intensities are all equal,

$$\alpha = 1 - \exp \left\{ - \frac{1}{d} \int_{-\infty}^{+\infty} \left[1 - \exp \left[- \frac{S_0 w d}{\pi(\bar{\nu}^2 + \gamma^2)} \right] \right] d\bar{\nu} \right\} \quad (2-55)$$

When the lines saturate at their centers, Eqs. 2-54 and 2-55 reduce to

$$\alpha = 1 - \exp \left[- \frac{2}{d} \sqrt{S_0 \gamma w} \right] \quad (2-56)$$

When there is little overlap between lines,

$$\sqrt{\frac{S_0 \gamma w}{d^2}} \ll 1$$

and Eq. 2-56 is reduced to Eq. 2-53.

The band parameters relevant to the Goody model Eqs. 2-54 and 2-56 are $\frac{S_0}{d}$ and $\frac{S_0^*}{2\pi\gamma}$. These parameters for H₂O and O₃ are tabulated in Ref. 14. These values for H₂O are reproduced in Table 2-7 (for sea level conditions). The coefficient γ_0 that appears in Table 2-7 is defined by Eq. 2-44 and corresponds to a pressure $P_0 = 1\text{mm Hg}$ and to a temperature $T_0 = 300^\circ\text{K}$.

2-4.2.3.5 Other Less Frequently Used Models

Other band models developed are variations of those mentioned above and do not differ sufficiently to justify a detailed discussion here.

The random Elsasser model is a model in which several Elsasser bands with different line spacings and intensities overlap in a given wavelength interval.

In the doublet model, one considers the absorption due to two Lorentz lines of the same intensity which overlap.

The Curtis model is a variation on the Elsasser band model in which the line intensities are not equal.

Another model takes into account occasional gaps which may occur between lines in a band and which have a strong influence on the transmission behavior of the band for very long paths. In this model, a gap of varying width between two random arrays of lines is considered and the transmission characteristics are related to the gap width.

The quasi random model is the most complicated in that it takes into account the fact that lines are neither uniformly spaced nor completely randomly spaced. A detailed knowledge of the band structure is required and the aid of an electronic computer is essential¹⁰.

Most of the band models are discussed in Ref. 13.

2-4.2.3.6 Selective Absorption of Plume Radiation

The previous discussion applies only to the absorption of graybody radiation. In some applications, however, the emitter (target) is a hot gas (i.e., plume or flame radiation), and the emission spectrum is composed of many narrow emission

lines. If the emitting gas is the same as one of the minor constituents of the atmosphere (CO₂ or H₂O, for example), the target radiation will be subjected to selective absorption by the atmosphere. The result will be higher average absorptance for this radiation than for blackbody radiation. If the emitter is sufficiently hot ($T > 600^\circ\text{K}$ for CO₂ and $T > 1200^\circ\text{K}$ for H₂O), or thick enough so that its emittance approaches one; then (1) this selective absorption of the atmosphere will be small²⁸; (2) the emitting gas may be assumed to radiate as a graybody insofar as transmission calculations are concerned; and (3) the results of the previous paragraphs may then be applied.

2-4.2.4 Absorption Calculation

In order to apply the theoretical analysis of par. 2-4.2.3 to the actual calculation of molecular absorption in the atmosphere, two more points need examination: (1) spectral location and bandwidth of detection system, and (2) conversion of actual paths through the atmosphere to equivalent sea-level paths.

The ideal situation would be that in which the spectral resolution of the detection system is the same as that of the laboratory data available. The direct use of laboratory data is then possible. But this is rarely the case. In general, one must refer to laboratory data of higher resolution than that of the detection system. If the bandwidth of the system is larger than 50 cm⁻¹, the band models discussed in par. 2-4.2.3 can be used to calculate the (average) transmittance at each wavenumber inside the bandwidth of the detection system and the average transmittance over the band can be derived by averaging. If the spectral bandwidth of the detecting system is so large that it completely encompasses one or more absorption bands, transmission calculations can be simplified by calculating the total absorptions of the bands rather than the absorptances at each wavelength.

The narrow band absorption data to which band models can be applied are discussed in par. 2-4.2.4.1. The use of wideband absorption data for the determination of total band absorption is presented in par. 2-4.2.4.2. Justification for the use of equivalent sea-level paths and their method of calculation are given in par. 2-4.2.4.4. Some sample problems are worked out in par. 2-4.2.4.4.

* Note that the overlap parameter $\frac{2\pi\gamma}{d}$ is the ratio of these two parameters.

Extensive tabulations of CO₂, and H₂O transmittances for various atmospheric paths and absorber contents have been compiled^{11,12,29}.

pressed in Table 2-9.) The experimental data on CO₂ at 2.7 microns in Fig. 2-12 is fitted to an error function curve.

Ref. 14 contains a description of a computer program which can be used for calculating transmissions between 1 and 20 microns.

2-4.2.4.1 Narrow-band Absorption Data

Narrow-band absorption is that for which the spectral resolution of the measuring instrument is 10 to 50 cm⁻¹. This resolution is sufficiently narrow such that only a small portion of an absorption band is measured, but sufficiently wide such that the theoretical considerations of par. 2-4.2.3 (Absorption Models) apply. A great amount of laboratory data on absorption by CO₂²⁹, H₂O³⁰, and by other minor atmospheric constituents^{29,31} except ozone are available. Unfortunately, only little laboratory data on ozone are available^{32,33}. Other data for the atmosphere as a whole^{34,35} are available for sea-level paths of various lengths.

Many attempts have been made since the publication of laboratory data^{29,30,31} to fit the data to the band models discussed here. Tables 2-8 and 2-9 give a summary of the data and references to investigators who reduced the data.

The band parameters derived for CO₂ and H₂O from the experiments in Refs. 29 to 31 are listed in Tables 2-6 and 2-7. From these parameters, it is possible to calculate the coefficients entering in Eqs. 2-52 (CO₂) and 2-54 (H₂O), and to compute the transmission at any wavelength if the amount of absorber w is known.

An example of the data available on the 6.3-micron vapor band, taken from Ref. 30, is shown in Fig. 2-11. The curves in the figure represent absorption across the band for a single water-vapor path-length as a function of total pressure. Table 2-9 from Ref. 14 lists the absorption bands and absorption data source references.

An example of the use of these data for finding the transmission curve is given in Fig. 2-12³⁸. (Note that units on the abscissa of Fig. 2-12 are expressed in "atmospheric kilometers" rather than "atmospheric centimeters" as ex-

2-4.2.4.2 Wide-band Absorption Data

Wide-band absorption is that which is measured by an instrument with a spectral bandwidth completely encompassing an absorption band. For example, if all lines of a given band are between the wavelength limits of 1.75 and 2.00 microns, the wide-band absorption would be measured by an instrument with a spectral passband between 1.5 and 2.5 microns. To avoid problems with instrument passband width, which for the above-mentioned band could extend in width from 0.25 micron to infinity, wide-band absorption is measured in absolute units, microns. An absorption of 0.1 micron would mean that the integrated absorption in the band would be equivalent to total absorption in a 0.1-micron interval. Thus, for the 1.75- to 2.00-micron band above, total absorption can range from 0 to 0.25 micron. The wide-band absorption data for the various bands of carbon dioxide and water vapor are listed in Tables 2-10 and 2-11. These tables list the effective pressure p_e as total pressure plus the absorber partial pressure. For atmosphere transmission problems, the absorber partial pressure can be neglected.

2-4.2.4.3 Atmospheric Windows

As illustrated in Fig. 2-6, attenuation by the atmosphere is weak in the following window regions:

Microns
1 — 1.1
1.2 — 1.3
1.5 — 1.8
2.1 — 2.4
3.5 — 4
4.5 — 5
8 — 14

TABLE 2-7. BAND MODEL PARAMETERS S/d AND $S/(2\pi\gamma_0)$ FOR H_2O

WAVELENGTH, μ	S/d	$S/(2\pi\gamma_0)^*$
2.16000	0.7030E-03**	0.8675E+00
2.18000	.9430E-03	.1157E+01
2.20000	.1680E-02	.2078E+01
2.24000	.7590E-03	.9356E+00
2.28000	.3070E-01	.3791E+02
2.33100	.5650E-01	.6790E+02
2.33645	.5660E-01	.6800E+02
2.34192	.7930E-01	.8210E+02
2.34742	.7980E-01	.7880E+02
2.35294	.8390E-01	.8240E+02
2.35849	.8820E-01	.8640E+02
2.36407	.9310E-01	.8670E+02
2.36967	.9890E-01	.9270E+02
2.37530	.1040E+00	.9910E+02
2.38095	.1090E+00	.9920E+02
2.38663	.1150E+00	.1030E+03
2.39234	.1210E+00	.1050E+03
2.39808	.1250E+00	.1050E+03
2.40385	.9580E-01	.5260E+02
2.40964	.1370E+00	.9790E+02
2.41546	.1500E+00	.1030E+03
2.42131	.1620E+00	.9810E+02
2.42718	.1860E+00	.1060E+03
2.43309	.2180E+00	.1320E+03
2.43902	.2490E+00	.1690E+03
2.44499	.2910E+00	.1760E+03
2.45098	.3970E+00	.2490E+03
2.45700	.6460E+00	.4390E+03
2.46305	.7490E+00	.4850E+03
2.46970	.4380E+01	.5110E+05
2.47400	.2530E+01	.2320E+05
2.48020	.6650E+01	.2110E+05
2.48320	.5280E+01	.3920E+05
2.48760	.5630E+01	.3140E+05
2.49380	.1000E+02	.2150E+05
2.50130	.9860E+01	.1670E+05
2.50500	.1030E+02	.5090E+05
2.50880	.1590E+02	.3630E+05
2.51180	.1390E+02	.3070E+05
2.51890	.2600E+02	.2480E+05
2.52400	.3450E+02	.1730E+06
2.52840	.5160E+02	.9290E+05
2.53610	.9200E+02	.1150E+06
2.53940	.7220E+02	.1030E+06
2.54450	.1440E+03	.1520E+06
2.54970	.9060E+02	.5650E+06
2.55620	.1120E+03	.2700E+06

* The values in this column correspond to a pressure of 1 mm Hg.

For sea level conditions the values in this column should be multiplied by 760.

** 0.7030E-03 = 0.7030×10^{-3} .

TABLE 2-7 (Continued)

WAVELENGTH, μ	S/d	$S/(2\pi\gamma_0)^*$
2.56280	0.1410E+04	0.6690E+07
2.56610	.4570E+03	.8500E+06
2.57070	.2590E+03	.1310E+06
2.57730	.2320E+03	.1150E+06
2.58400	.8130E+03	.1300E+07
2.58930	.5980E+03	.7880E+06
2.59200	.1020E+04	.1310E+07
2.59740	.2880E+03	.1310E+06
2.60210	.4950E+03	.2020E+06
2.60890	.2940E+03	.1270E+06
2.61440	.4070E+03	.1360E+06
2.62190	.2510E+03	.1740E+06
2.62880	.2380E+03	.6220E+05
2.63370	.9650E+02	.4900E+05
2.63990	.1260E+03	.5670E+05
2.64340	.1130E+03	.7030E+05
2.65040	.1930E+03	.7880E+05
2.66740	.6180E+03	.1530E+06
2.67240	.4890E+03	.1190E+06
2.67380	.6090E+03	.1850E+06
2.68020	.3050E+03	.8040E+05
2.68310	.3090E+03	.8640E+05
2.68820	.2150E+03	.7070E+05
2.69110	.2590E+03	.7980E+05
2.69400	.3070E+03	.8880E+05
2.69690	.1470E+03	.4340E+05
2.70270	.1310E+03	.4830E+05
2.70860	.2490E+03	.3050E+05
2.71370	.2130E+03	.1200E+06
2.72110	.5790E+03	.3090E+06
2.73220	.1240E+03	.7180E+05
2.73970	.4950E+03	.2020E+06
2.74730	.1390E+03	.6150E+05
2.75480	.2780E+03	.6890E+05
2.75790	.2730E+03	.1100E+06
2.76090	.2660E+03	.1520E+06
2.76630	.2940E+03	.6690E+05
2.76850	.2500E+03	.6640E+05
2.77390	.1710E+03	.6460E+05
2.77780	.1900E+03	.7200E+05
2.78010	.1800E+03	.7630E+05
2.78550	.2300E+03	.8460E+05
2.79170	.1130E+03	.6270E+05
2.79410	.8740E+02	.4970E+05
2.80270	.2550E+03	.1320E+06
2.81290	.1000E+03	.1150E+06
2.81530	.1050E+03	.9170E+05
2.81770	.1360E+03	.9230E+05

* The values in this column correspond to a pressure of 1 mm Hg.
For sea level conditions the values must be divided by 760.

TABLE 2-7 (Continued)

WAVELENGTH, μ	S/d	$S/(2\pi\gamma_0)^*$
2.82410	0.8170E+02	0.1300E+06
2.82810	.6120E+02	.9380E+05
2.83450	.1070E+03	.6000E+05
2.84330	.3740E+02	.6240E+05
2.85140	.6000E+02	.5740E+05
2.85550	.8030E+02	.6880E+05
2.86200	.3870E+02	.3490E+05
2.86860	.2830E+03	.5200E+05
2.87520	.1500E+02	.1800E+05
2.87770	.1490E+02	.1600E+05
2.88100	.1500E+02	.1780E+05
2.88600	.1540E+02	.7930E+04
2.89440	.5910E+01	.8930E+04
2.90280	.3890E+02	.5700E+05
2.91040	.8030E+01	.1130E+05
2.91460	.8730E+05	.1070E+05
2.91630	.8160E+01	.1550E+05
2.92400	.2600E+02	.2480E+05
2.93080	.4140E+01	.4920E+04
2.93260	.3810E+01	.9710E+04
2.94120	.7170E+01	.6610E+04
2.94810	.1560E+02	.3020E+05
2.95070	.1210E+02	.5430E+05
2.95510	.1160E+02	.1720E+05
2.96120	.2320E+01	.2470E+04
2.97180	.1570E+02	.1240E+05
2.97620	.1340E+02	.2130E+05
2.98950	.2050E+01	.6270E+04
2.99400	.8180E+01	.1630E+05
3.00300	.6850E+01	.3000E+05
3.00750	.8010E+01	.8370E+05
3.01390	.4740E+01	.1500E+05
3.02110	.1120E+02	.9920E+04
3.02480	.7720E+01	.5220E+05
3.03030	.8140E+01	.1490E+05
3.03580	.9810E+01	.6650E+04
3.03950	.8430E+01	.2450E+05
3.04410	.1010E+02	.2390E+05
3.04880	.1670E+02	.1770E+05
3.05340	.7600E+01	.3210E+05
3.06000	.8280E+01	.1940E+05
3.06750	.9680E+01	.1190E+05
3.07220	.7190E+01	.4480E+05
3.07790	.1280E+02	.2190E+05
3.08360	.7030E+01	.1050E+05
3.08830	.8860E+01	.7010E+04
3.09410	.8630E+01	.3130E+05
3.09890	.6250E+01	.4900E+04

* The values in this column correspond to a pressure of 1 mm Hg.
For sea level conditions the values must be divided by 760.

TABLE 2-7 (Continued)

WAVELENGTH, μ	S/d	$S/(2\pi\gamma_0)^*$
3.10750	0.9860E+05	0.1660E+05
3.11620	.6430E+01	.1150E+06
3.12110	.9780E+01	.1440E+05
3.12500	.8120E+01	.9550E+04
3.12990	.2200E+01	.2480E+04
3.13480	.1420E+01	.1470E+04
3.13970	.7670E+01	.9380E+04
3.14470	.7100E+01	.7250E+04
3.14960	.4280E+01	.3540E+04
3.15460	.9240E+00	.8140E+03
3.15960	.4570E+00	.2300E+03
3.16460	.2700E+00	.1260E+03
3.16960	.2290E+00	.1020E+03
3.17460	.4260E+00	.3300E+03
3.17970	.1300E+01	.1310E+04
3.18470	.1560E+01	.1280E+04
3.18980	.7340E+01	.8010E+04
3.19490	.1130E+02	.1380E+05
3.20000	.1100E+02	.7690E+04
3.20510	.1000E+02	.8070E+04
3.21030	.1290E+02	.1100E+05
3.21540	.1110E+02	.1000E+05
3.22060	.1290E+02	.1070E+05
3.22580	.1450E+02	.7960E+04
3.23100	.1110E+02	.6420E+04
3.23620	.8780E+00	.5260E+03
3.24150	.4870E+01	.8410E+04
3.24680	.1020E+02	.1400E+05
3.25200	.6470E+00	.5070E+03
3.25730	.4350E+01	.9140E+04
3.26260	.1500E+02	.4610E+05
3.26800	.3330E+01	.4670E+04
3.27330	.6400E+00	.4150E+03
3.27870	.1210E+01	.1070E+04
3.28400	.6470E+00	.5820E+03
3.28950	.1940E+01	.3610E+04
3.29490	.1480E+02	.1590E+05
3.30030	.8470E+01	.8880E+04
3.30580	.5160E+01	.4640E+04
3.31130	.3830E+01	.4090E+04
3.31670	.2010E+01	.3860E+04
3.32230	.1370E+01	.1560E+04
3.32780	.1710E+00	.9100E+02
3.33330	.1090E+00	.6100E+02
3.33890	.4560E+00	.5050E+03
3.34450	.1870E+01	.2780E+04
3.35000	.2880E+00	.1670E+03
3.35570	.5690E+00	.5050E+03

* The values in this column correspond to a pressure of 1 mm Hg.
For sea level conditions the values must be divided by 760.

TABLE 2-7 (Continued)		
WAVELENGTH, μ	S/d	$S/(2\pi\gamma_0)^*$
3.36130	0.5300E+01	0.9430E+04
3.36700	.1120E+01	.1150E+04
3.37270	.1130E+01	.1090E+04
3.37840	.2020E+00	.1310E+03
3.38410	.8970E+00	.1220E+04
3.38980	.1790E+01	.2220E+04
3.39560	.1730E+01	.2150E+04
3.40140	.2480E+00	.1640E+03
3.40720	.1680E+00	.1030E+03
3.41300	.8310E+00	.1050E+04
3.41880	.7170E+00	.8840E+02
3.42470	.3320E+00	.2800E+03
3.43050	.2030E+00	.1330E+03
3.43640	.3060E+00	.1980E+03
3.44230	.5290E+00	.5510E+03
3.44830	.2090E+00	.1590E+03
3.45420	.1720E+00	.9160E+02
3.46020	.1130E+00	.5260E+02
3.46620	.1110E+00	.8360E+02
3.47220	.2280E+00	.1600E+03
3.47830	.1190E+00	.5210E+02
3.48430	.5310E-01	.3610E+02
3.49040	.8090E-01	.4460E+02
3.49650	.1130E+00	.7350E+02
3.50260	.9140E-01	.7050E+02
3.50880	.8840E-01	.3830E+02
3.51490	.8620E-01	.3520E+02
3.52110	.1290E+00	.4770E+02
3.52730	.8300E-01	.5230E+02
3.53360	.8390E-01	.5400E+02
3.53980	.8380E-01	.5270E+02
3.54610	.5250E-01	.3780E+02
3.55240	.1490E+00	.6220E+02
3.55870	.7630E-01	.4830E+02
3.56510	.4390E-01	.2310E+02
3.57140	.1550E+00	.5310E+02
3.57780	.1300E+00	.7100E+02
3.58420	.1140E+00	.7830E+02
3.59070	.1900E+00	.1270E+03
3.59710	.3280E-01	.3700E+02
3.60360	.4260E-01	.4600E+02
3.61010	.7680E-01	.4670E+02
3.61660	.3830E-01	.2620E+02
3.62320	.3470E-01	.4360E+02
3.62980	.5920E-01	.5410E+02
3.63640	.4990E-01	.4060E+02
3.64300	.3820E-01	.2830E+02
3.64960	.5970E-01	.3140E+02
3.65630	.4700E-01	.3650E+02

* The values in this column correspond to a pressure of 1 mm Hg.
For sea level conditions the values must be divided by 760.

TABLE 2-7 (Continued)

WAVELENGTH, μ	S/d	$S/(2\pi\gamma_0)^*$
3.66300	0.5570E-01	0.6290E+02
3.66970	.3780E+00	.2020E+03
3.67650	.3920E+00	.1070E+03
3.68320	.1420E+00	.4180E+02
3.69000	.8360E-01	.2240E+02
3.69690	.5330E-01	.1730E+02
3.70370	.3540E-01	.2590E+02
3.71060	.5580E-01	.4030E+02
3.71750	.3530E-01	.3110E+02
3.72440	.2320E-01	.3740E+02
3.73140	.6800E-01	.5990E+02
3.73830	.5100E-01	.4260E+02
3.74530	.5890E-01	.1230E+03
3.75230	.6220E-01	.5760E+02
3.75940	.5880E-01	.4920E+02
3.76650	.2320E-01	.3890E+02
3.77360	.4420E-01	.4390E+02
3.78070	.7120E-01	.5250E+02
3.78790	.2710E-01	.5420E+02
3.79510	.2290E-01	.2650E+02
3.80230	.5940E-01	.4740E+02
3.80950	.4120E-01	.4130E+02
3.81680	.2190E-01	.2760E+02
3.82410	.3480E-01	.3410E+02
3.83140	.4780E-01	.3550E+02
3.83880	.2030E-01	.2970E+02
3.84620	.2070E-01	.2980E+02
3.85360	.3790E-01	.3000E+02
3.86100	.2900E-01	.2920E+02
3.86850	.1940E-01	.3000E+02
3.87600	.2380E-01	.3280E+02
3.88350	.3180E-01	.2620E+02
3.89110	.2400E-01	.3350E+02
3.89860	.1940E-01	.4070E+02
3.90630	.2220E-01	.2830E+02
3.91390	.2270E-01	.2450E+02
3.92160	.2700E-01	.3510E+02
3.92930	.1990E-01	.5500E+02
3.93700	.2120E-01	.2770E+02
3.94480	.2010E-01	.3180E+02
3.95260	.2230E-01	.5290E+02
3.96040	.1960E-01	.3400E+02
3.96830	.2120E-01	.3420E+02
3.97610	.1940E-01	.3870E+02
3.98410	.2340E-01	.5750E+02
3.99200	.2180E-01	.3870E+02
4.00000	.2440E-01	.3930E+02
4.00800	.2110E-01	.4200E+02
4.01600	.2000E-01	.4120E+02

* The values in this column correspond to a pressure of 1 mm Hg.
For sea level conditions the values must be divided by 760.

TABLE 2-7 (Continued)

WAVELENGTH, μ	S/d	$S/(2\pi\gamma_0)^*$
4.02400	0.2090E-01	0.4160E+02
4.03200	.3400E-01	.6320E+02
4.04000	.2570E-01	.4680E+02
4.04900	.2150E-01	.4190E+02
4.05700	.2260E-01	.4090E+02
4.06500	.2200E-01	.4000E+02
4.07300	.4970E-01	.7810E+02
4.08200	.3280E-01	.5280E+02
4.08900	.2200E-01	.3910E+02
4.09800	.2610E-01	.3880E+02
4.10700	.4970E-01	.7320E+02
4.11500	.9700E-01	.1660E+03
4.12400	.2490E-01	.3870E+02
4.13200	.2340E-01	.4160E+02
4.14100	.3190E-01	.4770E+02
4.14900	.2740E-01	.3870E+02
4.15800	.2380E-01	.3770E+02
4.16700	.2560E-01	.4810E+02
4.17500	.3550E-01	.5820E+02
4.18400	.4990E-01	.6110E+02
4.19300	.2750E-01	.3910E+02
4.20200	.2800E-01	.3570E+02
4.21100	.2530E-01	.4050E+02
4.21900	.5360E-01	.6970E+02
4.22800	.1170E+00	.2070E+03
4.23700	.3480E-01	.3700E+02
4.24600	.3360E-01	.3860E+02
4.25500	.2980E-01	.3360E+02
4.26400	.3190E-01	.3490E+02

* The values in this column correspond to a pressure of 1 mm Hg.
For sea level conditions the values must be divided by 760.

**TABLE 2-8. SUMMARY OF BAND-MODEL METHODS FOR COMPUTING
ATMOSPHERIC ABSORPTION¹⁴**

AUTHOR	GAS	BAND MODEL	WAVELENGTH RANGE, μ	EXPERIMENTAL DATA
Bradford	CO ₂	Elsasser	4.184 - 4.454	Bradford, McCormack, and Selby (Ref. 36)
Thomson and Downing	CO ₂	Elsasser	4.0 - 4.5	Theoretical
Elsasser	CO ₂	Empirical	11.77 - 18.2	Cloud, Howard, et al. (Ref. 30)
	H ₂ O	Statistical	4.39 - 250	Palmer, Howard, et al.
	O ₃	Empirical	8.85 - 16.4	Summerfield, Walshaw (Ref. 32)
Oppel	CO ₂	Elsasser	2.64 - 2.88	Burch, et al. (Refs. 29, 31)
			4.15 - 4.52	
	H ₂ O	Statistical	1.08 - 4.0	Burch, et al.; Howard, et al.;
			4.0 - 5.0	Stull, Wyatt, and Plass
	N ₂ O	Elsasser	4.36 - 4.74	Burch, et al.
	CH ₄	Statistical	3.02 - 4.16	Burch, et al.
	CO	Statistical	4.4 - 5.0	Burch, et al.
Altshuler	CO ₂	Empirical	1.0 - 15.0	Howard, et al.
	H ₂ O	Statistical	1.0 - 9.0	Howard, et al.
			9.1 - 20.0	Taylor and Yates (Refs. 34, 35)
			20 - 40	Palmer, et al.
			40 - 250	Stanevich
	O ₃	Elsasser	4.4 - 16.5	Strong (Ref. 33)
	N ₂ O	Elsasser	3.8 - 18.0	Shaw
Zachor	CO ₂	(a) Elsasser	1.0 - 5.3	Howard, et al.
		(b) Two overlapping Elsasser bands	1.0 - 5.3	

TABLE 2-8. (Continued)

AUTHOR	GAS	BAND MODEL	WAVELENGTH RANGE, μ	EXPERIMENTAL DATA
Howard, Burch, and Williams	O ₃	Elsasser	9.3 - 10.2	Walshaw, et al.
	H ₂ O	Statistical	1.0 - 10.6	Howard, et al.
	CO ₂	Elsasser	4.167 - 4.51	Theoretical
	H ₂ O	Statistical	1.0 - 9.2	Howard, et al.
Carpenter	H ₂ O	Statistical	1.0 - 10.0	Howard, et al.
	CO ₂	Statistical	1.0 - 10.0	Burch, et al.
	H ₂ O	Statistical	1.0 - 10.0	Howard, et al.
	H ₂ O	Statistical	1.0 - 10.0	Burch, et al.
Lindquist	O ₃	Statistical	9.3 - 10.2	Walshaw, et al.
	N ₂ O	Statistical	4.4 - 4.6	Burch, et al.
	CH ₄	Statistical	3.15 - 3.45	Burch, et al.
	CO	Statistical	4.15 - 4.85	Burch, et al.
Green and Griggs	CO ₂	Quasi-random	1.0 - 20.0	Theoretical*
	H ₂ O	Quasi-random	1.0 - 20.0	Theoretical*
	H ₂ O	Empirical	0.7 - 5.9**	See appropriate paragraph
	H ₂ O	Empirical	14 - 20	Stauffer and Walsh ^{35A}

* The results of Stull, Wyatt, and Plass were normalized against the laboratory data of Howard, et al. for each absorption band.

** The results of Elder and Strong give average window transmission for seven windows in the wavelength range.

TABLE 2-9. SUMMARY OF LABORATORY MEASUREMENTS OF HOMOGENEOUS-PATH ABSORPTION SPECTRA¹⁴

GAS	BAND, μ	OBSERVED INTERVAL, cm^{-1}	RANGE OF PRESSURES* mm Hg	RANGE OF ABSORBER, w^{**}	NO. OF CURVES	RESOLUTION† APPROX.	RESEARCHERS
CO ₂	1.6 & 1.4	6000 - 7200	75 - 760	540 - 8100	13	0.12 μ	Howard, et al. ³⁰
	2.0	4600 - 5400	10 - 760	108 - 8630	32	0.9 μ	Howard, et al.
	2.7	3300 - 4100	1 - 755	11 - 1619	67	0.07 μ	Howard, et al.
	2.7	3450 - 3850	14.2 - 2065	0.164 - 24.4	32	10 - 15 cm^{-1}	Burch, et al. ^{29, 31}
	4.3	2200 - 2450	3.8 - 2115	0.0108 - 22.8	53	5 - 10 cm^{-1}	Burch, et al.
	4.3 & 4.8	2000 - 2500	1 - 735	9 - 1570	43	0.1 μ	Howard, et al.
	4.3	2250 - 2450	38 - 760	1.0 - 300	10	10 cm^{-1}	Bradford ³⁶
	5.2	1800 - 2000	10 - 735	104 - 1570	9	0.1 μ	Howard, et al.
	9.398 & 10.41	900 - 1100	103 - 3800	48 - 11,200	25	5 - 10 cm^{-1}	Burch, et al.
		720 - 875	103 - 3800	305 - 11,200	14	5 - 10 cm^{-1}	Burch, et al.
	15	500 - 900	20 - 745	1 - 863	37	0.5 μ	Howard, et al.
		495 - 875	0.26 - 3190	0.0118 - 2470	30	5 - 10 cm^{-1}	Burch, et al.
H ₂ O	1.1	8250 - 9500	9.8 - 740	0.03 - 1.93	41	0.13 μ	Howard, et al.
	1.38	6500 - 8000	3 - 740	0.026 - 3.85	62	0.12 μ	Howard, et al.
	1.875	4000 - 6000	3 - 740	0.026 - 3.85	62	0.1 μ	Howard, et al.
	1.875	4950 - 5800	27.5 - 862	0.0033 - 0.101	14	20 cm^{-1}	Burch, et al.
	2.7 & 3.2	2800 - 4400	2 - 750	0.017 - 2.1	114	0.07 μ	Howard, et al.
	2.7	3000 - 4300	27.5 - 862	0.0033 - 0.101	5	20 cm^{-1}	Burch, et al.
	6.3	1000 - 2200	2.5 - 742	0.021 - 1.49	69	0.4 μ	Howard, et al.

* Pressure designated is generally the equivalent pressure.

** w is expressed in precipitable centimeters for H₂O and in atmospheric centimeters for the other gases.

† Resolution specified is ordinarily center-band resolution and is used only to give an approximate designation.

TABLE 2-9. (Continued)

GAS	BAND, μ	OBSERVED INTERVAL, cm^{-1}	RANGE OF PRESSURES,* mm Hg	RANGE OF ABSORBER, w^{**}	NO. OF CURVES	RESOLUTION† APPROX.	RESEARCHERS
H ₂ O	6.3	1200 - 2200	14.0 - 805	0.0041	15	6 cm^{-1}	Burch, et al.
		200 - 500	0.76 - 600	0.0041 - 0.143		5 - 10 cm^{-1}	Palmer
O ₃	9.6	1000 - 2560	11.2 - 744	0.00278 - 1.968		7 cm^{-1}	Walshaw ³²
CO	4.666	2000 - 2250	1 - 3210	0.00096 - 22.2	147	25 cm^{-1}	Burch, et al.
	2.347	4100 - 4400	54 - 756	36.6 - 1140	26	15 - 20 cm^{-1}	Burch, et al.
CH ₄	3.311	2700 - 3200	2 - 3085	0.015 - 188	88	25 cm^{-1}	Burch, et al.
	6.452 & 7.657	1100 - 1800	3.8 - 3050	0.026 - 188	86	10 cm^{-1}	Burch, et al.
N ₂ O	4.0	2400 - 2650	22.4 - 746	0.38 - 18.6	8	20 cm^{-1}	Burch, et al.
	4.5	2100 - 2300	1.0 - 3120	0.00016 - 76.4	177	25 cm^{-1}	Burch, et al.
	4.5	2100 - 2300	99.8 - 849	0.01 - 2.3	65		Abels ³⁷
	7.78 & 8.57	1100 - 1400	3.2 - 3035	1.37 - 46.7	11	10 cm^{-1}	Burch, et al.
	14.45 & 16.98	500 - 800	4.5 - 851	1.89 - 359	7	6 cm^{-1}	Burch, et al.

* Pressure designated is generally the equivalent pressure.

** w is expressed in precipitable centimeters for H₂O and in atmospheric centimeters for the other gases.

† Resolution specified is ordinarily center-band resolution and is used only to give an approximate designation.

TABLE 2-10. WIDE-BAND ABSORPTION OF CARBON DIOXIDE ³⁰

Band and Limits	Total Absorption ($\alpha \Delta \bar{\nu}$ in μ^{-1})	Remarks
15 μ ; 11.7 - 18.5 μ	$-0.15 + 1.24 \log w + 1.06 \log p_e$	Also see Refs. 29, 31
10.4 μ and 9.4 μ		For data see Ref. 29
5.2 μ ; 5.05 - 5.35 μ	$6.5 \times 10^{-5} w^{1/2} p_e^{0.4}$	Also see Ref. 31
4.8 μ ; 4.65 - 5.05 μ	$2.75 \times 10^{-4} w^{1/2} p_e^{0.37}$	Also see Ref. 31
4.3 μ ; 4.0 - 4.65 μ	$0.051 + 0.063 \log w + 0.058 \log p_e$	Also see Refs. 29, 31
2.7 μ ; 2.66 - 2.82 μ	$-0.100 + 0.056 \log w + 0.050 \log p_e$	$w < 4$ atm-km
	$-0.126 + 0.078 \log w + 0.067 \log p_e$	$w > 4$ atm-km
	$-0.012 \log w \log p_e$	Also see Refs. 29, 31
2.0 μ ; 1.92 - 2.1 μ	$+ 1.97 \times 10^{-4} w^{1/2} p_e^{0.39}$	Total absorption $< 0.02\mu$
	$-0.2144 + 0.0552 \log w + 0.0456 \log p_e$	Total absorption $> 0.02\mu$
		Also see Ref. 31
1.6 μ ; 1.52 - 1.66 μ	$1.61 \times 10^{-5} w^{1/2} p_e^{0.38}$	Also see Ref. 31
1.4 μ ; 1.38 - 1.47 μ	$1.14 \times 10^{-5} w^{1/2} p_e^{0.41}$	Also see Ref. 31

NOTE: 1. All logs to the base 10.

2. w = atm-cm; p_e = mm Hg.

TABLE 2-11. WIDE-BAND ABSORPTION OF WATER VAPOR ³⁰

Band and Limits	Total Absorption ($\alpha\Delta\bar{\nu}$ in μ^{-1})	Remarks
6.3 μ ; 4.75 - 8.7 μ	$1.21 + 0.87 \log w + 0.62 \log p_e$	Questionable validity for $w < 0.001$ pr-cm or $p_e < 10$ mm Hg. Also see Ref. 31
3.2 μ ; 3.08 - 3.57 μ	$0.041 w^{1/2} p_e^{0.3}$	Also see Ref. 31
2.7 μ ; 2.3 - 3.08 μ	$0.23 w^{1/2} p_e^{0.32}$	Valid for total absorption < 0.15 μ
	$0.246 + 0.180 \log w + 0.109 \log p_e$	Valid for total absorption > 0.15 μ Also see Ref. 31
1.87 μ ; 1.67 - 2.08 μ	$0.053 w^{1/2} p_e^{0.3}$	Valid for total absorption < 0.097
	$0.0445 + 0.0810 \log w + 0.0505 \log p_e$	Valid for total absorption > 0.097 Also see Ref. 31
1.38 μ ; 1.19 - 1.56 μ	$0.0304 w^{1/2} p_e^{0.3}$	Valid for total absorption < 0.067
	$0.0384 + 0.0875 \log w + 0.0376 \log p_e$	Valid for total absorption > 0.067
1.1 μ ; 1.05 - 1.19 μ	$0.00375 w^{1/2} p_e^{0.26}$	
0.94 μ ; 0.89 - 1.00 μ	$0.00335 w^{1/2} p_e^{0.27}$	

NOTE: 1. All logs to the base 10.
2. w = pr-cm; p_e = mm Hg.

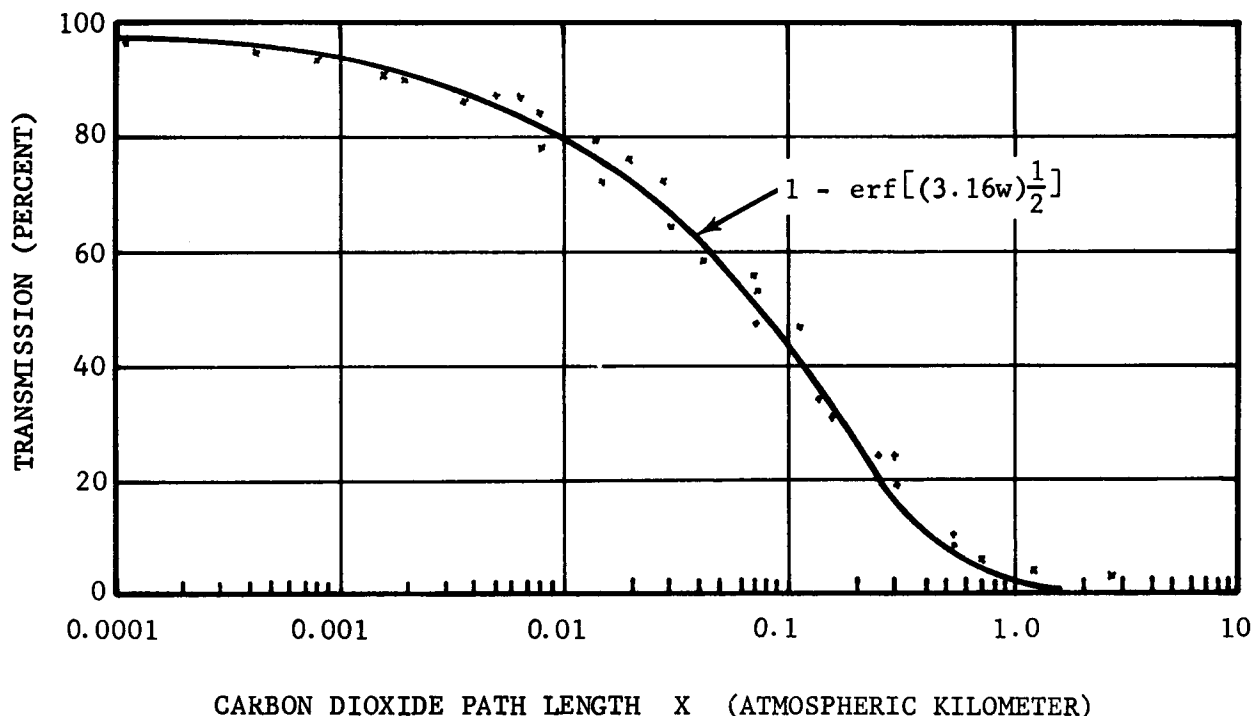


FIGURE 2-12. Experimental Fit of Burch and Williams Data to Error Function Absorption at 2.7 Microns

By far the largest window extends from 8 to 14 microns. Elder and Strong³⁹ and Streete^{39A} have related the wide-band transmission in each window to the amount of water vapor in the path. Their data should be used with caution since it is difficult to eliminate the effect of aerosol scattering (especially at wavelengths less than 5 microns) from absorption due to water vapor. The transmittance inside a window region is expected to vary as follows:

$$t = (1 - C\sqrt{w}) \exp [-(\alpha w + \beta_a X)] \quad (2-57)$$

where

C = constant to be determined

α = continuum absorption coefficient due to water vapor

w = amount of water vapor in the path

β_a = aerosol scattering coefficient
(par. 2-4.3.1)

X = path length

The second term on the right hand side of Eq. 2-57 is due to the few water vapor lines that

may exist in the window and is only important for short paths. The continuum absorption coefficient α is the sum of the contributions of all the distant water vapor lines in the neighboring bands and is a slowly varying function of wavelength. The measurements of Ref. 39 clearly show the effect of the exponential in Eq. 2-57 and the exponential variation of transmittance with w . Careful measurements in the 8- to 14-micron window have been performed in Refs. 40 and 41 to separate the effect of water vapor absorption from aerosol scattering. A plot of α in Eq. 2-57 vs wavelength λ is shown in Fig. 2-13. Transmission curves in the 8- to 14-micron window taking into account all these effects can be found in Ref. 42. Recent unpublished measurements by Burch indicate that absorption due to water vapor in the 8- to 14-micron window is strongly dependent on water vapor partial pressure. Thus at altitudes above a few kilometers where this partial pressure is down by an order of magnitude as compared to sea level, absorption due to water vapor should be negligible. This should apply also to the other windows.

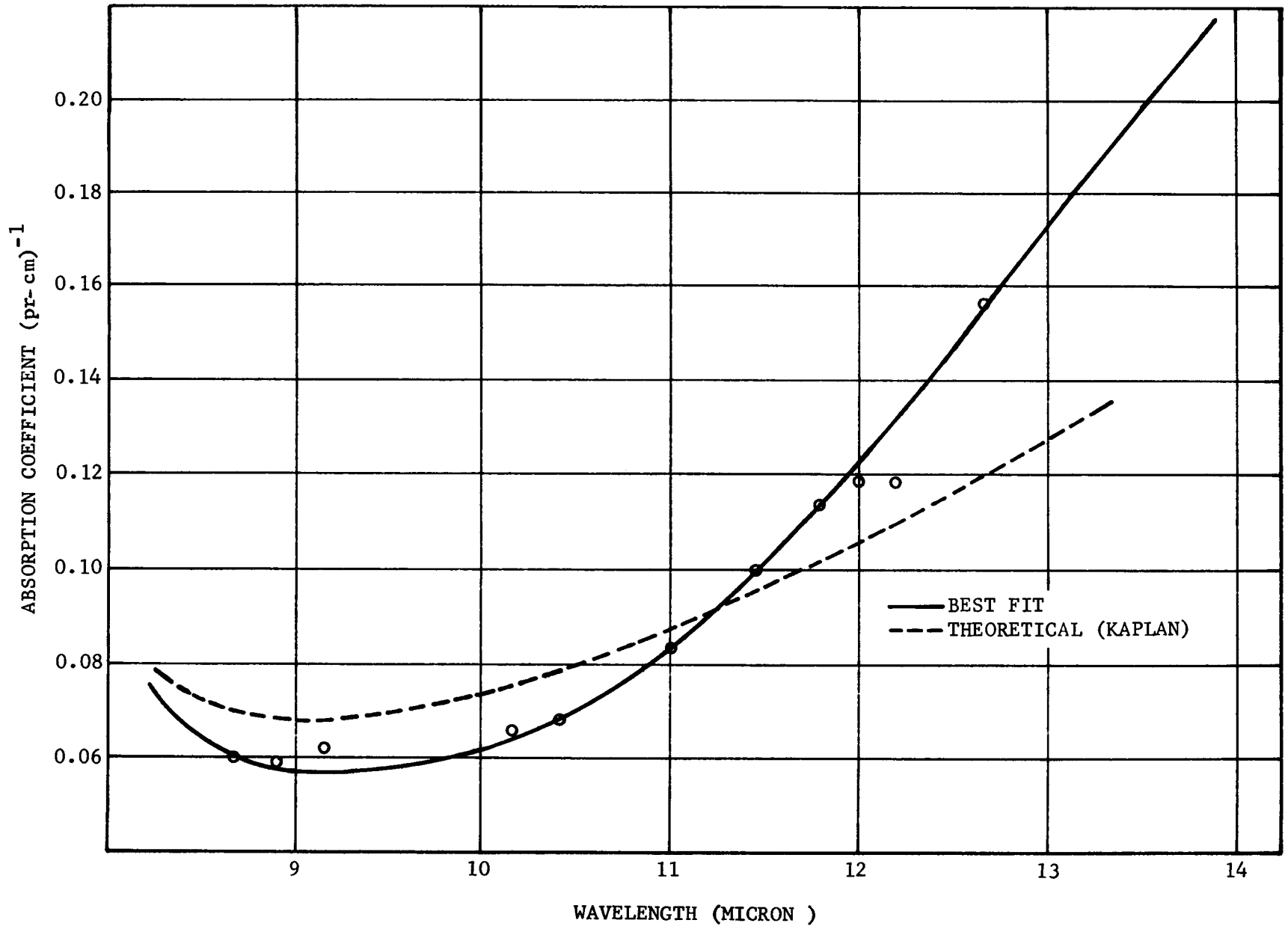


FIGURE 2-13. Variation of Continuum Absorption Coefficient vs Wavelength

2-4.2.4.4 Equivalent Sea-level Path

The problem of atmospheric absorption is complicated by the fact that in most cases the paths considered are slant paths along which the temperatures and pressures vary. The discussion and results in the previous paragraphs apply only to the case of constant pressure and temperature paths.

2-4.2.4.4.1 Equivalent-path Absorption Calculations

It is possible under certain conditions, however, to reduce a slant path through the atmosphere to an equivalent sea level path in which pressure and temperature are constant. The reduction can be easily justified if either the weak line or the strong line approximation holds²⁷. If the line intensities are not too dependent on temperature, the results are as follows:

(1) Weak Line Approximation:

The equivalent absorber content is w given by

$$w = \int_{Path} \zeta(h) \frac{dh}{\cos \theta} \quad (2-58)$$

where $\zeta(h)$ is the absorber concentration (atm-cm km⁻¹), h is the altitude (km), and θ is the zenith angle. The absorptance will be given by the first of Eq. 2-50.

(2) Strong Line Approximation:

The pressure and temperature corrected absorber content in a slant path is defined by⁴³

$$\bar{w} = \int \zeta(h) \left(\frac{dh}{\cos \theta} \right) p(h) \left[\frac{273}{T(h)} \right]^{1/2} \quad (2-59)$$

and the average pressure in the path is

$$\bar{p} = \frac{\bar{w}}{w} \quad (2-60)$$

where $p(h)$ is the pressure in atmospheres at altitude h , T is the temperature in degrees Kelvin and w is given by Eq. 2-58. Transmission through a slant path can then be obtained from any of the models discussed above (see the second part of Eqs. 2-50 and 2-56) either by replacing w wherever it occurs by \bar{w} , or by replacing γ by $\gamma\bar{p}$ where γ is the line half-width at sea level.

To evaluate the integrals in Eqs. 2-58 and 2-59, it is necessary to know $\zeta(h)$, $T(h)$, and $p(h)$. A discussion of absorber concentration was given in par. 2-4.2.2 and $\zeta(h)$ can be obtained from Table 2-5. A typical temperature profile is given in Fig. 2-9 and the pressure, which can be assumed to decrease exponentially with altitude, is given by

$$p = \exp(-h/7.5), \text{ atmospheres}$$

where h is in km and 7.5 km represents the average scale length of the atmosphere.

In the case of the Goody model, it can be shown⁴⁴ that the absorptance is given by an equation analogous to Eq. 2-54 which holds in both the weak and the strong line limits.

$$\alpha = 1 - \exp \left[- \frac{wS_0}{d \left(1 + \frac{wS_0}{\pi\gamma\bar{p}} \right)^{1/2}} \right] \quad (2-61)$$

where \bar{p} is defined by Eqs. 2-59 and 2-60, and w by Eq. 2-58.

2-4.2.4.4.2 Equivalent-path Absorber Contents

A typical atmospheric measurement situation is illustrated in Fig. 2-14, in which observer A, at an altitude h_1 , views object B, at altitude h_2 , along a slant path, at zenith angle θ . The exact calculations of absorber content along this path are quite complex. There are certain simplifications however, which, for most problems, will permit rapid estimates of absorber contents to be made. If the zenith angle θ is less than 85 deg, the curvature of the earth can be ignored and absorber contents estimated by dividing vertical path contents by $\cos \theta$. Values for w (uncorrected curve) and \bar{w} (pressure-corrected curve), for a vertical path extending from any altitude to a point outside the earth's atmosphere, may be obtained from Fig. 2-15 for any gas with constant mixing ratios (CO₂, CH₄, etc.). Values for w and \bar{w} are given in atm-km but may be converted to atm-cm by using Table 2-5. Water vapor w and \bar{w} values can be obtained from Fig. 2-16 for a dry model atmosphere and a wet model atmosphere⁴⁵.

Another situation which lends itself to simplified calculations involves slant paths near horizontal and path altitudes which vary only slightly (they can only occur for path lengths

less than 100 km). In this case, for a uniformly distributed absorber such as CO₂,

$$\bar{w} = w_o \exp[-h/7.5] \quad (2-62)$$

and

$$\bar{w} = w_o \exp[-2h/7.5] \quad (2-63)$$

where

h = path altitude, km
 w_o = absorber content for the same path length at sea level

Absorber values w for ozone and water vapor may be approximated from Figs. 2-7 and 2-9, respectively. It should be understood, however, that values for any actual problem can vary considerably from those given in these figures. Approximate values for \bar{w} for ozone and water vapor can be obtained by multiplying the w values by $\exp(-h/7.5)$.

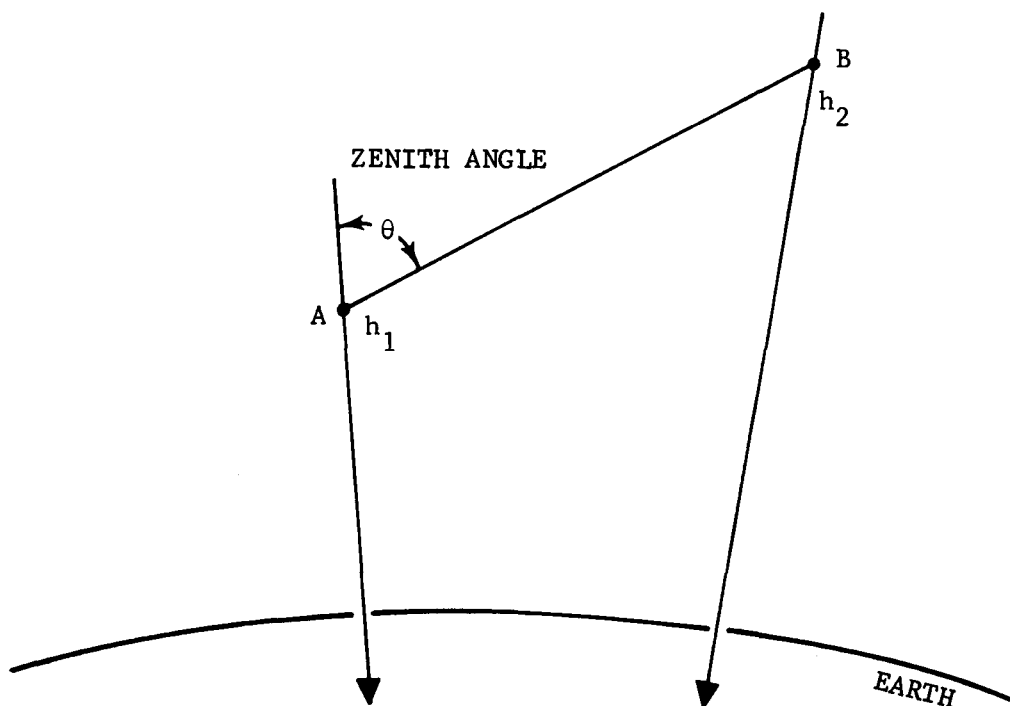


FIGURE 2-14. Geometrical Relation Between Observer A and Object B

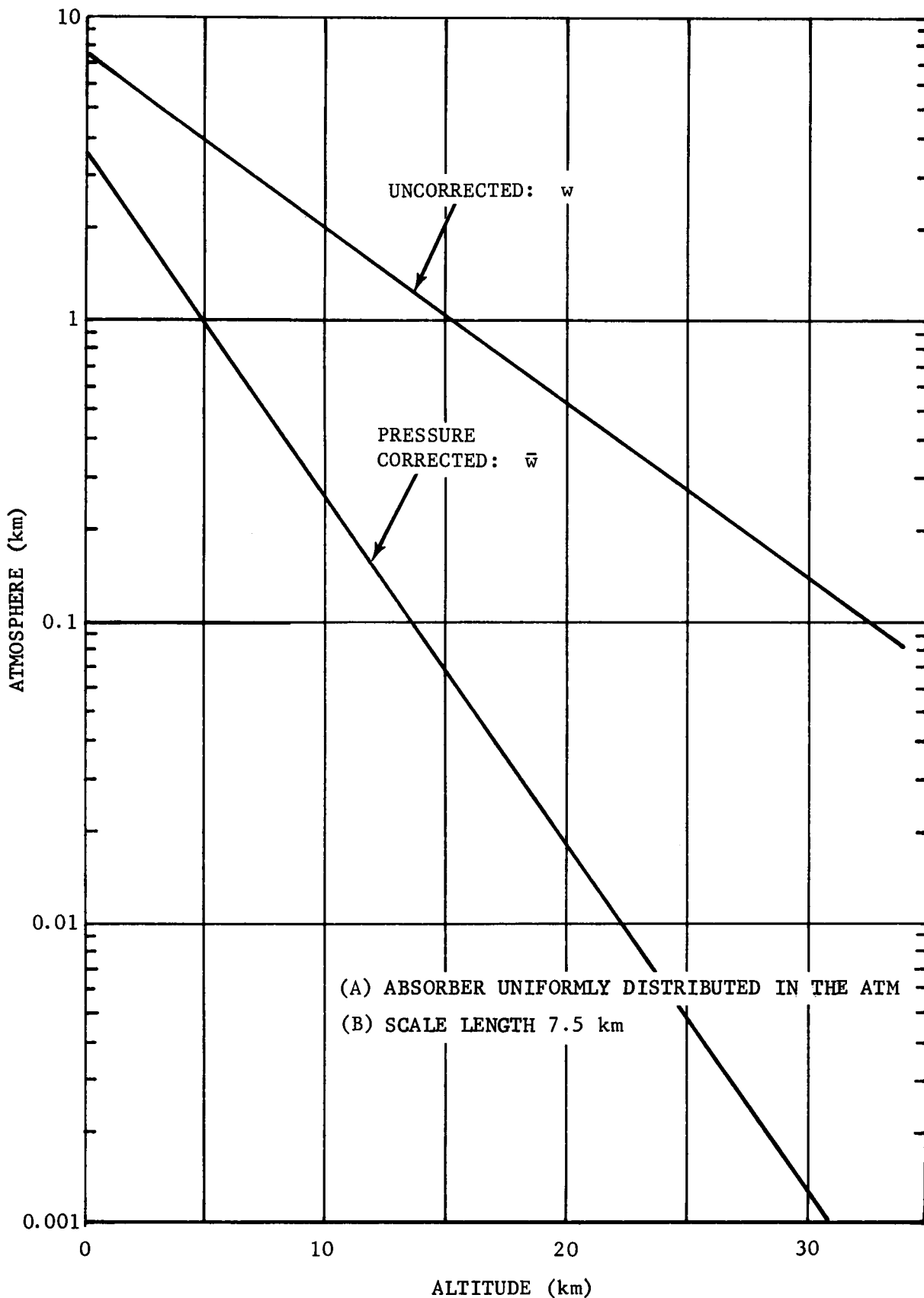


FIGURE 2-15. IR Absorber Content Above a Given Altitude

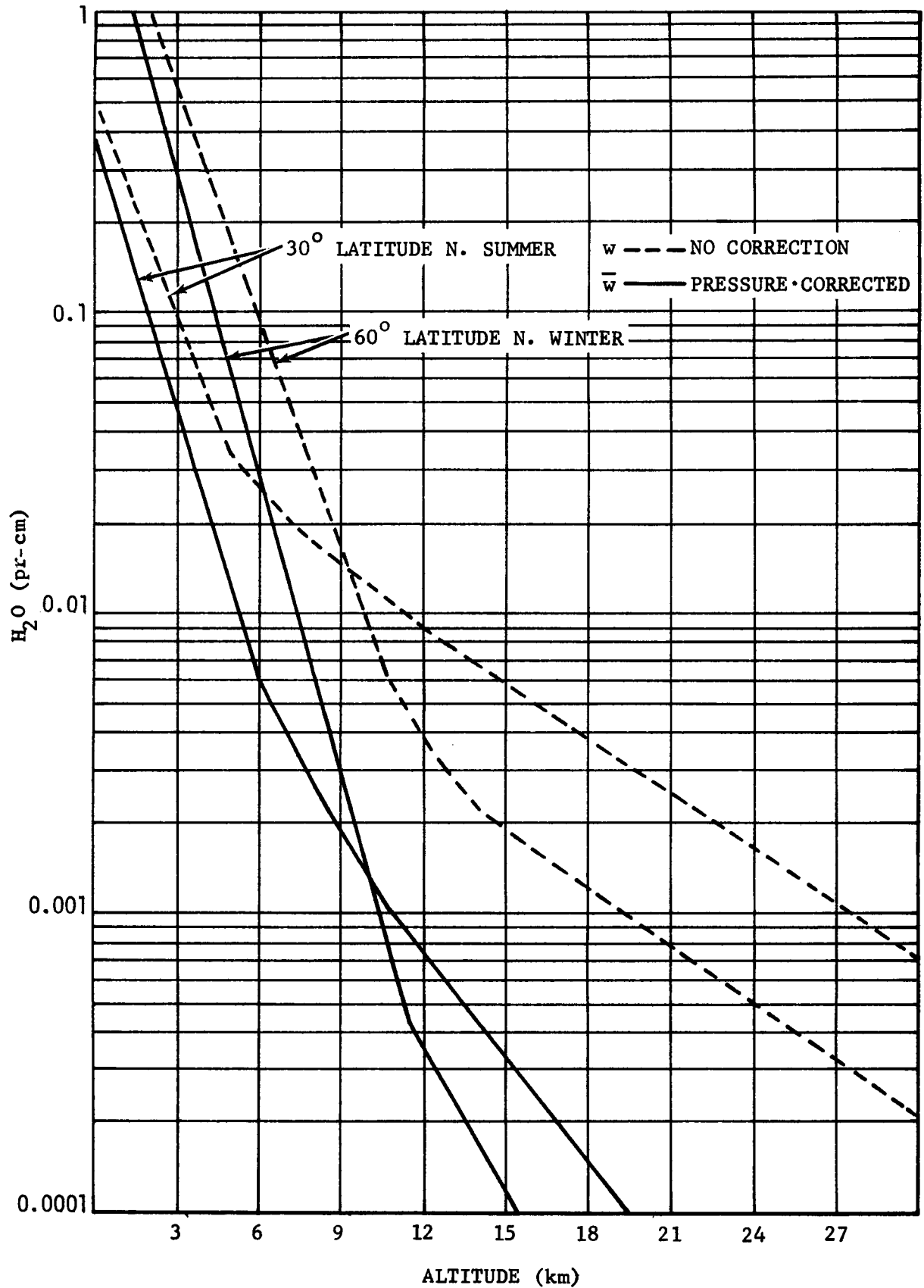


FIGURE 2-16. Water Vapor Content Above a Given Altitude

CHAPTER 3

IR SYSTEM COMPONENTS*

3-1 INTRODUCTION

The various major components and techniques which enable active as well as passive IR systems to emit, focus, detect, and process IR signals for any of a number of end uses are discussed here. The interrelated functions of the individual components when joined to form a variety of standard as well as specialized IR systems are then analyzed in Chapters 4 and 5.

A thorough understanding of the function of these components is essential in order to make possible the economical design of an operationally optimum IR system. The functional relationship of the major disciplines of IR technology and the associated design specialties are indicated in Fig. 3-1. The essential elements used in IR systems are identified and discussed in the following paragraphs within this chapter:

- 3-2 Optics
- 3-3 Emitters and Illuminators
- 3-4 Detectors
- 3-5 Cooling Systems
- 3-6 Signal Processing
- 3-7 Data Display and Recording
- 3-8 Testing IR and Associated Equipment
- 3-9 Ancillary IR Components and EMI Rejection Techniques

An attempt is made in this chapter to update information previously published regarding these components and techniques. Specifically, recent technological advancements in the following areas are thought to merit special attention:

a. Long wavelength IR (LWIR) multi-sensor arrays and associated electronics attained the level of development which now makes possible thermal mapping of terrestrial expanses in the 8- to 14-micron region. The use of LWIR arrays in space for object detection and in satellite communication systems represents a major achievement in space technology.

b. Cryogenic electronics have been developed for use in processing the output of high-sensitivity LWIR sensors. This electronic advancement is treated here in the context of the components discussion and in AMCP 706-128 in terms of systems application.

c. Other components such as lasers, illuminators, and displays are discussed in fairly detailed form because of their novelty and the increasing interest in their application. The advent of the lasers and, especially, the recent development of high-power IR lasers has opened new frontiers in optical range finding and detection. The relative novelty of lasers, compared to other IR components, is responsible for the lack of detailed published data on the subject; consequently, a comprehensive discussion is included here as the preface for the design criteria discussion on laser systems. The remaining material included in the lasers chapter appears in current IR publications; however, an attempt is made here to update that material by including any new significant developments.

d. The requirement for real-time observation of high data-rate IR information in performing surveillance and tactical tasks has prompted detailed discussions of display systems, man-machine interface considerations, and human engineering techniques. These are discussed partly in this chapter and partly in Chapter 5.

*Written by K. Seyrafi.

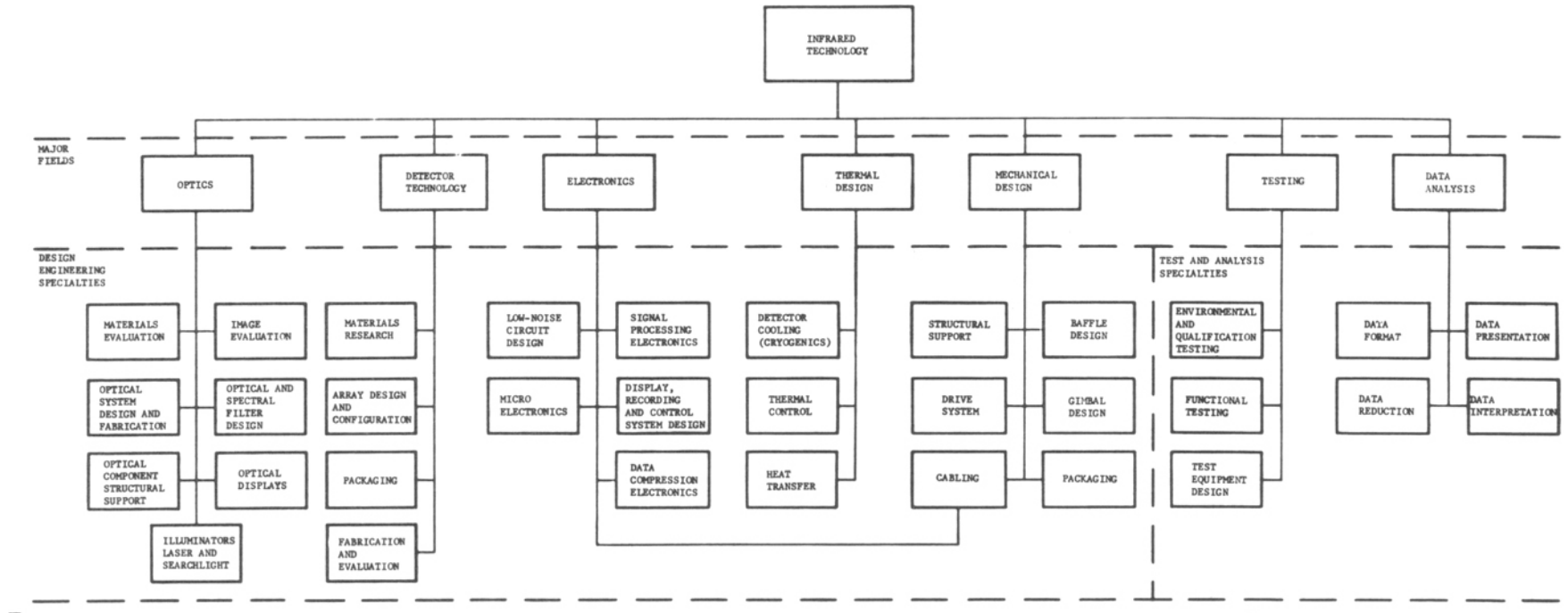


FIGURE 3-1. Functional Relationship of the Major Disciplines and Associated Design Specialties

3-2 OPTICS

3-2.1 OPTICAL MATERIALS

3-2.1.1 Material Types

3-2.1.1.1 *Refractive Materials*

Infrared transmitting materials include various types of glass, crystals, and plastics. In the glass category are the oxide (regular optical, high silica and fused quartz, and special oxide glasses) and nonoxide materials. Although physically suited for IR applications, the transmission range of oxide glasses is limited to wavelengths of 6 microns or less. Oxide glasses usually exhibit absorption in the 2.7- to 3.3-micron region due to the water content in the material; however, some "water free" types have been developed. Nonoxide glasses which transmit to longer wavelengths (some to 20 microns) tend to be softer and have lower softening points. Significant improvements are being made in the nonoxide chalcogenide (sulfur, selenium, and tellurium) glasses¹. Results of investigations of many combinations and variations of glasses are reported in some of the open literature listed in the bibliography.

Crystalline materials can be either single crystalline or polycrystalline. The single crystal materials have been used primarily at the longer wavelengths, but available size, cost, and unsuitable physical properties have been limiting factors in many engineering applications. The number and size of polycrystalline materials have increased significantly during recent years. Among these are chiefly ITRAN* materials made by Eastman Kodak and KRS-5 materials.

Plastic materials, in general, are considered unsuitable for use as optical components in IR instruments—mainly because of poor mechanical properties, low scratch resistance, temperature instability, instability due to water absorption, and difficult surface finishing characteristics. The following exceptions should be noted:

1. Metal-backed epoxy mirrors can be successfully fabricated by a molding (replication) technique. Aspheric surfaces can be readily produced, thereby, resulting in components which are generally adequate for condenser systems.

2. Polystyrene has a large number of stable narrow absorption bands in the IR region. This characteristic makes it an excellent standard in the form of thin sheet for wavelength calibration of IR spectrometers and related instruments.

The index of refraction for all commercially available plastics ranges between the limits 1.49 for Lucite or Plexiglas to 1.59 for polystyrene.

3-2.1.1.2 *Reflective Materials*

The limited selection of suitable IR transmitting materials along with limiting size considerations have promoted the use of reflective elements in IR systems. Substrate materials used include fused quartz, Pyrex, low-expansion fused silica, glass-ceramics and metals (especially beryllium and aluminum). Vacuum-deposited aluminum is most frequently used as a reflective coating, although silver, gold, copper, and rhodium are also effective. Protective coatings of silicon monoxide or magnesium fluoride, which may also increase the reflectivity of the primary coating, are usually applied.

Beryllium, stainless steel, aluminum, and fused quartz are used in fabricating mirror substrates for cold optical devices which must be cooled to cryogenic temperatures to avoid becoming performance-limited due to background photon fluctuations. From a thermal standpoint, the mirror substrate material must have high thermal conductivity and thermal diffusivity characteristics and, if possible, low thermal capacity. These combined characteristics determine the ease with which the optical element can be cooled to the required operating temperature and maintained in a thermal gradient-free condition.

*ITRAN is a proprietary name of Eastman Kodak Co. for optical materials which transmit in the 3-5 and 2-14 μ bands.

TABLE 3-1. SALIENT CHARACTERISTICS OF OPTICAL IR MATERIALS


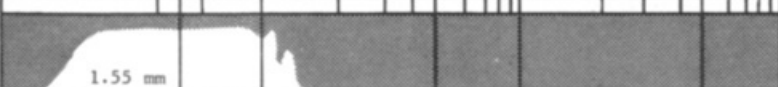
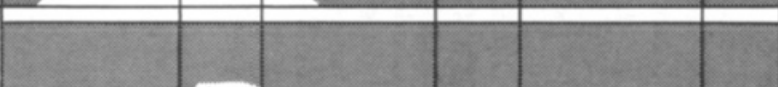






	MATERIAL	WAVELENGTH (MICRONS)								% REFL LOSS	REFRA INDEX n	WATER SOLUB g/100g	HDNS KNOOP	EXP COEF $10^{-6}/^{\circ}\text{C}$	SP GR
		0.5	1.0	2	5	10	20	30	50						
1	POTASSIUM DIHYDROGEN PHOSPHATE (KDP)									7	1.49-1.51	33			2.34
2	AMMONIUM DIHYDROGEN PHOSPHATE (ADP)									8	1.47-1.50	36.8			1.80
3	GALLIUM PHOSPHIDE (GaP)									40	3.0 at 2_{μ}			5.3	
4	OPTICAL GLASS									7-20	1.45-1.98	INSOL	300-600	4-10	2.5-36
5	SODIUM NITRATE (NaNO_3)	Details not available								4	1.334 at 0.67_{μ}	88	19.2	12	2.26
6	GALLIUM ANTIMONIDE (GaSb)									51	3.789 at 2.0_{μ}	INSOL		6.9	
7	QUARTZ, FUSED (SiO_2)									6	1.438 at 2.0_{μ}	INSOL	1600	0.55	2.20
8	Kel-F														
9	CALCIUM CARBONATE (CaCO_3)									11	1.624 at 2.0_{μ}	.0014	3 Moh	25	2.71
10	CALCIUM ALUMINATE GLASS									11	1.63 at 2_{μ}		600	8.3	3.07

TABLE 3-1. SALIENT CHARACTERISTICS OF OPTICAL IR MATERIALS (Continued)








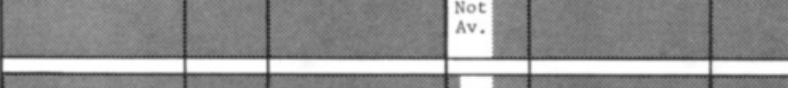

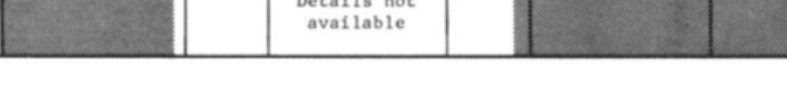
	MATERIAL	WAVELENGTH (MICRONS)						% REFL LOSS	REFRA INDEX n	WATER SOLUB g/100g	HDNS KNOBP	EXP COEF 10 ⁻⁶ /°C	SP GR
		0.5	1.0	2	5	10	20 30 50						
11	SPECIAL OXIDE GLASSES							15	1.8 at 2 _μ	INSOL	≥400	8-10	3.0- 6.0
12	SPINEL (MgO· 3.5Al ₂ O ₃)							13	1.724 at 0.66 _μ	INSOL	1140	5.9	3.61
13	TITANIUM DIOXIDE (TiO ₃)(Rutile)							29	2.399 at 2.0 _μ	INSOL	890	7-9	4.26
14	SAPPHIRE (Al ₂ O ₃)							13	1.73 at 2.2 _μ	INSOL	~1700	5.8- 7.7	3.98
15	STRONTIUM TITANATE (SrTiO ₃)							25	2.21 at 3.4 _μ		595	9.4	5.12
16	INDIUM ARSENIDE (InAs)							46	3.4 at 6 _μ	INSOL		5.3	
17	LEAD SULFIDE (PbS)(film)							54	4.10 at 3.0 _μ	8.6x10 ⁻⁵			7.5
18	LEAD SELENIDE (PbSe)(film)							58	4.5 at 2.2 _μ	INSOL		18.4	8.1
19	LEAD TELLURIDE (PbTe)(film)							64	5.35 at 3 _μ				8.16
20	LANTHANUM FLUORIDE (LaF ₃)							16	1.82 at 0.58 _μ	INSOL	MED HARD		5.94

TABLE 3-1. SALIENT CHARACTERISTICS OF OPTICAL IR MATERIALS (Continued)

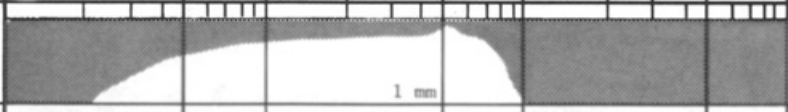
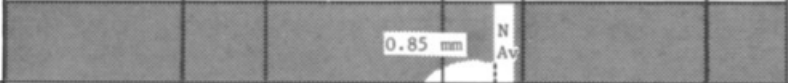

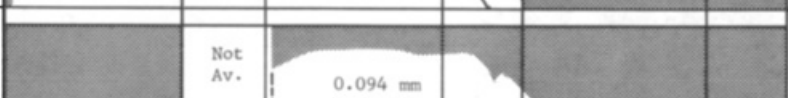
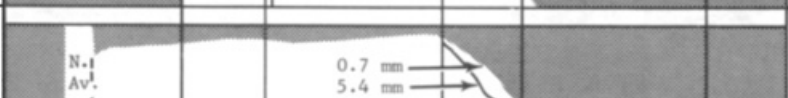
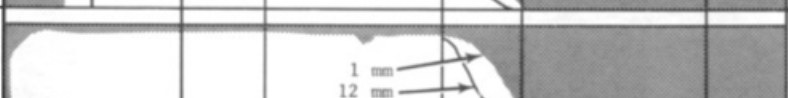

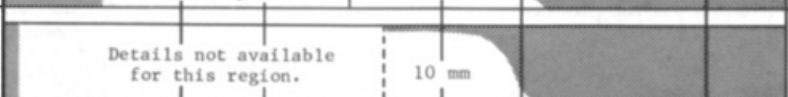
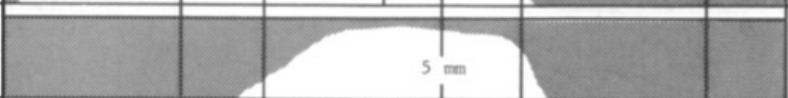
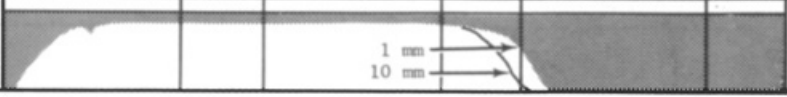
	MATERIAL	WAVELENGTH (MICRONS)	% REFL LOSS	REFRA INDEX n	WATER SOLUB g/100g	HDNS KNOOP	EXP COEF $10^{-6}/^{\circ}\text{C}$	SP GR
21	IRTRAN 5 (Polycrys. MgO)		7	1.482 at 8_{μ}	INSOL	640	11.5	3.58
22	TELLURIUM (Te)		60,69	4.83, 6.29 at 6.0_{μ}	INSOL	2.3 Moh	16.75	6.24
23	MAGNESIUM FLUORIDE (MgF_2)		5	1.38 at 0.70_{μ}	.0076	415	16.6	3.17
24	BARIUM TITANATE (BaTiO_3)		29	2.40			400	5.9
25	MAGNESIUM OXIDE (MgO)		12	1.68 at 3.3_{μ}	INSOL	690	13.8	3.57
26	LITHIUM FLUORIDE (LiF)		4	1.35 at 4.0_{μ}	0.3	110	3.7	2.64
27	CADMIUM FLUORIDE (CdF_2)		10	1.576 at 0.59_{μ}	4.4	3 Moh	22.0	6.34
28	MANGANESE FLUORIDE (MnF_2)		5	1.4 at 6_{μ}	.0076	MED HARD		3.98
29	T-12		6	1.41 at 3.3_{μ}	0.20	4.5 Moh	20.6	4.35
30	CALCIUM FLUORIDE (CaF_2)		5	1.40 at 5.0_{μ}	.0013	160	22	3.18

TABLE 3-1. SALIENT CHARACTERISTICS OF OPTICAL IR MATERIALS (Continued)

	MATERIAL	WAVELENGTH (MICRONS)								% REFL LOSS	REFRA INDEX n	WATER SOLUB g/100g	HDNS KNOOP	EXP COEF $10^{-6}/^{\circ}\text{C}$	SP GR
		0.5	1.0	2	5	10	20	30	50						
31	STRONTIUM FLUORIDE (SrF_2)									6	1.439 at 0.58μ	.0117	4 Moh		4.28
32	CESIUM FLUORIDE (CsF)									7	1.478 at 0.59μ	.367 at 18°			3.59
33	IRTRAN 3 (Polycrys. CaF_2)									3	1.300 at 10μ	.0017	200	24	3.18
34	IRTRAN 2 (Polycrys. ZnS)									24	2.151 at 13μ	INSOL	354	6.8	4.09
35	INDIUM PHOSPHIDE (InP)									40	3.0 at 10μ				
36	ZINC SULFIDE (ZnS) (film)														4.1
37	INDIUM ANTIMONIDE (InSb)									52	3.95 at 10μ			5.5	
38	CADMIUM TELLURIDE (CdTe)									32	2.56 at 10μ			4.5	6.2
39	POTASSIUM FLUORIDE (KF)									5	1.361 at 0.57μ	92.3 at 18°			2.48
40	IRTRAN 1 (Polycrys. MgF_2)									4	1.34 at 4.87μ	.0076	576	10- 12	3.18

TABLE 3-1. SALIENT CHARACTERISTICS OF OPTICAL IR MATERIALS (Continued)

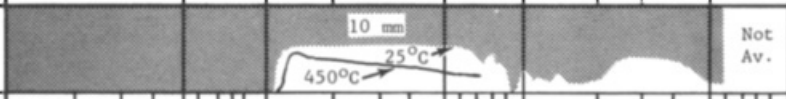
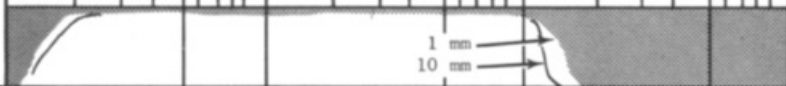
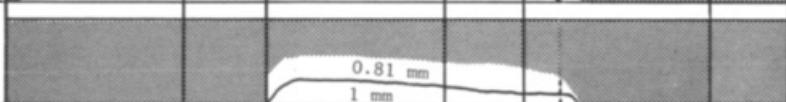


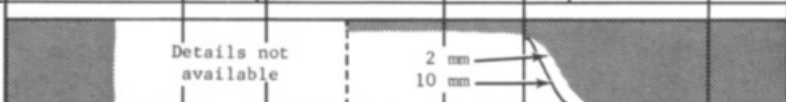
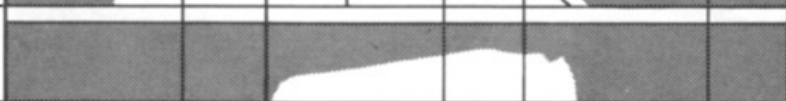
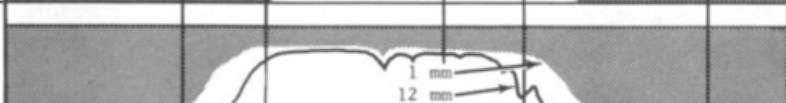
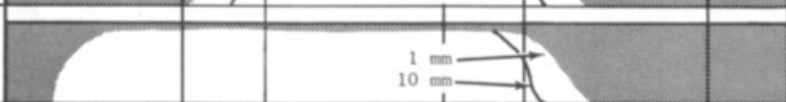
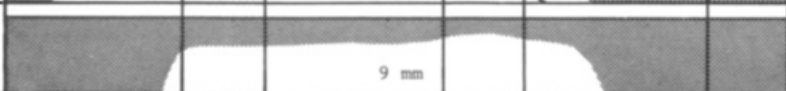
	MATERIAL	WAVELENGTH (MICRONS)						% REFL LOSS	REFRA INDEX n	WATER SOLUB g/100g	HDNS KNOOP	EXP COEF 10 ⁻⁶ /°C	SP GR	
		0.5	1.0	2	5	10	20 30 50							
41	SILICON (Si)							Not Av.	46	3.42 at 5.0 _μ	INSOL	1150	4.15	2.33
42	BARIUM FLUORIDE (BaF ₂)							7	1.45 at 5.2 _μ	0.12	82	15-18	4.83	
43	GALLIUM ARSENIDE (GaAs)							42	3.135 at 10 _μ	INSOL			5.7	
44	POLYETHYLENE													
45	POLYMETHYL METHACRYLATE							7	1.49 at .6 _μ				6.3	1.19
46	LEAD FLUORIDE (PbF ₂)							11	1.65 at 4.0 _μ	0.064	200			8.24
47	CADMIUM SULFIDE (CdS)							27	2.30 at 1.2 _μ	INSOL	122		4.2	4.82
48	ARSENIC TRISULFIDE GLASS (As ₂ S ₃)							29	2.41 at 5.0 _μ	INSOL	125		24.6	3.2
49	SODIUM FLUORIDE (NaF)							3	1.27 at 8.0 _μ	4.2	60		36	2.79
50	CuCl								1.93	6.2×10 ⁻³				3.53

TABLE 3-1. SALIENT CHARACTERISTICS OF OPTICAL IR MATERIALS (Continued)



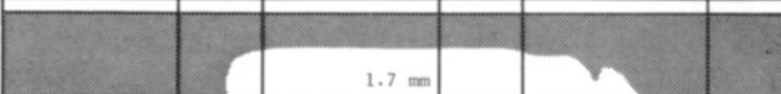
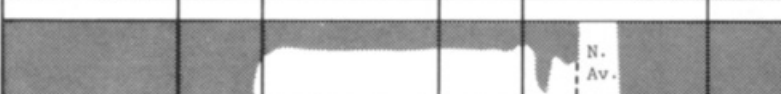
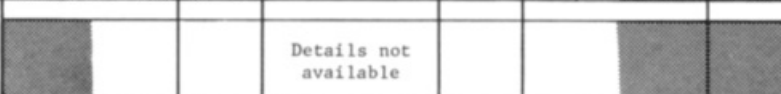
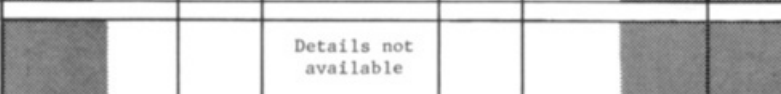
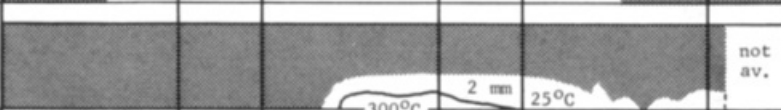
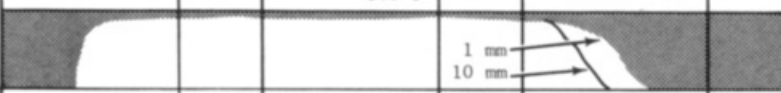
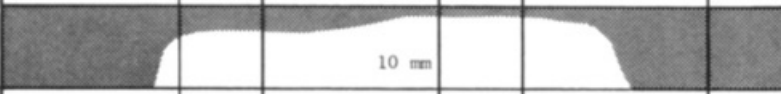

	MATERIAL	WAVELENGTH (MICRONS)	% REFL LOSS	REFRA INDEX n	WATER SOLUB g/100g	HDNS KNOOP	EXP COEF $10^{-6}/^{\circ}\text{C}$	SP GR
51	IRTRAN 4 ⁺ (Polycrys. ZnSe)		27	2.310 at 20 μ	INSOL	150	7.5	5.27
52	SILICON MONOXIDE (film) (SiO)				INSOL			
53	Cd Se				INSOL			5.81
54	ARSENIC SELENIUM GLASS (Se(As))		31	2.48 at 5.0 μ	INSOL		34	
55	SODIUM BROMIDE (NaBr)		11	1.638 at 0.61 μ	91			3.20
56	SODIUM IODIDE (NaI)		14	1.765 at 0.65 μ	180			3.67
57	GERMANIUM (Ge)		52	4.001 at 16 μ	INSOL	6.25 Moh	5.5-6.5	5.327
58	SODIUM CHLORIDE (NaCl)		8	1.495 at 10.0 μ	36	15.2	44	3.16
59	SILVER CHLORIDE (AgCl)		19	1.95 at 15.0 μ	INSOL	9.5	30	5.59
60	SELENIUM (AMORPHOUS) (Se)		30	2.45 at 2.5 μ			36.8	4.26

TABLE 3-1. SALIENT CHARACTERISTICS OF OPTICAL IR MATERIALS (Continued)

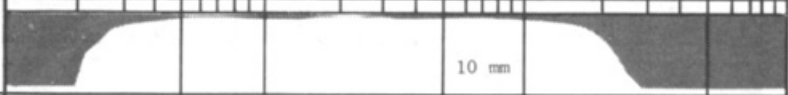
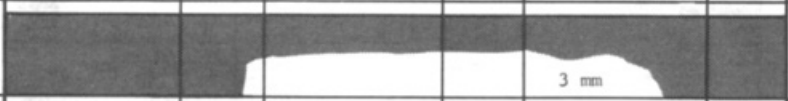
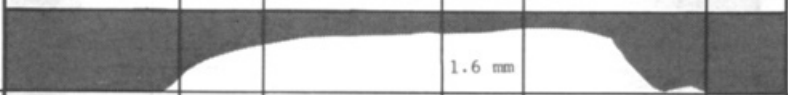
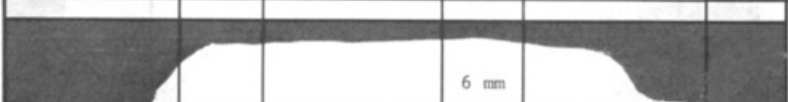
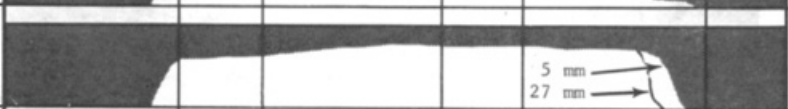
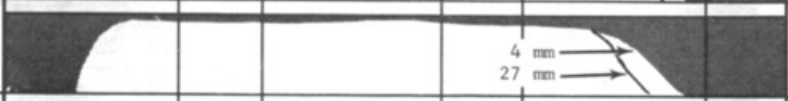
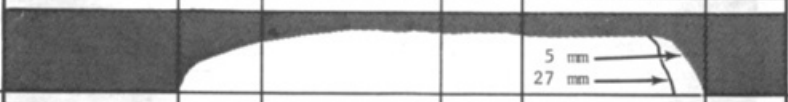
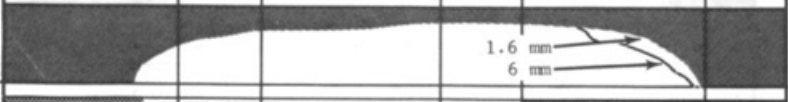



	MATERIAL	WAVELENGTH (MICRONS)						% REFL LOSS	REFRA INDEX n	WATER SOLUB g/100g	HDNS KNOOP	EXP COEF $10^{-6}/^{\circ}\text{C}$	SP GR
		0.5	1.0	2	5	10	20 30 50						
61	POTASSIUM CHLORIDE (KCl)							5	1.363 at 23μ	34.7	7.2 9.3	36	1.99
62	IRTRAN 6 ⁺ (Polycrys. CdTe)							34	2.673 at 10μ	INSOL	45	5.7	5.85
63	CESIUM CHLORIDE (CsCl)	Details not available						11	1.644 at 0.54μ	186			3.97
64	THALLIUM CHLORIDE (TlCl)							24	2.193 at 10μ	0.32	12.8	53	7.02
65	KRS-6 (TlBr-TlCl)							24	2.18 at 9.0μ	0.32	30	50	7.19
66	SILVER BROMIDE (AgBr)							25	2.232 at 0.67μ	INSOL		34.9	6.47
67	POTASSIUM BROMIDE (KBr)							8	1.524 at 11.0μ	65.2	27	43	2.75
68	KRS-5 (Tl(Br,I))							28	2.371 at 10μ	0.05	40.2	58	7.37
69	THALLIUM BROMIDE (TlBr)							28	2.338 at 9.98μ	0.05	11.9	51	7.45
70	POTASSIUM IODIDE (KI)	Details not available						11	1.62 at 10μ	144	5	42.6	3.13

TABLE 3-1. SALIENT CHARACTERISTICS OF OPTICAL IR MATERIALS (Continued)

	MATERIAL	WAVELENGTH (MICRONS)												% REFL LOSS	REFRA INDEX n	WATER SOLUB g/100g	HDNS KNOOP	EXP COEF $10^{-6}/^{\circ}\text{C}$	SP GR
		0.5	1.0	2	5	10	30	20	50										
71	CESIUM BROMIDE (CsBr)													11	1.64 at 20μ	124.3	19.5	47.9	4.44
72	CESIUM IODIDE (CsI)													13	1.727 at 20μ	85	SOFT	50	4.53
73	DIAMOND (C)													29	2.417 in.vis.	INSOL	10 Moh	1.38	3.51

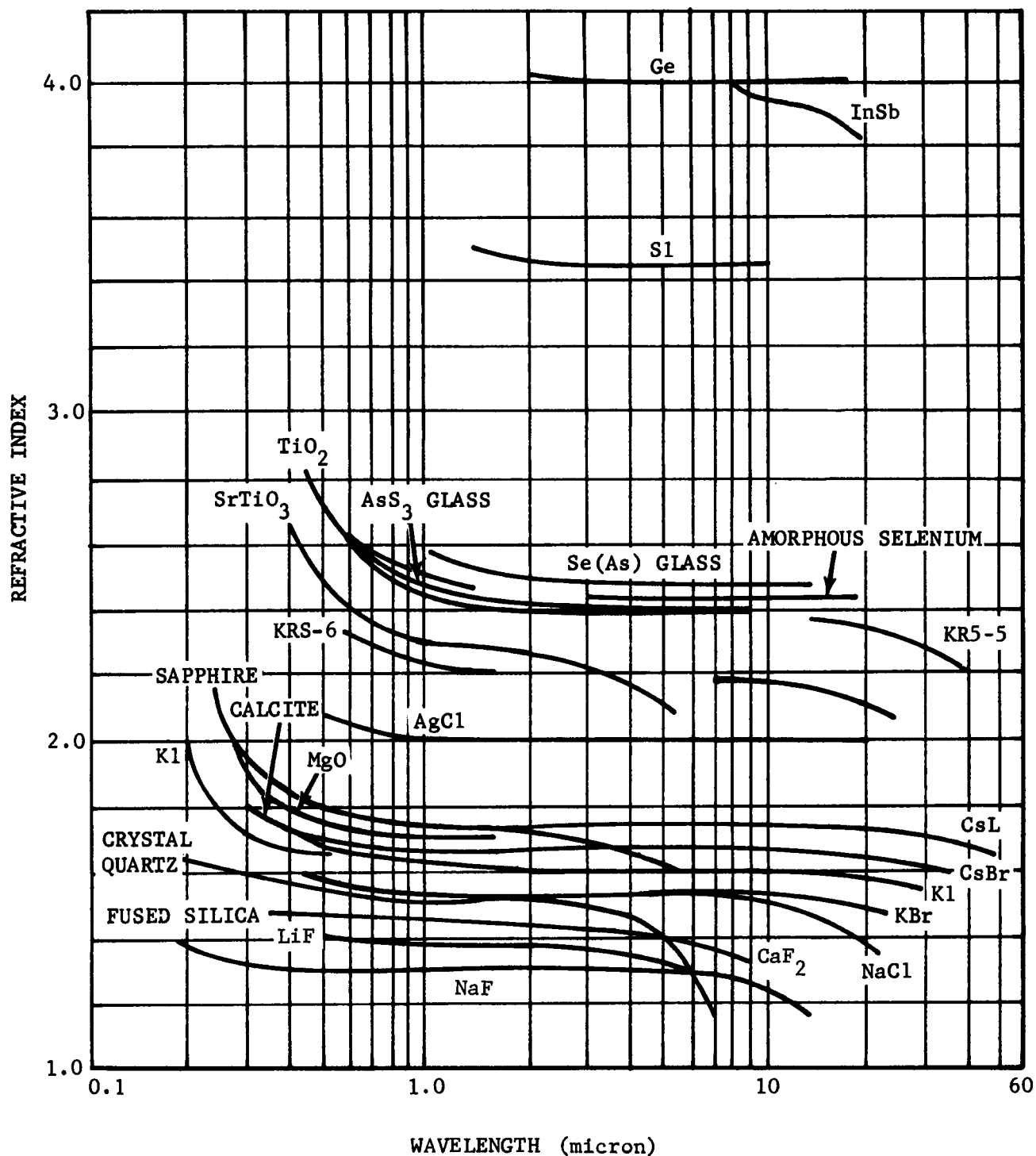


FIGURE 3-2. Refractive Index vs Wavelength for Several Optical Materials

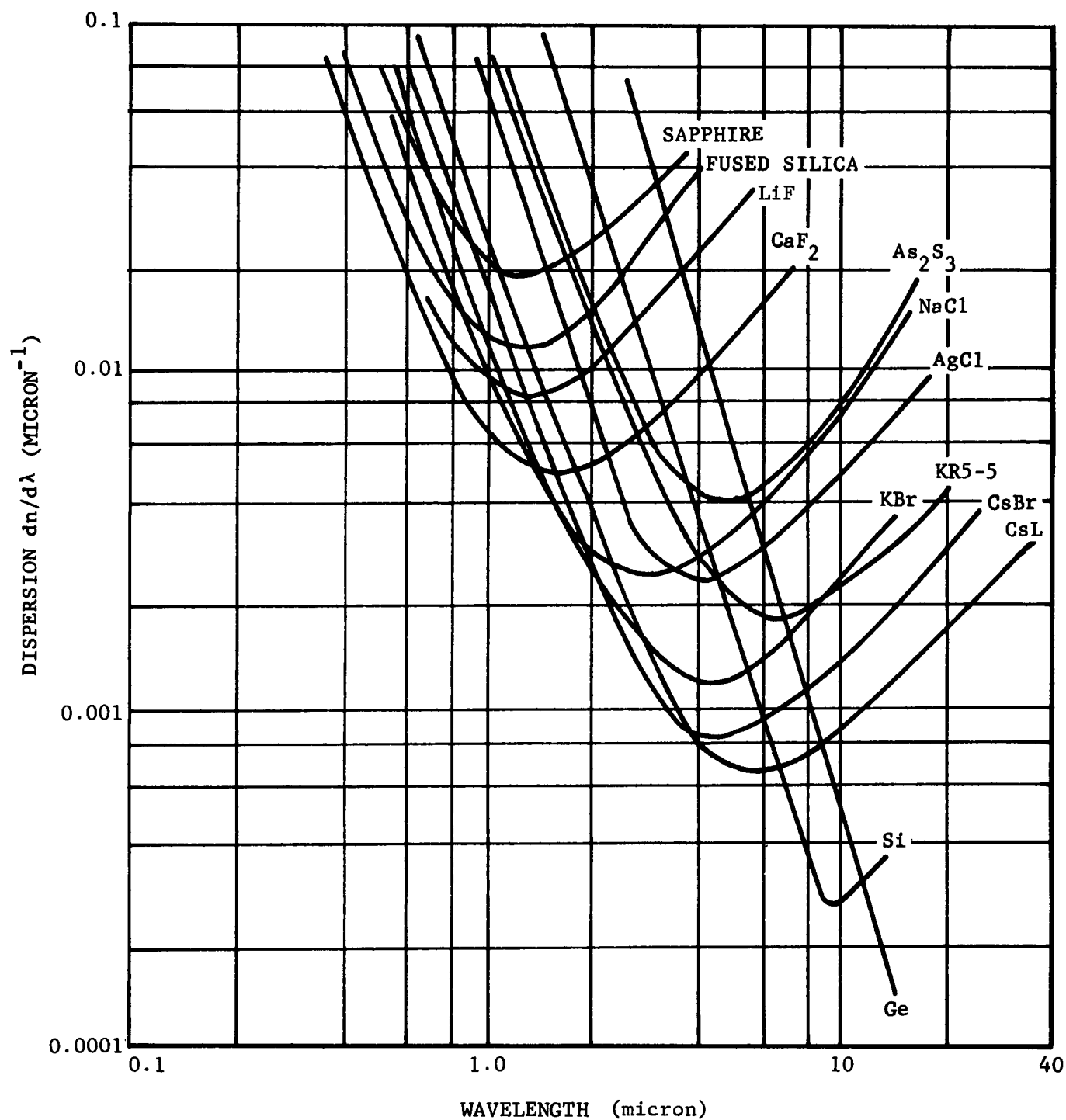
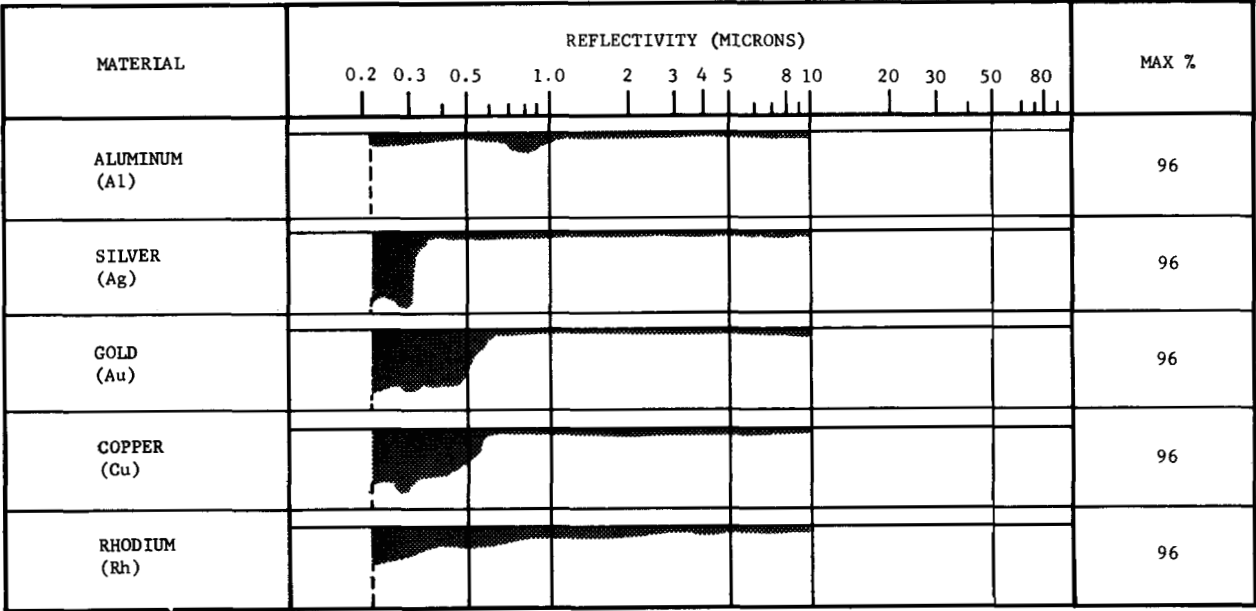


FIGURE 3-3. Dispersion vs Wavelength for Several Optical Materials

TABLE 3-2. MIRROR MATERIALS

MATERIAL	SPECIFIC GRAVITY	EXPANSION COEFFICIENT, $10^{-6} / ^\circ\text{C}$	MELTING POINT, $^\circ\text{C}$	YOUNG'S MODULUS, 10^6 psi	THERMAL CONDUCTIVITY, $\text{cal cm}^{-1} \text{sec}^{-1} ^\circ\text{C}^{-1}$	SPECIFIC HEAT	HARDNESS, KNOOP
Fused Quartz	2.20	0.55	1600	10.5	0.0033	0.188	460
Pyrex (7740)	2.23	3.2	820	9.5	0.0027	0.233	480
Vycor (7900 series)	2.18	0.80	1500	6.7	0.0035	0.19	530
Glass-ceramics							
Pyroceram (9606)	2.61	5.7	1350	17.3	0.0087	0.230	698
Pyroceram (9608)	2.50	0.4 - 2.0	1250	12.5	0.0047	0.235	703
CER-VIT C-101	2.50	0.15		13.4	0.0040	0.217	540
Aluminum	2.70	23.9	680	6.9	0.53	0.215	2.0 Moh
Beryllium	1.82	12.4	1300	28.0	0.38	0.516	
Invar (36% Ni)	8.0	1.30		14.8	0.026	0.095	
Magnesium	1.74	26		4.5	0.38	0.25	2.0 Moh
Titanium	4.54	8.5		11.6	0.042	0.126	

TABLE 3-3. REFLECTIVITY CHARACTERISTICS OF COMMON MIRROR COATINGS



CHAPTER 4

IR SYSTEMS DESCRIPTION*

Even a cursory survey of the various infrared systems that have been produced, delivered, or proposed leaves the uninitiated with the impression of a bewildering array of different uses and techniques. In this chapter it will be shown that a coherent set of underlying principles exist which allow IR systems to be described and

understood in terms of a relatively few functional parameters. These parameters will be identified and used to describe and categorize the systems. The following chapter, Chapter 5, will expand the discussion into specific system analyses and design methods. Table 4-1 defines the terms used.

TABLE 4-1. INFRARED SYSTEM DEFINITIONS

SYMBOL	TERM	DEFINITION	UNITS
A_d	Detector area	Area of sensitive surface of a detector	cm^2
A_T	Target area	Cross-sectional area of a target	cm^2
<i>Airy disc</i>	Central bright portion of the diffraction pattern	----	----
c	Speed of light	$2.997925 \times 10^{10} \text{ cm sec}^{-1}$	
D^*	Detectivity	Detector figure of merit	$\text{cm Hz}^{1/2} \text{ w}^{-1}$
D_o	Optical diameter	Diameter of a circular entrance aperture of an optical system	cm
F	f/number (f/no.)	Ratio of focal length to optical diameter	dimensionless
$\ddagger \Delta f$	Noise equivalent bandwidth	Bandwidth of white noise which has the same integrated noise power as the total power of the actual noise	Hz
Δf_e	Electrical bandwidth	Bandwidth between the two half-power points of the amplitude response of the network	Hz

* Written by S. J. Halasz

\ddagger For a white noise and an ideal bandpass filter, the filter bandwidth and noise equivalent bandwidth are the same. However for nonwhite noise or practical filter, the filter bandwidth and noise equivalent bandwidth are different.

The noise spectrum of most IR detectors and systems are white or close to white (with the exception of the low frequency band below 10 or 20 Hz). The filter bandwidth and noise equivalent bandwidth have therefore, almost the same values.

TABLE 4-1. INFRARED SYSTEM DEFINITIONS (Continued)

SYMBOL	TERM	DEFINITION	UNITS
$*\Delta f'_e$	Optimum electrical bandwidth	----	Hz
f_d	Scanner spin rate	Rate of spin of a rotating mechanical scanner	revolutions per second (rps), rpm
fl	Focal length	Effective focal length of an optical system	cm
H	Irradiance	----	w cm ⁻²
ΔH	Change in spectral irradiance	Variation in irradiance caused by variation in scene temperature or emissivity	w cm ⁻²
H	Spectral irradiance	Irradiance per unit wavelength interval	w cm ⁻² μ^{-1}
h	Planck's constant	6.62554×10^{-27} erg sec	
h	Aircraft height	----	ft
$h\nu = \frac{hc}{\lambda}$	Photon energy	Energy of a quantum of radiation	erg
J	Radiant intensity	Radiant power per unit solid angle from a source	w sr ⁻¹
K_v	Velocity constant	$\dot{\theta}_s/\theta_E$	sec ⁻¹
K_1, K_2, K_3	Proportionality constants	----	----
N	Cycles per revolution of spinning reticle	Eq. 4-35	rev ⁻¹
N_d	Number of detectors	Number of detector elements that are employed to scan the total field of view	dimensionless
N_f	Number of prism faces	Number of individual sides on the rotating prism mirror of a down-looking line scanner	dimensionless

* For a white noise and an ideal bandpass filter, the filter bandwidth and noise equivalent bandwidth are the same. However for nonwhite noise or practical filter, the filter bandwidth and noise equivalent bandwidth are different.

The noise spectrum of most IR detectors and systems are white or close to white (with the exception of the low frequency band below 10 or 20 Hz). The filter bandwidth and noise equivalent bandwidth have therefore, almost the same values.

TABLE 4-1. INFRARED SYSTEM DEFINITIONS (Continued)

SYMBOL	TERM	DEFINITION	UNITS
<i>NEFD</i>	Noise equivalent flux density	Eq. 4-3	w cm ⁻²
<i>NEP</i>	Noise equivalent power	Eq. 4-2	w
<i>NET</i>	Noise equivalent temperature	ΔT within scene element (at constant emissivity and at some scene temperature, usually 300° K) which produces a change in electrical signal level that is numerically equal to the rms electrical noise	° K, ° C
<i>P_T</i>	Transmitted power	Radiant power generated by an illuminator	w
<i>R</i>	Range	Distance to target	cm
<i>R</i>	Reflection efficiency	Ratio of incident flux to reflected radiant energy from an illuminated target. A product of surface reflectivity and geometric losses	sr ⁻¹
<i>T</i>	Temperature	Temperature in absolute or Kelvin scale	° K
δT	Sample period	Pulse-width of a transmitted pulse of illumination for ranging purposes	sec
<i>t</i>	Dwell time	Time duration of a point in the image plane on a detector scanning across the point	sec
<i>t_f</i>	Frame time, rotation period of reticle	Time in which Ω is scanned	sec, min
<i>V_{AZ}</i>	Instantaneous voltage of scan drive in azimuth	Eq. 4-28	V
<i>V_{EL}</i>	Instantaneous voltage of scan drive in elevation	Eq. 4-28	V
<i>V_o</i>	Reference voltage	Voltage generated by an analog pickoff from the scanner drive	V
<i>v</i>	Aircraft velocity	----	ft sec ⁻¹

TABLE 4-1. INFRARED SYSTEM DEFINITIONS (Continued)

SYMBOL	TERM	DEFINITION	UNITS
v/h	Velocity-to-height ratio	Ratio of the forward ground velocity to the altitude of an aircraft	sr sec ⁻¹
W_s	Signal power	Product of irradiance and collecting aperture	w
W_λ	Spectral radiant emittance	Radiant emittance per unit wavelength interval	w cm ⁻² μ ⁻¹
\bar{W}_λ	Average radiant power	Average spectral power in a very narrow bandwidth	w
W_ϕ	Differential radiant emittance	Differential blackbody radiant density within a spectral bandwidth, for a small change in temperature	w cm ⁻² °K ⁻¹
		$\int \frac{\partial W_\lambda d\lambda}{\partial T}$	
$\Delta \bar{W}$	rms radiant power	Integral of \bar{W}_λ for all wavelengths	w
ϵ	Emissivity	Ratio of radiant power emitted by a body to that emitted by a blackbody at the same temperature	dimensionless
$\Delta \epsilon$	Change in emissivity	----	dimensionless
ϵ_o	Optical efficiency	Fraction of incident irradiance actually transmitted by an optical system after losses to absorption, reflection, blocking, etc.	dimensionless
ϵ_s	Scan efficiency	Factor describing the ratio of dwell time of an ideal scanner to the dwell time of a given scanner	dimensionless
ϵ_λ	Emissivity for a particular λ	----	dimensionless
η	Overall optical efficiency	Factor that combines all optical losses in a system	dimensionless

TABLE 4-1. INFRARED SYSTEM DEFINITIONS (Continued)

SYMBOL	TERM	DEFINITION	UNITS
$\eta_{\lambda d}$	Quantum efficiency of detector	Ratio of number of photons that are effective in generating carriers in the detector to the total number of photons incident at the detector	dimensionless
$\bar{\eta}_B$	Average number of background photoelectrons per sample period δT	----	dimensionless
$\bar{\eta}_s$	Average number of pulse-return photoelectrons per sample period δT	----	dimensionless
θ	Instantaneous angular position	Angular position of a scanning optical axis with reference to its mid position	rad
θ'	Full cone angle of cold shield for detector	Eq. 4-11	rad
θ_{AZ}	Azimuth angular position of detector with respect to center of Ω	Eq. 4-27	rad
θ_E	Error angle of scanner, instant angular displacement error	Eq. 4-25	rad
$\theta_{E(max)}$	Maximum error angle of scanner	Eq. 4-39	rad
θ_{EL}	Elevation angular position of detector with respect to center of Ω	Eq. 4-27	rad
θ_o	Constant reference angle	Eq. 4-27	rad
θ_S	Angular position of optical axis (center of field of view)	Eq. 4-25	rad
θ_T	Target angular position	Eq. 4-25	rad
$\dot{\theta}_M$	Direction of missile velocity	Eq. 4-26	rad sec ⁻¹

TABLE 4-1. INFRARED SYSTEM DEFINITIONS (Continued)

SYMBOL	TERM	DEFINITION	UNITS
$\dot{\theta}_s$	Rate of output angular displacement	----	rad sec ⁻¹
$\dot{\theta}_{S(max)}$	Maximum steady state tracking rate available from servo	Eq. 4-39	rad sec ⁻¹
$\ddot{\theta}_s$	Output acceleration	----	rad sec ⁻²
$\dot{\theta}_{TM}$	Line of sight angular rate in inertial coordinates	Eq. 4-26	rad sec ⁻¹
θ_α	Down-looking scan angle	Angular coverage perpendicular to the line of sight of a down-looking line scanner	rad
λ	Wavelength	Electromagnetic wave interval	cm
$\Delta\lambda$	Spectral band	Half-power spectral bandwidth	cm
λ_m	Longest significant wavelength in an expression for diffraction limited operation	----	cm
ν	Frequency	----	sec ⁻¹
τ_A	Atmospheric transmission	Fraction of radiance transmitted by the intervening atmosphere between source and instrument	dimensionless
Φ	Beam angle	Half-power subtended angle of a beam	rad
Ω	Total field of view	Solid angle that is repetitively sampled or scanned by one or more detector elements	sr, mrad ²

TABLE 4-1. INFRARED SYSTEM DEFINITIONS (Continued)

SYMBOL	TERM	DEFINITION	UNITS
ω	Instantaneous solid angle field of view	Small solid angle subtended by a detector element in the focal plane of an optical system	sr
ω_B	Solid angle through which ambient radiation enters detector	Eqs. 4-9, 4-9a	sr

4-1 PASSIVE SYSTEMS

For purposes of parametric description, it is convenient to separate passive IR systems into two broad categories: (1) scanning systems such as search, track, and imaging systems, and (2) measurement systems such as spectrometers, radiometers, and interferometers. Terms used in the discussion of passive systems are identified in Table 4-1.

Scanning systems scan and sample the radiant intensity distribution within a designated field. Their output may be a linear analog of this distribution for imaging purposes, or a simple indication of the presence of a target and its location as in search-track applications.

Measurement systems are intended for performing a measure on the irradiance directed at the system. The measure may be as simple as intensity level within some fixed radiation bandwidth, or a sequential measure of intensity within a variable center radiation bandwidth, or a simultaneous measure of intensity over a number of center bandwidths.

4-1.1 IMAGING SYSTEMS

At the present state-of-the-art in infrared imaging technology, the most frequent emphasis is on thermal imaging with systems using mechanical scanning in the 10-micron region, and somewhat less frequently in the 3- to 5-micron region. (Image tubes using electron focusing of a near-IR photo-emissive cathode onto a phosphor

screen are widely used for sights and viewing devices. These form a separate category which is described in par. 4-1.1.2.*)

The major portion of the IR scene radiance is in the 10-micron region, and sensitive detector elements and arrays as well as efficient optical components and detector cooling mechanisms are now available for this spectral region. Thus, it is possible to obtain maximum sensitivity to thermal variations in the structure of the scene.

A block diagram for a typical imaging system is shown in Fig. 4-1. The basic elements are a scanner which scans the scene (an object plane which can be assumed for all practical purposes to be located at infinity) with a sensor which responds to the IR radiance level within the instantaneous field of view of each detector element; amplification and filtering to convert the detector outputs into electrical signals to modulate corresponding light sources; and a display scan that moves the light sources in angular synchronism with the sensor scan in order to "paint out" a visible radiance distribution that is analogous to the scanned scene. The display scan may be the electron beam deflection on a CRT, or the optical deflection of a

* Other image conversion devices such as the Absorption Edge Image Converter, the Evapograph, and the Thermosensitive Phosphor Imaging System rely on some physical change in state with temperature that can be observed optically^{1,2}. They have had limited applicability to practical military systems. Baird-Atomic, Inc., Cambridge, Mass., has developed the Evapograph into a commercial instrument.

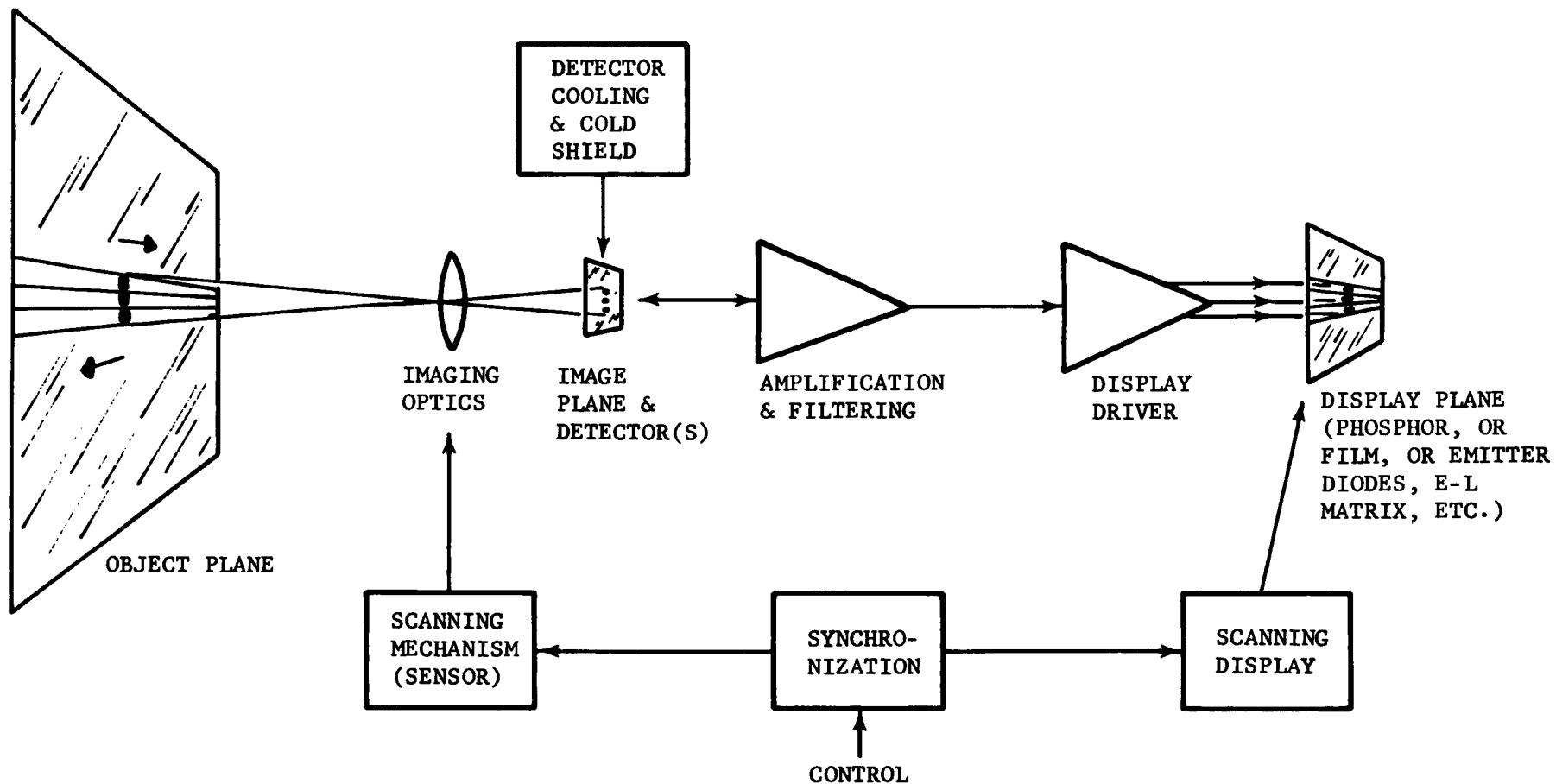


FIGURE 4-1. Typical Imaging System Block Diagram

light beam focused on a strip of film. If the scan rate is rapid enough to scan an entire designated scene repeatedly at a rate higher than the flicker frequency of the human eye, then an integrating display surface such as film or long-persistence phosphor is not needed. The display plane can be simply the focal plane onto which scanning modulated light sources such as diode emitters are focused. To the human observer the visible image will appear to reside in that plane.

Supporting system functions consist of the IR scanning mechanism, detector cooling mechanism (if needed), and a multiplexing subsystem for commutating the outputs of many detectors into one CRT (if needed). In some systems it may be desirable to transmit the scanner output signals to a remote recording and/or display station. This of course requires a transmitter-receiver data link to be included in the loop but does not change the generality of the approach.

4-1.1.1 Mechanical Scanners

For slow scanners, the simplest scan technique might be to move the optical telescope assembly on its gimbals through some programmed raster scan, spiral scan, or any path which avoids redundant scan and gaps in the field. This is adequate where many seconds or minutes are available for the scan of one frame. For higher speed scanning, schemes must be devised where less physical mass is to be moved. Common techniques are to direct the optical viewing path of the sensor at oscillating plane-mirrors located outside the collector aperture, or through counterrotating prisms as described in Chapter 3. Down-looking line scanners that operate from aircraft utilize the aircraft's motion to achieve scan in the forward direction, and a spinning four-sided mirror whose rotation axis is parallel to the direction of motion for scanning in the direction perpendicular to the line of flight.

In this chapter scanning imaging systems will be described in terms of functional parameters. First the sensitivity equations will be derived. There are two basic approaches to describing the sensitivity of the detector within the scanner. One approach is based on utilizing the detector figure of merit D^* which was described in par. 3-4. This approach regards the detector as a source of noise of a fixed level, the level being determined from measurements under con-

ditions similar to the conditions to be encountered by the detector when it is installed within the scanner. The other approach which is suitable only for BLIP detectors, regards the random arrival rate of photons from the background as being the ultimate source of detector noise. (Refer to par. 3-4 for definition of BLIP or background-limited operation.) Here the detector noise-power-density is calculated on the basis of photon rate and detector quantum efficiency. For situations where the number of signal photons is small in comparison to the number of background photons, the two approaches are equivalent since BLIP D^* is determined by background photon rate. For situations where the number of signal photons is larger than the average number of background photons, the noise due to the random arrival time of the signal photons predominates and D^* has no meaning. This situation, however, is less likely to occur in imaging systems than in systems where bright objects are located against dark backgrounds, as for example, in star trackers.

After deriving the sensitivity equations the optical parameters will be analyzed, then the effect of scan rate on system bandwidth will be described. Finally the sensitivity equation will be presented in parametric form, showing the trade-offs among operational parameters such as scan rate, field of view and resolution; and instrumentation parameters such as optical collector diameter, number of detector elements, and optical efficiencies.

4-1.1.1.1 Scanner Parameters

4-1.1.1.1.1 Noise Equivalent Temperature (Sensitivity)

Customarily, image forming scanners are not designed to respond to the absolute radiance level of a scene element, i.e., they are not designed for dc response. They are, however, designed to follow the changes in scene radiance as the scene is being scanned, down to very low frequencies corresponding to a gradual change in level over a large portion of the scan. Dc restoration may be used in the circuitry to restore the average scene level to some arbitrary average intensity level at the display output. There are two major reasons for not designing for absolute level or dc response. The first is that the possible range of radiance levels in a scene

spans a far greater range of levels than that which can be reproduced in a practical display system. Frequent periods of no brightness or complete saturation of the display output could result if absolute levels were maintained. The second reason is that both detectors and high gain dc amplifiers exhibit drift and high $1/f$ noise near zero frequency. (In cases where absolute radiance level measurement is a requirement, reference blackbody sources are supplied within the system, and provisions are made to allow the scanner to periodically scan them and present a reference output.)

The signal in the scene that is of significance to the imaging sensor is therefore the variation in irradiance H caused by variation in scene temperature or emissivity. This is expressed by

$$\Delta H = \frac{\omega}{\pi} \left(\Delta T \int_0^\infty \frac{\partial W_\lambda}{\partial T} d\lambda + \int_0^\infty \frac{\Delta \epsilon_\lambda}{\epsilon_\lambda} W_\lambda d\lambda \right), \text{ w cm}^{-2} \quad (4-1)$$

where

ω = instantaneous field of view, sr

T = temperature, °K

ϵ = emissivity

W_λ = spectral radiant emittance, $\text{w cm}^{-2} \mu^{-1}$

If the system noise is mainly detector noise, it can be expressed in terms of "noise equivalent flux density". This is the minimum signal irradiance that will produce a peak signal-to-rms-noise ratio of one.

The system noise equivalent power (NEP), in watts, is obtained from the figure of merit for the detector, denoted as D^* . This relationship can be expressed as

$$NEP = \frac{\sqrt{A_d \Delta f}}{D^*}, \text{ w} \quad (4-2)$$

where

A_d = area of sensitive surface of detector, cm^2

Δf = system noise bandwidth, Hz

D^* = detector figure of merit, $\text{cm Hz}^{1/2} \text{ w}^{-1}$

The signal power on the detector is equal to the optical collector area times the signal flux density. Therefore the system noise equivalent flux density ($NEFD$) is

$$NEFD = \frac{4\sqrt{A_d \Delta f}}{\pi D_o^2 D^* \epsilon_o}, \text{ w cm}^{-2} \quad (4-3)$$

where

D_o = diameter of aperture of optical system, cm

ϵ_o = optical efficiency

and other terms as previously defined.

Both ΔT and $\Delta \epsilon$ contribute to the differential radiant emittance ΔH of a thermal scene. However, by convention only the ΔT term in Eq. 4-1 is considered in sensitivity calculations. If the first integral in this equation is abbreviated to W_ϕ then Eq. 4-1 can be reduced to

$$\Delta H = \frac{\omega}{\pi} \Delta T W_\phi, \text{ w cm}^{-2} \quad (4-4)$$

The instantaneous field of view ω is defined by the area of the detector A_d and the optical focal length fl

$$\omega = \frac{A_d}{(fl)^2}, \text{ sr} \quad (4-5)$$

Substituting Eq. 4-5 into Eq. 4-3 gives

$$NEFD = \frac{4F\sqrt{\omega \Delta f}}{\pi D_o D^* \epsilon_o}, \text{ w cm}^{-2} \quad (4-6)$$

where F is the $f/\text{no.}$ of the optics.

The signal-to-noise (S/N) generated by the scanner is given by the ratio of ΔH to $NEFD$

$$S/N = \frac{\Delta T W_\phi D_o D^* \epsilon_o \sqrt{\omega}}{4F\sqrt{\Delta f}} \quad (4-7)$$

where all terms previously have been defined.

It should be noted that the spectral distribution of $\frac{\partial W_\lambda}{\partial T}$ is not the same as that for W_λ . For example, a 300°K blackbody, or a scene at this average temperature, will have its peak spectral energy density at approximately 10 microns, whereas the partial derivative with respect to temperature at an average temperature of 300°K will have a peak spectral energy density at approximately 8 microns. The difference is important when optical transmitting elements, filters, and detector responses are under consideration.

The ΔH actually seen by the sensor is modified by the spectral transmission of the optical components and by the spectral transmission of the

atmosphere. Generally, the integrals in Eq. 4-1 should also contain these factors as multiplying elements. In practice, however, sufficient accuracy can usually be achieved by applying averaged transmission values to these factors and retaining them as constant multipliers or as a single constant outside the integrals.

The sensitivity of an image forming scanner is expressed by "noise equivalent temperature", and is abbreviated as NET . It refers to that ΔT within the scene element (at constant emissivity and at some average scene temperature, usually 300°K) which produces a change in electrical signal level that is numerically equal to the rms electrical system noise. In a well-designed system, the system noise is mostly due to detector noise. The NET is determined by solving for ΔT in Eq. 4-7 for a signal-to-noise ratio equal to one. By incorporating the atmospheric transmission τ_A in Eq. 4-7, NET is obtained as

$$NET = \frac{4F\sqrt{\Delta f}}{\sqrt{\omega D_o D^* \epsilon_o \tau_A} W_\phi}, ^\circ\text{K} \quad (4-8)$$

In the derivation of Eq. 4-8, it was assumed that the value of the second term in the right-hand side of Eq. 4-1 $\int_0^\infty \frac{\Delta \epsilon_\lambda}{\epsilon_\lambda} W_\lambda d\lambda$, is negligible.

Given a particular imaging system whose parameters are known, Eq. 4-8 will express the temperature sensitivity of the system. Implicit assumptions are that the scene area over which the temperature differential ΔT occurs is significantly larger than the instantaneous field of view, and the detector D^* refers to the detector inside the instrument under its normal operating conditions. The D^* of a particular detector type will vary considerably from the generally published data owing to such factors as manufacturing process control for unusual sizes, cold-shielding efficiency, nonoptimum electrical bias and loading conditions, aging effects, background radiance effects, and aerodynamically heated optical window radiance.

In Eq. 4-8 the system noise was derived on the basis of detector D^* . For BLIP operation it is sometimes more useful to derive the rms noise value on the basis of the random fluctuation in arrival rate of incident photons on the detector. To obtain this photon noise, Poisson statistics are usefully invoked, which state that

the mean square value of the number of photons in a sample time period is equal to the average number of photons in that sample interval. If the average radiant power in a narrow spectral bandwidth is \bar{W}_λ , the average number of photons per period is $\bar{W}_\lambda \delta T / (h\nu)$ where δT is the sample period. The rms variation in the power is, therefore, $\sqrt{\bar{W}_\lambda h\nu / (\delta T)}$, w. Similarly, if the detector sees an average background spectral irradiance H_λ , it will see a random variation whose rms value is given by

$$\Delta \bar{W} = \left[2\Delta f \left(\frac{\omega_B}{\pi} \right) \left(\frac{\pi}{4} \right) D_o^2 \epsilon_o \int_{\lambda_1}^{\lambda_2} \eta_{\lambda d} H_\lambda \left(\frac{hc}{\lambda} \right) d\lambda \right]^{1/2}, w \quad (4-9)$$

where ω_B is *not* the solid angle subtended by the detector at the optical focal length, but the solid angle through which ambient radiation enters the detector. The term $\eta_{\lambda d}$ represents the quantum efficiency of the detector. It is the ratio of the number of photons that are effective in generating carriers in the detector to the total number of photons incident at the detector. The bandwidth Δf represents the effective noise bandwidth of the system, and the factor 2 is a consequence of the negative frequencies in the power spectrum of the noise. For photoconductive detectors, where both generation and recombination of carriers occur, an additional factor of 2 should be included under the radical. Eq. 4-9 when applied to a photoconductor can be simplified to

$$\Delta \bar{W} = \left[\Delta f \omega_B D_o^2 \epsilon_o \int_{\lambda_1}^{\lambda_2} \eta_{\lambda d} H_\lambda \left(\frac{hc}{\lambda} \right) d\lambda \right]^{1/2}, w \quad (4-9a)$$

As previously indicated, in Eq. 4-9, ω_B is *not* the solid angle subtended by the detector at the optical focal length, but the solid angle through which ambient radiation enters the detector. For a detector without cold shielding this angle is effectively π steradians. If a cold shield with a round aperture is employed, the value of ω_B is

$$\omega_B = \pi \sin^2 \theta' / 2 \quad (4-10)$$

where θ' is the full cone angle of the shield. The lower limit to this angle is set by the numerical aperture of the collector optics.

$$\sin(\theta'/2) = \frac{1}{\sqrt{4F^2 + 1}} \quad (4-11)$$

$$\text{and } \omega_B(\text{minimum}) = \frac{\pi}{4F^2 + 1} \quad (4-12)$$

The signal power W_s is the product of the irradiance (Eq. 4-1) and collecting aperture:

$$W_s = \frac{\omega \Delta T D_o^2 \epsilon_o}{4} \int_{\lambda_1}^{\lambda_2} \eta_{\lambda d} \left(\frac{\partial W_\lambda}{\partial T} \right) d\lambda, w \quad (4-13)$$

To obtain *NET* find the case where $W_s = \Delta \bar{W}$, i.e., the signal power is equal to background noise power. From Eqs. 4-9 and 4-13 we obtain

$$\frac{\omega \Delta T D_o^2 \epsilon_o}{4} \int_{\lambda_1}^{\lambda_2} \eta_{\lambda d} \left(\frac{\partial W_\lambda}{\partial T} \right) d\lambda = \left[\Delta f \omega_B D_o^2 \epsilon_o \int_{\lambda_1}^{\lambda_2} \eta_{\lambda d} H_\lambda \left(\frac{hc}{\lambda} \right) d\lambda \right]^{1/2}$$

NET or ΔT is, therefore,

$$\Delta T = \frac{4 \left[\Delta f \omega_B \int_{\lambda_1}^{\lambda_2} \eta_{\lambda d} H_\lambda \left(\frac{hc}{\lambda} \right) d\lambda \right]^{1/2}}{\omega D_o \sqrt{\epsilon_o} \int_{\lambda_1}^{\lambda_2} \eta_{\lambda d} \tau_A \left(\frac{\partial W_\lambda}{\partial T} \right) d\lambda} \quad (4-14)$$

4-1.1.1.1.2 Optical Gain and Resolution

From a viewpoint of system analysis, however, the parameters in Eq. 4-8 are not all independent. In the first place, the optical diameter D_o has to be sufficiently large to make diffraction effects compatible with the optical resolution requirements.

The central bright portion of the diffraction pattern, the Airy disc, contains 84 percent of the energy of an imaged point source. In a diffraction limited system this Airy disc should not be larger than the size of an individual detector element.

A classical Airy disc is produced only by monochromatic radiation, but an IR imaging system will be sensitive to the entire available spectral bandwidth, typically the 8.5- to 14-micron atmospheric window or the 3.2- to 5.0-micron window. Therefore, the intensity distribution within the diffraction pattern will be a superposition of the weighted values of all of the incoming wavelengths. The contribution from the edges of the window will be less significant than that from the central portion of the window. This intensity distribution is further modified by residual optical aberrations and imperfections. This intensity distribution or spot spread function is, therefore, not readily predictable analytically.

The focal plane image is a convolution of the object scene with this spread function. The scanning of this image plane by the detector represents, in effect, a second convolution between the detector area and the image. Each convolution of course degrades the image quality to some extent.

A basis for a rigorous relationship between optical spread function and detector area cannot be provided. An optimum error budget and cost budget exists if the spread function is approximately equal to the detector area. This criterion can be formulated approximately by requiring that the Airy disc diameter formed by the longest significant wavelength in the window, e.g., the one-half power point on the atmospheric transmission curve, be equal to or less than the size of the detector.

If the detector area is square, and it subtends an instantaneous solid angle field of view ω , then according to Rayleigh criteria:

$$\sqrt{\omega} = \frac{2.44\lambda_m}{D_o} \quad (4-15)$$

where λ_m is the longest significant wavelength in an expression for diffraction limited operation. The the *NET* of a diffraction limited imaging system is

$$NET = \frac{1.6F\sqrt{\Delta f}}{\lambda_m D^* \epsilon_o \tau_A W_\phi}, \text{ } ^\circ\text{K} \quad (4-16)$$

where Δf is noise equivalent bandwidth. Thus the sensitivity of a diffraction limited system is independent of optical diameter. The trade-off is only between optical diameter and resolution.

4-1.1.1.1.3 Scan Rate and Bandwidth

The electrical bandwidth Δf_e is determined by the scan rate. It is proportional to the reciprocal of the dwell time of an image point on the scanning detector. The electrical filter can be optimized, in principle, to maximize the signal-to-noise ratio, if the characteristics of the signal and noise can be completely described. This process is described in Chapter 3 and in Ref. 3. In practice, however, the optimum filter is usually not realizable physically, and in an imaging system utilizing many detectors and amplifiers, even a piecewise approximation to the optimum filter for each detector channel might require an excessive number of electronic components. A relatively simple bandpass filter consisting of a flat response with low- and high-frequency cutoff is often adequate and provides a signal-to-noise ratio very nearly equal to the theoretical optimum. A few decibels of peaking near the high frequency end of the filter will result in improved definition of small details in the scene, at the expense of a slight increase in noise.

At this point in the filter design, many design trade-offs are possible. Most of these trade-offs will relate to the aesthetic appeal of the displayed scene or to compensating for system component characteristics. For example, high frequency enhancement, which is analogous to differentiation, will enhance the edges of objects within the scene by causing light and dark banding in the direction of scan. In the extreme, the scene can be reduced very nearly to a stick drawing over a uniform intensity background level. Or, contrast can be traded for fine-detail

definition by adjusting the slope of the high-frequency cutoff. Compression and expansion can be implemented to compensate for nonlinearities and dynamic range in the display element. If bandwidth compression is an important consideration, the statistical constraints among picture samples and the properties of human vision can be exploited to achieve an order of magnitude reduction in bandwidth⁴.

In most instances, however, the desire is for a displayed output scene whose intensity distribution is a reasonably linear analog of the thermal intensity distribution in the scanned scene, and to obtain this with maximum economy. If a simple low-pass filter were used, its optimum electrical bandwidth $\Delta f'_e$ for best peak signal-voltage-to-rms-noise ratio would be approximately⁵

$$\Delta f'_e = \frac{3}{4t}, \text{ Hz} \quad (4-17)$$

The constant of proportionality of 3/4 between the bandwidth and the reciprocal of dwell-time t is not rigorous because the assumed signal pulse does not have zero rise time and because the bandwidth does not have a mathematically sharp cutoff. But an important factor to be kept in mind for this type of analysis is that the constant of proportionality is not at all critical in value. Goldman⁵ has shown, for example, that, if the bandwidth is reduced by a factor of one-third (to a proportionality constant of 1/2), the peak signal-to-noise ratio is reduced only by 6.5 percent and, if the bandwidth is increased by one-third (to a proportionality constant of 1), the signal-to-noise ratio is reduced only by 3 percent. Therefore the approximation of Eq. 4-15 is well within the accuracy requirements of a system trade-off study.

If a total field of view of Ω steradians is scanned at a constant rate, without redundancy, by an instantaneous field of view of ω steradians and the scan is completed in a frame time period t_f , the dwell time t of a point on the detector is $t_f \times \omega/\Omega$. Because of mechanical scan rate limitations, a linear scan rate is usually difficult to achieve, with the result that the dwell time in some parts of the field will be reduced by a factor ϵ_s called scan efficiency. This requires an increased electrical filter bandwidth, and is commonly expressed as scan efficiency or scan overshoot. The required bandwidth is then

$$\Delta f''_e = \frac{3\Omega\epsilon_s}{4\omega t_f}, \text{ Hz} \quad (4-18)$$

In reality this refers to the upper cutoff frequency because it is impractical to design for dc response. However, the lower cutoff frequency is typically very low—of the order of a few Hertz—in order to allow the scanner to accurately reproduce the low frequency features within the scene. The upper cutoff frequency is typically of the order of tens of kHz so that it is numerically very nearly equal to the total bandwidth. If a number N_d of detectors are used to simultaneously scan the field Ω , then the required bandwidth $\Delta f''_e$ is proportionately reduced.

The equivalent noise bandwidth Δf will generally be somewhat larger than $\Delta f''_e$ owing to excess $1/f$ noise, amplifier noise, and the gradual cutoff of simple R-C filters. The equivalent noise bandwidth is obtained by integrating the noise power spectrum in $\Delta f''_e$ and equating it to the integration of an ideal white noise power spectrum.

4-1.1.1.4 Performance Requirements and Instrumentation Parameters

Expressed in terms of scan rate, the *NET* of a scanning system is

$$NET =$$

$$\left(\frac{1}{\omega} \sqrt{\frac{\Omega}{t_f}} \right) \left(\frac{F}{D_o D^* W_\phi \sqrt{N_d}} \right) \left(\frac{2\sqrt{3\epsilon_s}}{\epsilon_o \tau_A} \right) \quad (4-19)$$

The terms in Eq. 4-19 have been separated into three groups by the use of parentheses in order to illustrate the nature and effect of the different parameters involved.

a. First Group of Terms:

The first group, ω, Ω , and t_f —which are instantaneous field*, total field, and frame time, respectively—represents the system performance requirements. These parameters are governed by

* Instantaneous field is also commonly referred to as the "resolution" of the system since it relates to the resolvable detail within the scene. It is important to note that this is not the same definition of resolution as the Rayleigh criterion, or those definitions that relate to photographic or television resolutions.

the operational or tactical demands on the system and are derived from a larger system analysis such as that for an integrated fire control-navigation system, weapon delivery system, etc.

b. Second Group of Terms:

The terms in the second set of parentheses represent the instrumentation parameters, or tools, which the designer has at his disposal for synthesizing an IR imaging system to meet the requirements. Actually, he will find that the flexibility and range of values at his disposal are quite restricted and that he cannot design for any arbitrary set of performance specifications. Similarly, the system analyst who defines the performance requirements soon becomes aware that he cannot request any arbitrary set of performance specifications. He, therefore, must perform judicious trade-offs among the performance parameters in order to constrain the net demands to the state-of-the-art in instrumentation. For example, Eq. 4-19 (first parentheses) shows that sensitivity or *NET* trades off as the square root of scan rate, and inversely as resolution or instantaneous field of view. Thus if high resolution is important, then it may be necessary to relax scan rate. If frame time cannot be increased, then the total field of view that is to be scanned might be decreased. Or, the *NET* specification may have to be relaxed.

Among the instrumentation parameters in the second set of parentheses, the number of detector elements N_d is probably the only parameter that allows for a wide range of values. The number of detectors used in imaging systems vary from one to a few hundred. The other parameters are less flexible.

Optical diameter D_o is typically of the order of a few inches to a foot. Weight and cost increase much more rapidly than gains in sensitivity for sizes larger than this range. On the other hand, for optical sizes much smaller than this range, system sensitivity and resolution decrease much more rapidly than overall system cost or weight. Therefore, practical consideration constrains optics diameter to this range of sizes. The optimum diameter depends on a close analysis of the overall instrumentation approach.

The *f*/number for sensitive systems is similarly constrained to a narrow range of values, typically between *f*/1.5 and *f*/3.0. Again, values

significantly less than *f*/1.5 are very difficult and costly to achieve, and the cost trade-off is poor. For narrow field of view, high-resolution systems, analogous to telephoto lens cameras, a longer focal length and, therefore, a higher *f*/number is necessary. A practical lower limit to the size of detector elements that can be fabricated is of the order of a few thousandths of an inch. Therefore, a limit is reached where decreased instantaneous field can only be achieved by increasing the focal length.

The selection of the detector type to be used is one of the most critical steps in the design process. The choice depends not only on the wavelength band of operation and available D^* but also on cooling requirements, cost and availability in the specific configuration called for, reliability and aging characteristics, and particular characteristics such as time constant, responsivity, sensitivity contours and uniformity, spectral filtering requirements, etc.

The last parameter in this group, W_ϕ , is the differential radiant emittance from the scene. In the 3- to 5-micron window for an average scene temperature of 240°K, W_ϕ has a value of approximately $1.5 \times 10^{-5} \text{ w cm}^{-2} \text{ }^\circ\text{K}^{-1}$, depending considerably on atmospheric and meteorological conditions. In the 8.5- to 14-micron window, the value is approximately $2.1 \times 10^{-4} \text{ w cm}^{-2} \text{ }^\circ\text{K}^{-1}$, again depending on the atmospheric absorption path and meteorological conditions. Thus, the available energy is considerably higher in the 10-micron region; however, cooling requirements are usually more severe for detectors operating in this region than for those operating in the 3- to 5-micron window. The optical diffraction limit is worse for the longer wavelength region, and optical materials such as refractors and filters tend to be significantly more costly for the longer wavelengths.

c. Third Group of Terms:

The terms in the last set of parentheses represent specific engineering design efficiency parameters. Optical transmission efficiency ϵ_o and scan efficiency ϵ_s are parameters that have to be maximized during the detailed design layout phase. Optical transmission in particular can become a critical or pacing item, especially in the longer wavelength system. Optical materials such as germanium or zinc sulfide have very high indexes of refraction, resulting in high

reflection losses at each surface. For example, if a fast, high-resolution optical system design requires four air-spaced refractive elements and if a transmission loss of 50 percent were suffered at each two surfaces, the net transmission would be reduced to $(0.5)^4$ or 0.0625 owing to this effect alone. To make up for this loss by increasing the optical diameter would require an increase of D_o by a factor of almost 16 which, of course, would be absurd. A multi-layered anti-reflection coating can reduce the reflection loss to about 2 percent at each surface, depending on the specific material to be coated and the width of the spectral band that is to be subtended. A 2 percent reflection loss per surface would result in a net transmission of 0.92 percent.

The atmospheric transmission τ_A is actually beyond the control of the system designer. It is merely a factor to be considered in the analysis and selection of the wavelength band of operation.

4-1.1.1.2 Thermographs

A thermograph is essentially a scanning radiometer. (See par. 4-1.4 for a description of radiometers.) A typical configuration produced by the Barnes Engineering Company utilizes an oscillating plane mirror mounted at 45 deg in front of the 8-in. diameter radiometer optics. The mirror is cam-driven in a horizontal scan with a quick return. During the return, the mirror tilts up one linewidth, thus generating a line-by-line scan of the scene. The back of the same plane mirror scans a light spot from a glow modulator tube over photographic film. The light spot is made proportional in size to the instantaneous field of the radiometer, and is intensity modulated by the radiometer output. Since the same mirror scans both the IR scene and the light output, excellent synchronization is maintained between the two.

The dynamic range and average intensity level of the output can be varied by electronic controls. The radiometer measures the level of the scene radiance by comparing it to a built-in reference blackbody source. It also supplies a set of reference signal levels which register as reference gray scale levels on the film.

By utilizing an immersed thermistor bolometer, characteristic performance is a *NET* of 0.04°C

for $\omega = 1 \text{ mrad}^2$, $\Omega = 10^\circ \times 10^\circ$, or 0.03 sr; and $t_f = 17 \text{ min}$. Instruments similar to the thermograph are also produced by Servo Corporation of America and Radiation Electronics Corporation.

4-1.1.1.3 Down-looking Line Scanners

For air-to-ground IR reconnaissance mapping, a down-looking line scanner is a configuration that utilizes the forward motion of the aircraft as one dimension of scan. The instantaneous field ω is caused to scan through an angle θ_α at right angles to the direction of motion. Typically, θ_α is made large enough to provide nearly horizon-to-horizon coverage. The rate of scan is adjusted to the forward speed of the aircraft so that successive scans cover adjacent strips on the ground.

To provide the scan pattern, a rotating mirror in the form of a prism with a number of faces is placed in front of the imaging optics. As each face rotates past the optics, the optical line of sight is deviated along with it. Two basic configurations are: (1) faces at 45 deg to the optics, and (2) a folded system where the faces on the prism are parallel to the direction of motion, and the receiving optics are separated into two halves to receive the reflection from two sides of the rotating prism.

The scan rate for this configuration is equivalent to

$$\text{scan rate} = \frac{\theta_\alpha v}{h}, \text{ sr sec}^{-1} \quad (4-20)$$

where v and h are aircraft velocity and height, respectively, and θ_α is expressed in radians. The dwell time on the detector is approximately

$$t = \frac{\omega v}{\theta_\alpha h}, \text{ sec} \quad (4-21)$$

and the spin rate of the mirror that is required is

$$f_d = \frac{60v}{\omega N_f h}, \text{ rpm} \quad (4-22)$$

where N_f is the number of sides on the rotating prism mirror. For low-altitude, high-speed flight, the work load imposed on the scanner is relatively severe. For example, for a v/h ratio of one steradian per second (i.e., 1000-ft altitude and 1000-ft sec^{-1} velocity) and an instantaneous

field of 1 mrad^2 , the scan rate is approximately $\pi \text{ sr sec}^{-1}$, the dwell time t is approximately $3 \times 10^{-7} \text{ sec}$, and the spin rate f_d for a four-sided mirror ($N_f = 4$) is 15,000 rpm. Using more than one detector relieves some of the work load, but

increases the distortion and scene rectification problem.

Fig. 4-2 illustrates one part of the distortion. The angular resolution of the detector is constant,

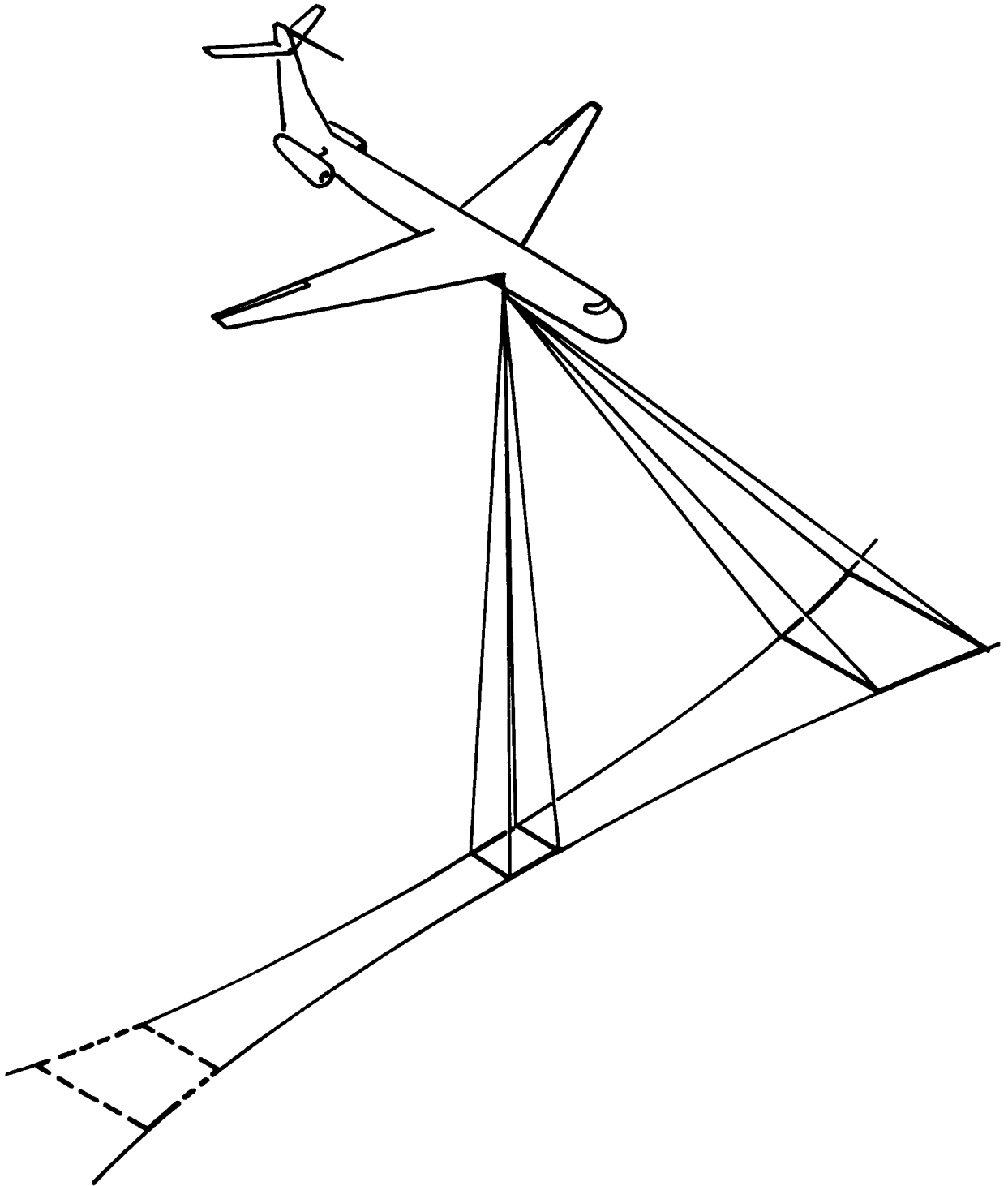


FIGURE 4-2. *End of Scan Distortion*

CHAPTER 5

IR SYSTEM DESIGN*

5-1 SYSTEM APPROACH TO INFRARED DESIGN

The system approach to infrared design engineering is a technique whereby all aspects of the total system are considered in the design of each individual subsystem and component. This systematic approach entails defining of the total mission objectives; the priority rankings and relative weightings of each individual mission objective; the operational environment in which the system must function; the target, background, and transmission characteristics; the measures of effectiveness against which alternate designs and requirements can be evaluated; and, finally, a methodology by which a final system design can be synthesized. For the system to perform effectively in the operational environment, detailed consideration must be given to reliability, maintainability, logistics, and ground support equipment.

The first task in the evolution of system design involves the identification of the mission objectives and subsequent translation of these objectives into a set of functional requirements to be satisfied in the design of the sensor system. For example, the functional requirements for an IR search system might include threat warning, threat identification, and threat priority assignment. Each may have different (and perhaps conflicting) implications on the performance parameters of the sensor system. The output of the functional requirement analysis includes characteristics associated with the operational performance of the system such as detection range, detection probability, minimum signal-to-noise ratio, sensitivity, false alarm[†] rate, frame time, total field of view, resolution, and tracking rates. It should always be remembered that this baseline set of operational parameters must be continuously re-evaluated in light of cost effectiveness considerations.

Cost effectiveness is the mission performance achieved at a given cost for one system approach. This determination must be made in the broadest possible sense; i.e., the measure(s) of effectiveness must be appropriate and all the costs, amortized over the sensible life of the system, must be included. The question of whether increased effectiveness at increased cost should be provided depends on the allocation of resources between qualitatively different systems and is beyond the scope of the analysis to be performed by the infrared system designer.

Following the delineation of functional requirements, a set of baseline sensor parameters are established to satisfy the performance requirements. These parameters include optical diameter, optical speed (f/no.), number of detectors, detector size and aspect ratio, detector type, the operating spectral region, electrical bandwidth, and the desired output display or format. Since most of these parameters are interrelated and are functions of the performance parameters, the actual selection of numerical values must follow a detailed parametric trade-off analysis in which the possible constraints of size, weight, power, and cost effectiveness considerations are evaluated. The output of this phase of analysis will be a baseline preliminary design specification.

At this point, the mission objectives should be re-examined, several alternative sets of functional requirements established, and a set of sensor parameters developed for each requirement. The optimum set of performance parameters and sensor parameters can then be resolved through the synthesis and development of a cost effectiveness model that can relate sensor and performance parameters to mission effectiveness and cost. The end result will then be the performance and design specification which defines the final system.

5-2 REQUIREMENTS

Systematic evaluation of mission requirements, functional requirements, targets, back-

* Written by S. Braunheim and K. Seyrafi

† When a signal waveform amplitude exceeds a preset threshold level due to noise, this excess of threshold is called false alarm.

grounds, and the effects of atmospheric transmission establishes the basic framework within which systems are designed and optimized. The interrelationships among the various sensor parameters and performance parameters, and the constraints and objectives of the mission constitute the analytical and quantitative base for establishing cost effectiveness relationships.

5-2.1 SYSTEM ANALYSIS

The paragraphs which follow describe the methodology through which functional requirements are established. A specific example is assumed throughout the remaining paragraphs to provide a few concrete situations in what must be an otherwise fairly-general discussion. For this purpose, the design of an IR sample-data tracker for use on an inexpensive surface-to-air missile (SAM) was selected. Table 5-1 lists and defines the symbols used.

5-2.1.1 Operational Environment

The operational environment delineates the mission characteristics and objectives in such a manner as to permit the development of the functional requirements. Thus, it is at this point that mission profiles and overall objectives should be established.

The geometric and kinematic relationships between the sensor platform and the target provide the initial clues into the requirements for detection range, field of view, tracking rates, and frame times. For example, assume that the mission of the sample SAM is to provide point defense capability for such targets as bridges, command posts, supply dumps, etc., against low-altitude attack jet aircraft armed with conventional low-drag ordnance. An analysis of the ordnance ballistics and other characteristics would show that, for a given drop altitude and

TABLE 5-1. LIST OF SYMBOLS

SYMBOL	DEFINITION	UNITS
A	Maximum amplitude of angular scan	rad
A_{bkd}	Background area in receiver field of view	m^2
A_d	Detector area	cm^2
A_i	Inherent availability	—
A_{is}	Area of illuminated spot	m^2
A_o	Optics collecting area	cm^2
A_r	Receiver area	m^2
A_t	Finite area of target	m^2
B	Background radiance	$w\ cm^{-2}\ sr^{-1}$
$B(\lambda)$	Background spectral radiance	$w\ sr^{-1}\ \mu^{-1}$
B_a	Radiance of the intervening atmosphere at ambient temperature	—
C	Contrast of target and background	—
c	Speed of light	$cm\ sec^{-1}$ or $m\ sec^{-1}$
D^*	Detector specific detectivity	$cm\ Hz^{1/2}\ w^{-1}$
\hat{D}^*	Detectivity of detector before roll-off	$w\ cm^{-2}$

TABLE 5-1. LIST OF SYMBOLS (cont'd)

SYMBOL	DEFINITION	UNITS
D_o	Optical diameter	cm
	Aperture diameter	cm
	Minimum object dimension	m
$D_o(max)$	Maximum diameter constraint	cm
DL	Diffraction limit	rad
d	Detector linear dimension	cm
d_{min}	Minimum linear dimension of element	
E	Acquisition threshold level	Hz
e	Charge on the electron	$1.602 \times 10^{-19} \text{ C}$
f	Frequency	Hz
$f/no.$	Optical speed	—
f_a	Lower cutoff frequency	Hz
f_b	Upper cutoff frequency of filter	Hz
f_c	Filter center frequency	Hz
Δf	Noise equivalent bandwidth	Hz
$\Delta f'$	Electrical (filter) bandwidth	Hz
f_r	Natural frequency of servo	Hz
f_s	Detector aspect ratio (height-to-width)	—
	Sampling rate of servo	—
G	Electron multiplier gain	—
H	Irradiance at the collecting aperture	w cm^{-2}
H_B	Apparent background irradiance	w cm^{-2}
	Total background radiant intensity	w cm^{-2}
$H_c(\lambda)$	Background radiant intensity	$\text{w cm}^{-2} \mu^{-1} \text{ sr}^{-1}$
H_t	Target irradiance	w cm^{-2}
H_λ	Spectral irradiance on ground	$\text{w m}^{-2} \mu^{-1}$
h	Planck's constant	or $6.625 \times 10^{-34} \text{ w sec}^{-2}$ $6.625 \times 10^{-34} \text{ J-sec}$
h/σ	Threshold-to-rms noise ratio	—
I	Moment of inertia of rotating seeker components about the spin axis	in.-oz sec^2
i_{bkd}	Background induced current	A
i_d	Photomultiplier dark current	A

TABLE 5-1. LIST OF SYMBOLS (cont'd)

SYMBOL	DEFINITION	UNITS
i_s	Signal current	A
J	Radiant intensity	W sr^{-1}
$J(\lambda)$	Spectral radiant intensity of target Spectral radiant intensity from target	$\text{W sr}^{-1} \mu^{-1}$ $\text{W sr}^{-1} \mu^{-1}$
$J_a(\lambda)$	Apparent spectral radiant intensity from target	$\text{W sr}^{-1} \mu^{-1}$
K_1, K_2	Proportionality constants	—
K	Number of linear resolution elements required for identification	—
K_d	Scan efficiency	—
k	Boltzmann's constant	$1.38 \times 10^{-23} \text{ J/}^\circ\text{K}^{-1}$
N	Radiance of illuminated spot on the ground Rms system noise	W m^{-2} W cm^{-2}
NEI	Noise equivalent input (sensor sensitivity)	W cm
N_{fa}	False alarm rate	crossings per sec
n_b	Number of bars	—
n_d	Number of detectors	—
n_{do}	Required number of detectors	—
n_g	Number of resolution elements in the acceptance gate	—
n_ℓ	Number of looks required for detection	—
n_{tot}	Total number of resolution elements in the field of view	—
$P_{bk d}$	Background power level	W
P_d	Reflected power impinging upon detector	W
P_ℓ	Laser power	W
p	Probability that a noise pulse exceeds the threshold in any given resolution element	—
\hat{p}	Probability of an initiating noise pulse occurring	—
\bar{p}	Probability that at least one noise pulse will exceed threshold in acceptance box	—
p_d	Detection probability	—
p_f	Probability of a false alarm	—
p_s	Probability that any one of n_ℓ looks exceeds the threshold	—
$p(v)$	Probability distribution function of noise	—
Q_B	Incident photon flux density	$\text{phot cm}^{-2} \text{ sec}^{-1}$

TABLE 5-1. LIST OF SYMBOLS (cont'd)

SYMBOL	DEFINITION	UNITS
R	Range	cm
R_c	Visible detection range of target due to cloud cover	m
R_d	Weapon release range to target	m
R	Load resistor	ohm
R_{min}	Minimum acceptable detection range	m
R_s	Safety margin range	m
r_s	Scan rate	rad sec ⁻¹
S/B	Signal-to-background noise ratio	—
S/N	Signal-to-noise ratio	—
S	Amplitude of signal	—
T	Threshold level of system	—
	Torque	in.-oz
	Time	sec
	Temperature	°K
ΔT	Effective temperature contrast between target and background	°K
T/σ	Number of levels the threshold level is above the noise level	—
t_d	Dwell time of an individual detector	sec
	Time required for a point image to cross a detector	sec
t_{fa}	Mean time between false alarms	sec
	Time period	sec
t_m	Time of flight of missile	sec
t_o	Frame time that would produce the roll-off knee frequency (3 dB point) for a given size detector	sec
t_r	Reaction time prior to launching the SAM	sec
t_s	Frame time	sec
	Frame (scan) time	sec
$t_s(opt)$	Optimum scan time	sec
$t_s(max)$	Maximum frame time	sec
$t_s(max)$	Maximum scan time	sec
V_m	Missile velocity	m sec ⁻¹
V_t	Attacking aircraft velocity	m sec ⁻¹
	Velocity of target	m sec ⁻¹
	Target speed	m sec ⁻¹

TABLE 5-1. LIST OF SYMBOLS (cont'd)

SYMBOL	DEFINITION	UNITS
v	Instantaneous noise voltage	V
X	Detector linear dimension	cm
	Detector height	cm
Y	Detector linear dimension	cm
	Detector width	cm
	Empirically determined number	—
α	Receiver field of view	rad
	Instantaneous field of view	sr
α_{min}	Limiting field of view	sr
α_r	Angular resolution required of system	rad
ϵ_e	Coefficient which relates the peak or rms value of the signal output to the input irradiance	—
ϵ_o	Optical efficiency	—
$\epsilon(S)$	Error for a ramp input	—
$\epsilon(t)_{peak}$	Peak value of error	—
η	Quantum efficiency of detector	—
	Photocathode quantum efficiency	—
θ	Angle between laser beam and normal to surface	rad
$\theta_{x/y} (min)$	Minimum angular dimension of an individual detector	rad
θ_x	Detector angular resolution in direction of scan	rad
	Detector's angular dimension	rad
	Detector width	rad
θ_y	Detector's angular dimension	rad
θ_s	Sinusoidal scan angle	rad
$\dot{\theta}_s$	Angular scan rate	rad sec ⁻¹
$\dot{\theta}$	Angular rate	rad sec ⁻¹
λ_c	Long-wavelength cutoff	cm
λ_1	Short-wavelength cutoff	cm
λ_2	Long-wavelength cutoff	cm
$\Delta\lambda$	Spectral bandpass	μ
	Spectral bandwidth of receiver optical filter	μ
ρ	Reflectance	—
ρ_m	Minimum signal-to-noise requirement	—
ρ_β	Signal-to-background plus noise ratio	—
ρ_N	Signal-to-noise ratio S/N	—

TABLE 5-1. LIST OF SYMBOLS (cont'd)

SYMBOL	DEFINITION	UNITS
σ	Rms value of noise	V
τ	Transmittance	—
$\tau(\lambda)$	Atmospheric transmission for target	—
$\tau_B(\lambda)$	Atmospheric transmission for background	—
τ_a	Atmospheric transmission	—
τ_B	Transmission of the atmospheric path between the optical system and the background	—
$\tau(\lambda, R)$	Atmospheric transmission as a function of wavelength and pathlength	—
τ_{io}	Transmission factor of illuminator optics	—
τ_{ro}	Transmission factor of receiver optics	—
ϕ	Field of view in the direction of scan	rad
Ω	Total field of view	mrad or sr
Ω_v	Angular precession velocity about output axis	rad sec ⁻¹
ω	Scan rate of system Angular velocity of scanner	rad sec ⁻¹ rad sec ⁻¹
ω_α	Angular subtense of detector	sr
ω_{max}	Maximum angular scanning rate of field of view	rad sec ⁻¹
ω_r	Seeker spin velocity	rad sec ⁻¹

speed, the weapons must be released some distance R_d prior to reaching the target in order for the weapon to hit the target and for the attacking aircraft to safely clear the area. It is necessary for the defense missile to intercept the aircraft with some safety margin prior to the aircraft reaching the range R_d . If we represent the safety margin range as R_s and the missile velocity as V_m , the time of flight t_m of the missile may be calculated as (it is implicitly assumed that the aircraft altitude relative to range is small)

$$t_m = \frac{R_d + R_s}{V_m} \quad (5-1)$$

If the reaction time prior to launching the SAM is t_r and the attacking aircraft velocity is V_t , then the minimum acceptable detection range may be calculated by

$$R_{min} = V_t(t_m + t_r) \quad (5-2)$$

Analogous expressions can be developed for the search field frame time and other sensor performance parameters. For an infrared instrument, the minimum signal-to-noise ratio is determined by the required detection probability and the false alarm rate. If the false alarm rate requirement is very stringent, the system must operate at a high threshold level which would be significantly higher than the rms noise values of the system. This implies that the peak signal must be at least equal to the threshold level. If the detection probability requirement is 99 percent and the system noise is Gaussian white noise (normal), then the minimum signal must be at least 2.33 times noise standard deviations (usually expressed as root mean square-rms-noise) above the threshold in order to assure this

probability of detection. If the threshold setting based on false alarm rate considerations must be 6 times rms noise, then the minimum signal-to-noise ratio for 99 percent detection probability would be 8.33:1. In this manner (clearly simplified at this point), the mission requirements and operational environment determine the functional requirements.

5-2.1.2 Functions

The mission objectives and requirements determine the sensor parameters and sequence of functions that the sensor must perform, thereby, dictating the functions of the subsystems and components within the overall system. A definite delineation of these generic functions is imperative if reasonable and realistic requirements are to be allocated. Again consider the IR seeker on the SAM. Prior to initiation of the SAM launch sequence it is necessary to detect and acquire the target. This requires prior acquisition of the target by some other element of the SAM system (e. g., infrared or radar acquisition system) and then a transfer of this acquisition information to the IR seeker. The pointing accuracy of the initial acquisition system determines, in large measure, the field of view requirements of the IR seeker. If target acquisition is also a requirement of the IR seeker, it must be capable of rejecting background clutter and providing the sensitivity necessary to detect and lock on a target at the desired range. Thus, the acquisition function in conjunction with the operational environment will establish the ground rules governing the field of view, background clutter rejection, and sensitivity requirements.

The second function of the seeker is to track the target and to provide guidance error signals. In this mode of operation, the seeker must reject the countermeasure response of the target and provide data at the rate and resolution required to achieve the desired kill probability. It must possess the necessary gimbal freedom for maintaining the target in the field of view despite target maneuvers. A sufficiently-high angular tracking rate capability must be provided to maintain a small miss-distance at the intercept point. In order to establish numerical requirements for these functions, the missile and target motion usually undergo dynamic simulation on an analog computer. However, as is often the

case, the volume weight or power constraints of the missile nose will not permit the installation of a seeker which provides the full desired mission capability. As a consequence, the designers of both the IR seeker and the mounting platform must determine whether the mission performance can be resolved if the power required can be reduced; or whether more power, weight, or volume can be allocated to the seeker.

It can now be seen that the mission objectives, operational environment, and the functional requirements have begun to yield a preliminary set of performance specifications from which the sensor characteristics can be developed.

5-2.1.3 Requirement Analysis

Following the definition of the functional requirements, the system designer can begin to formulate the sensor system parameters. In general, these are derived analytically from the system sensitivity equations; the considerations of optical, mechanical, and electrical design; cooling requirements and power constraints; and size and weight constraints.

Assume a target of radiant intensity J in w sr^{-1} at a given range R in cm through an atmosphere that provides transmittance τ . The irradiance at the collecting aperture is expressed as

$$H = \frac{J\tau}{R^2}, \text{ w cm}^{-2} \quad (5-3)$$

based on the inverse-square law. The sensor sensitivity or noise equivalent input (NEI) is given by Eq. 5-4, which is discussed further in par. 5-3.3.1.

$$NEI = \frac{\sqrt{A_d \Delta f}}{\epsilon_o \epsilon_e A_o D^*}, \text{ w cm}^{-2} \quad (5-4)$$

where

A_d = detector area, cm^2

Δf = noise equivalent bandwidth, Hz

ϵ_o = optical efficiency

ϵ_e = coefficient which relates the peak or rms value of the signal output to the input irradiance (a unique function of the filter characteristics and input waveforms)

A_o = optics collecting area, cm^2

D^* = detector specific detectivity, $\text{cm Hz}^{1/2} \text{W}^{-1}$

If the minimum signal-to-noise requirement is ρ_m then the noise equivalent input can be rewritten as:

$$NEI = H = \frac{J\tau}{R^2 \rho_m} = \frac{\sqrt{A_d \Delta f}}{\epsilon_o \epsilon_e A_o D^*} \quad (5-5)$$

It is thus shown (for this example) how the functional requirement for detection at range R is related to the sensor parameters of Eq. 5-4. It is also apparent that there is no unique solution to Eq. 5-5 since an infinite combination of numerical values will satisfy the equation.

Assume the need to scan the total field of view Ω steradians once per t_s seconds, and n_d detectors of instantaneous field of view α steradians to scan the field at 100 percent duty cycle, then the dwell time t_d of an individual detector is expressed as

$$t_d = \frac{n_d t_s \alpha}{\Omega}, \text{ sec} \quad (5-6)$$

The filter (electrical) bandwidth $\Delta f'$ for scanning systems is often given as

$$\Delta f' = \frac{1}{2t_d}, \text{ Hz} \quad (5-7)$$

in which case the system response will be reduced by a factor of 0.60 to 0.70 of its maximum amplitude. Theoretically, one would like to have $\Delta f' = \infty$ so that there would be no degradation in system response. However, because of the increase in noise power with bandwidth, Δf should be limited. Practically, the selection of $\Delta f'$ as indicated by the relationship of Eq. 5-7 is a compromise between system response and noise. In this case the response has been reduced by a factor of 0.6–0.7, depending on its application. The detector area A_d can be

expressed as follows in terms of optical speed, aperture, and field of view:

$$A_d = (f/no.)^2 D_o^2 \alpha \quad (5-8)$$

where

$f/no.$ = optical speed

α = instantaneous field of view, sr

D_o = optical diameter, cm

The background clutter rejection capability of a sensor is often expressed in terms of the signal-to-background noise ratio. This reflects the fact that the higher the ratio, the higher the threshold can be set (given adequate sensitivity) and, thus, the more background clutter that can be eliminated. Since background radiance is a complete random function, a frequently-used criterion is a "worst case" or peak background radiance. The signal-to-background noise ratio S/B may be computed as

$$S/B = \frac{J\tau}{\alpha BR^2} \quad (5-9)$$

where

B = background radiance, $\text{W cm}^{-2} \text{sr}^{-1}$

Eq. 5-9 applies when the target is a point source and the background is an extended source such as a cloud. Both the signal-to-background and signal-to-noise ratios can be improved by making the instantaneous field of view α small in the equation. This is done at the expense of cost and complexity compared to a system of equal size and performance, since the number of scanned elements in a frame time is Ω/α . The frame time can be achieved by using additional detectors. There are also physical constraints on the minimum dimension d_{min} of current state-of-the-art detectors which can be fabricated to form large arrays. Thus, the constraint imposed dictates that

$$d_{min} \leq f/no. D_o \theta_{x/y} (min) \quad (5-10)$$

where $\theta_{x/y} (min)$ is the minimum angular dimension in radians of an individual detector. Since total package size, weight, and volume are

strongly influenced by $f/no.$ and diameter; severe penalties can result from using small detectors.

For sensors wherein the limiting source of noise is the internal system noise—provided this noise is Gaussian distributed with a flat amplitude (white) spectrum—the ratio of threshold to the rms noise required for any prescribed false alarm rate is

$$\frac{T}{N} = \sqrt{\frac{2}{n_\ell} \ln \left[\Delta f n_d t_{fa} (n_g)^{n_\ell - 1} \right]} \quad (5-11)$$

where

- T = threshold level of the system
- N = rms noise
- n_ℓ = number of looks required for detection
- n_d = number of detectors
- Δf = noise equivalent bandwidth, Hz
- t_{fa} = mean time between false alarms, sec
- n_g = number of resolution elements in the acceptance gate

The proof of Eq. 5-11 (see Eqs. A-1 through A-12 in the Appendix to this chapter) assumes Rayleigh-distributed white noise such that the probability density functions $p(v)$ can be written as

$$p(v) = \frac{v}{\sigma} \exp \left[-\frac{1}{2} \left(\frac{v}{\sigma} \right)^2 \right] \quad (5-12)$$

where

- $p(v)$ = probability distribution function of noise
- v = instantaneous noise voltage, V
- σ = rms value of noise, V

and the probability that a noise pulse exceeds any given threshold T is

$$\begin{aligned} p(v > T) &= \int_T^\infty \frac{v}{\sigma} \exp \left[-\frac{1}{2} \left(\frac{v}{\sigma} \right)^2 \right] dv \\ &= \exp \left[-\frac{1}{2} \left(\frac{T}{\sigma} \right)^2 \right] \end{aligned} \quad (5-13)$$

Eq. 5-11 is the result of σ being defined as the rms value of the noise which is denoted as N .

Also it can be shown that the signal-to-noise ratio S/N required for any given detection probability p_d when $S \gg N$, is

$$\frac{S}{N} = \frac{T}{N} + \sqrt{2 \ln \left[\frac{1}{1 - (p_d)^{\frac{1}{n_\ell}}} \right]} \quad (5-14)$$

Given a signal of amplitude S , a threshold value T , and noise N , all the same units (volts, for example), and a detection rule of n_ℓ looks; the detection probability can be derived in the manner which follows. First, the probability p_s that any one of the n_ℓ looks exceeds the threshold is expressed as

$$p_s = 1 - \exp \left[-\frac{1}{2} \left(\frac{S - T}{\sigma} \right)^2 \right] \quad (5-15)$$

Assuming that an overall detection probability of p_d is required, then

$$p_d = (p_s)^{n_\ell} \quad (5-16)$$

or

$$p_s = (p_d)^{\frac{1}{n_\ell}} \quad (5-17)$$

Substituting Eq. 5-15 into Eq. 5-17 gives

$$(p_d)^{\frac{1}{n_\ell}} = 1 - \exp \left[-\frac{1}{2} \left(\frac{S - T}{\sigma} \right)^2 \right] \quad (5-18)$$

and

$$\exp \left[-\frac{1}{2} \left(\frac{S - T}{\sigma} \right)^2 \right] = 1 - (p_d)^{\frac{1}{n_\ell}} \quad (5-19)$$

or

$$\frac{S - T}{\sigma} = \sqrt{2 \ln \left[\frac{1}{1 - (p_d)^{\frac{1}{n_\ell}}} \right]} \quad (5-20)$$

Substituting N for σ and rearranging terms, results in Eq. 5-14.

For example, assume the target analysis as having shown that, in the spectral band of interest (3.8 to 4.8 microns for instance), the radiant intensity of the target is 7 w sr^{-1} , and the mission analysis as having indicated a detection range of 9 km through an atmosphere that provides 0.3 transmittance. From Eq. 5-3 the irradiance will then be

$$H = \frac{7 \times 0.3}{(9 \times 10^5)^2} = 2.6 \times 10^{-12} \text{ w cm}^{-2}$$

Let us also assume the background analysis as having shown the effective peak-background-radiance in the band to be $3 \times 10^{-5} \text{ w cm}^{-2} \text{ sr}^{-1}$ and that a signal-to-background noise ratio of 2.0 is necessary for background clutter rejection. Then from Eq. 5-9

$$2.0 = \frac{2.6 \times 10^{-12}}{\alpha \times 3 \times 10^{-5}}$$

The instantaneous field of view α must be approximately $4.4 \times 10^{-8} \text{ sr}$ which implies a detector instantaneous field of view of $2.1 \times 10^{-4} \text{ rad}$, assuming a 1:1 aspect ratio. With a total field of view Ω of $10 \times 10 \text{ mrad}$ dictated by pointing accuracy requirements and a need to search the field with a single-bar linear array, the required number of detectors would be

$$n_d = \frac{10 \times 10^{-3}}{2.1 \times 10^{-4}} \cong 48$$

Let it also be assumed that in order to provide an adequate information rate, the system must scan the complete field 30 times per sec; then from Eq. 5-6

$$t_d = \frac{48 \times 0.033 \times 4.4 \times 10^{-8}}{100 \times 10^{-6}} = 7 \times 10^{-4} \text{ sec}$$

and from Eq. 5-7

$$\Delta f' = \frac{1}{2 \times 7 \times 10^{-4}} = 710 \text{ Hz}$$

If a detection probability requirement of 0.99 is required, an average false alarm rate of one per hour is acceptable, and a single-look detection criterion is used, a threshold setting of 6.4 (Eq. 5-11) and signal-to-noise ratio of 9.5 (Eq. 5-14) will be required. From Eq. 5-5 the required sensitivity is determined to be

$$NEI = \frac{2.6 \times 10^{-12}}{9.5} = 2.74 \times 10^{-13} \text{ w cm}^{-2}$$

It is now assumed that an analysis has shown lead selenide (PbSe) to be potentially the most suitable detector material and that an average D^* of $4 \times 10^{10} \text{ cm Hz}^{1/2} \text{ w}^{-1}$ can be expected when the detector is cooled to -80°C . By replacing A_d and A_o of Eq. 5-4 by their respective terms,

where

$$A_d = (f/no.)^2 D_o^2 \alpha \quad [\text{Eq. 5-8}]$$

and

$$A_o = \left(\frac{\pi}{4}\right) D_o^2$$

(representing the detector and collector area, respectively), NEI can be expressed as

$$NEI = \frac{4 f/no. \sqrt{\alpha \Delta f}}{\pi \epsilon_o \epsilon_e D_o D^*} \quad (5-21)$$

or

$$D_o = \frac{4 f/no. \sqrt{\alpha \Delta f}}{\pi \epsilon_o \epsilon_e D_o D^* NEI} \quad (5-22)$$

By further assuming an $f/no.$ of 3.0 for purposes of optical resolution and packaging and an optical efficiency ϵ_o of 0.5,

$$\begin{aligned} D_o &= \frac{4 \times 3 \times \sqrt{4.4 \times 10^{-8} \times 710}}{3.14 \times 0.5 \times 0.65 \times 4 \times 10^{10} \times 2.74 \times 10^{-13}} \\ &= 5.8 \text{ cm} \approx 2.3 \text{ in.} \end{aligned}$$

Next, a check is made to verify that neither the Rayleigh diffraction limit criterion or the cell size limit have been exceeded. The required resolution was $2.1 \times 10^{-4} \text{ rad}$. The diffraction limit equation is

$$DL = \frac{2.44 \lambda_c}{D_o} \leq \sqrt{\alpha} \quad (5-23)$$

Assuming the limiting wavelength to be 4.8 microns, then

$$DL = \frac{2.44 \times 4.8 \times 10^{-4}}{5.8} = 2 \times 10^{-4} \text{ rad}$$

and thus the diffraction limit is not exceeded. Assume next that the minimum linear dimension d_{min} of a PbSe element is 0.001 in. or $2.5 \times 10^{-3} \text{ cm}$. From Eq. 5-10 it is shown that the detector dimension

$$d = 5.8 \times 3.0 \times 2.1 \times 10^{-4} = 3.65 \times 10^{-3} \text{ cm}$$

which is greater than the assumed d_{min} of $2.5 \times 10^{-3} \text{ cm}$.

5-2.1.4 Block Diagrams

One of the most effective methods of describing all manner of complex systems is by means

of simple pictorial diagrams. This technique is, of course, well-suited for illustrating the overall scope, internal functions, and interfacings of typical IR systems (see Fig. 5-1).

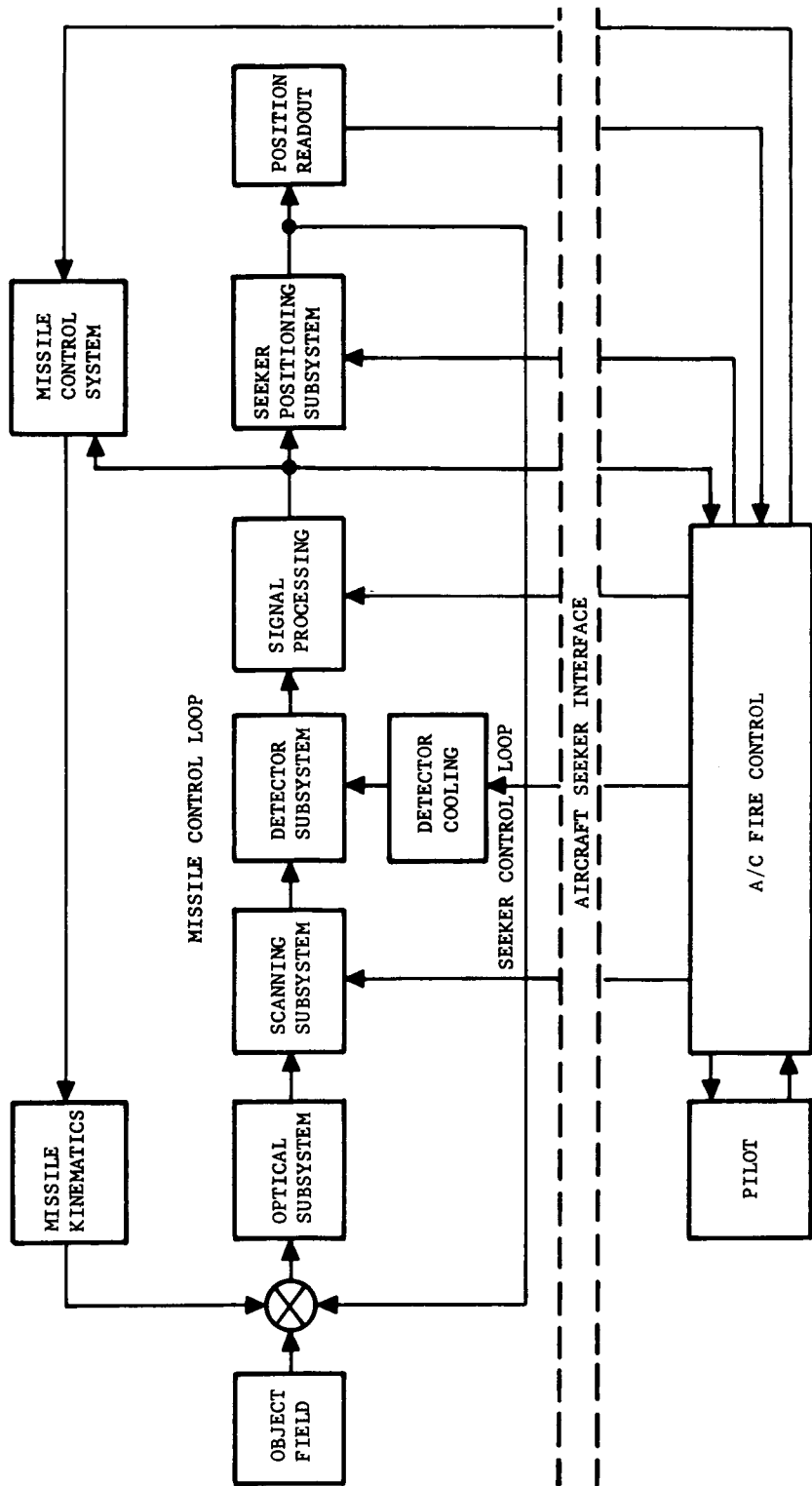


FIGURE 5-1. Infrared Missile Seeker Block Diagram

5-2.2 TARGET DEFINITION

The mission objectives and the generic class of targets of interest in any given application determine the functional role of the IR sensor. The target characteristics of interest in a reconnaissance or mapping mission are in most cases distinctly different from those of interest in a threat warning application. The spectral, spatial, temporal, and amplitude characteristics of the surrounding background, in large measure, determine the overall effectiveness of the system. If no significant distinguishable target characteristics exist relative to its background, the target is essentially camouflaged. In general, there will always be some distinguishable aspects of the target. The question is then relative to the type of detection system required and to its cost. Par. 2-6.2 and AMCP 706-128 discuss in detail some of the salient characteristics of military targets. The following two paragraphs describe the manner in which the system designer makes use of this information.

5-2.2.1 Spectral Radiant Intensity Bounds

The spectral characteristics of many military targets are often the most dominant differenti-

ating feature of the target description. As a result, spectral optimization has become a highly effective tool in providing increased background rejection. Thus, it is extremely important for the system designer to have, or to be able to generate, an accurate spectral representation of a (minimum) target under the operating conditions expected to be encountered in the field.

For example, the spectral signature of a jet aircraft at side aspect is significantly different from that of the same aircraft viewed from the tail. In the first case, the signature is characterized by emission bands of H_2O and CO_2 combustion products at 2.7 and 4.4 microns, while in the second case, the signature is characterized by the blackbody emission of the hot tailpipe. Fig. 5-2 shows the various aspect emissions. When viewed from the nose aspect, the signature may be dominated by graybody emission from the relatively cool surface of the aircraft.

Ground targets, which exhibit relatively little energy compared to airborne targets, are generally characterized by small temperature differences between the target and the surrounding background.

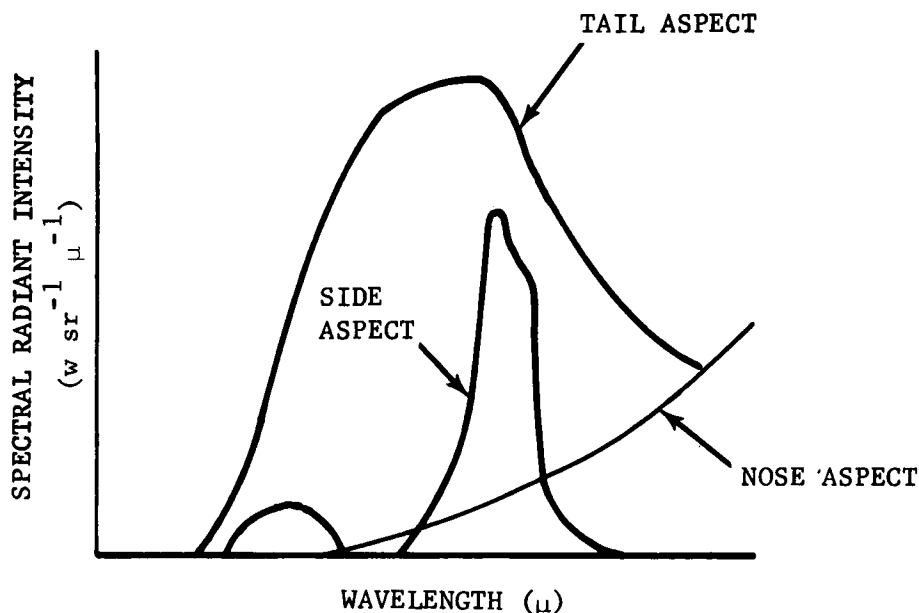


FIGURE 5-2. Spectral Characteristics of Aircraft vs Viewing Aspect

5-2.2.2 Radiance Gradients

Virtually all infrared sensors operate on the modulated gradient between the target and its surrounding background. Thus, from a signal standpoint, the effective signal is the difference between the target and the background. Thus, for example, a 300°K blackbody target contrasted against a 300°K blackbody background would not produce a discernible gradient. In many cases it is not required that the contrast be positive because negative gradients can also be processed. In the case of thermal imaging systems, targets are often specified in terms of the effective temperature contrast ΔT between target and background. For example, a sampan on a river might be said to have a $5^\circ \Delta T$ gradient. It should be noted that this temperature gradient is the result of both emissivity and temperature differences. In the 8- to 14-micron region a ± 5 percent emissivity difference around $\epsilon = 0.95$ is equivalent to approximately a 7°C temperature difference at 300°K ambient.

5-2.3 BACKGROUND DEFINITION

The spectral and spatial characteristics of the background relative to the target determine the degree of background clutter that must be processed and the resulting false alarm rate if background is the dominant source of noise. To this date there has been no satisfactory statistical representation of the underlying stochastic process of background noise. Weiner spectra representations of backgrounds have never been found to adequately represent the spatial distribution of backgrounds. As a result, the system designer must generally utilize concepts such as the signal-to-background ratio which can be quantitatively translated into false alarm rates only through complete knowledge of the probability distribution function. However, if the signal-to-background ratio is defined in terms of the minimum signal-to-maximum background and the ratio is significantly greater than unity, then in most cases the background can be adequately thresholded to a point where the false alarm rate will be within tolerable limits.

5-2.3.1 Terrain, Sea

The spectral signature of most ground backgrounds are characterized by diffusely reflected solar energy in the short wavelengths during daylight hours; and lunar, stellar, and air glow

illumination at night. In the longer wavelengths (above 4 microns) the spectral characteristics are dominated by graybody emission at or near ambient temperature. Since most natural objects tend to have high emissivities in the long wavelengths the spectral signatures approach that of a blackbody. These subjects are discussed in greater detail in par. 2-6.1. The spectral absorptive properties of the intervening atmosphere and the re-emission of the atmosphere in the absorption bands tend to modify the spectral characteristics of the background in a fashion which in many cases is to the advantage of the designer. In many cases, terrain backgrounds will be at a range greater than or equal to the target range, which means that the background will be attenuated as much as or more than the target. It should also be noted that the relative position of the sun, the type and amount of cloud cover, and the type of terrain also affect the amplitude and spectral signature of backgrounds.

The spatial characteristics of terrain are usually dominated by a large low-frequency component and roll-off at about $1/f^2$ beginning at relatively low spatial frequencies. Many targets of interest may be characterized by point objects with corresponding high-frequency components. This tends to improve the background clutter problem if the proper spatial and electrical filters are used. In general, these filters limit the low-frequency response of the system. This reduces signal energy, but at a much slower rate than background energy, and thus improves the signal-to-background ratio.

5-2.3.2 Clouds

Clouds, or more exactly cloud edges, have been the traditional enemy of IR system designers because of the large radiance gradient between blue sky and a cloud edge. There are few analogous situations in the case of terrain backgrounds that produce gradients of this magnitude. As a result, systems that are designed to operate in a cloud environment must be carefully designed with respect to their spectral and spatial filtering properties.

As in the case of terrain, the spectral signature of clouds are dominated by emitted energy in the long wavelengths and reflected energy in the shorter wavelengths as illustrated in Fig. 5-3.

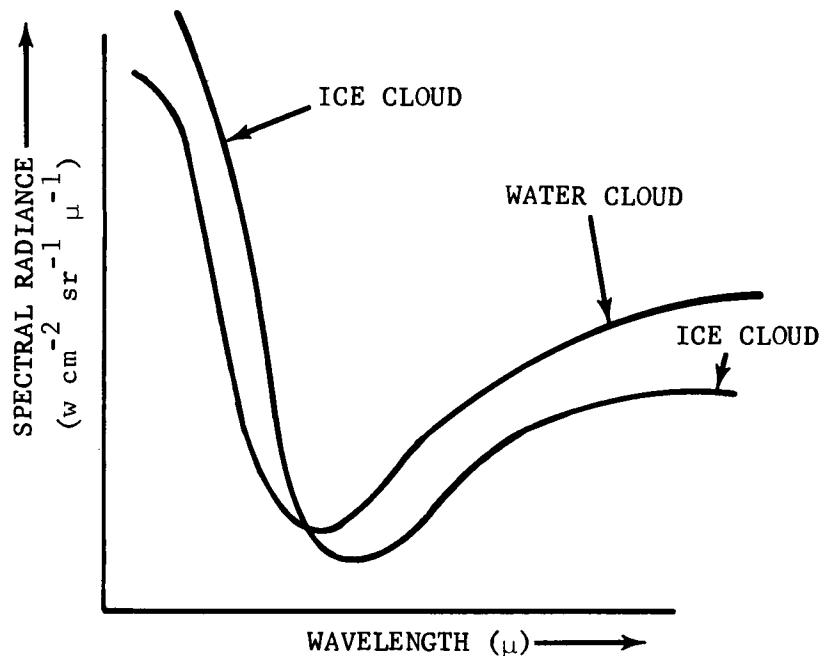


FIGURE 5-3. Typical Sunlit Cloud Radiances vs Wavelength

(Refer to par. 2-6 for more detailed information.) The spectral radiance of clouds in the reflected region is strongly affected by the solar scattering angle and the cloud altitude. High-altitude ice clouds tend to be better reflectors in the short wavelengths but, because of their cooler temperatures, have lower radiance than the low-altitude water clouds in the longer wavelengths.

5-2.3.3 Stellar Backgrounds

The stellar background provides two sources of background radiation. The first comes from the bright stars that are resolved or detected by the sensor. The number and position of resolvable stars can often be predicted in advance through the use of star tapes and ephemeris catalogues. When this information is stored in processing computers, these false targets can be eliminated. Another technique of stellar discrimination is based on the spectral signature of stars. Since most stars radiate as 5000° - 6000° K blackbodies, an instrument operating in two spectral regions has a potential for rejecting these objects relative to much cooler targets. In the regions of high-stellar density such as the galactic equator it is often impossible to process the information in real-time and as a consequence these regions are often avoided. A

second source of stellar radiation is the noise emission from many unresolved stars. In some long-wavelength applications this may be the limiting noise source.

5-2.4 TRANSMISSION

The selective absorption of radiated infrared energy by the intervening atmosphere influences both the spectral characteristics and amplitude of the received target signal. As a consequence, a comprehensive understanding of absorption phenomena is mandatory for successful system design. The primary constituents that absorb infrared energy are the vibration and rotation bands of water vapor and carbon dioxide. Secondary absorption sources include nitrous oxide, ozone, methane, and other minor atmospheric gases. Particulate matter causes scattering of the infrared energy. The phenomenology of this subject is discussed in par. 2-4.

5-2.4.1 Absorption

The dominant absorption bands in the infrared are the 2.7-micron band of H_2O and CO_2 , the 6.3-micron band of H_2O , and the 15-micron band of CO_2 . Because of these absorption bands and the spectral characteristics of target radiation, the traditional operating bands which have

evolved include: 1.8 to 2.7 microns, 3 to 5 microns, and 8 to 14 microns. It should be noted that, since the atmosphere absorbs in the same bands where hot-gas plumes emit, only a small fraction of these strong emission bands is transmitted even through relatively short atmospheric paths. However, temperature and pressure broadening of the plume emission bands results in a small residual skirt of energy that is transmitted as shown in Fig. 5-4. It is apparent from Fig. 5-4 that unless both the spectral characteristics of the target and transmissions are well understood, the estimation of the transmitted target energy can be significantly in error. It should also be noted that nonhomogeneities in the atmosphere in the absorption regions can be a significant source of external scanning noise.

Model atmospheres have been developed to represent the differing climatological environments in which an infrared system may operate. For example, a model temperate atmosphere describes the altitude dependence of CO_2 , H_2O , temperature, and pressure for mid-latitude regions. Similar models exist for tropical and arctic regions. In addition, transmission models by such authors as Thomas Altshuler¹ greatly facilitate the calculation of slant path transmission.

5-2.4.2 Obscuration

In addition to being a background problem, clouds are also a source of obscuration of

infrared energy. This is often characterized by probability curves of cloud free line-of-sight as shown qualitatively in Fig. 5-5. The point A on the curve indicates that at an altitude of about 20 kft and an observer-target distance of 5 mi there is 80 percent probability of a cloud-free line of sight. While at the same altitude but for a 6 - mi observer-target distance, point B on the curve, there is 70 percent probability of a cloud-free line of sight. Curves such as those in Fig. 5-5 are especially useful in cost effectiveness studies. For example, from the point of view of aircraft detection it may be desirable to have a detection range of 20 km. If, however, there is only a 1 percent chance of having a cloud-free line of sight to that altitude, it may not be economical to provide that range capability. In addition, the relationships of Fig. 5-5 are useful in determining the expected range at which targets may emerge from cloud cover. This information is often required in determining frame rate requirements. For example, if a system must detect a target by some minimum range R_{min} and the cloud data indicate that there is a high probability that the target is not visible until some other range R_c and the velocity of the target is V_t , then the maximum frame time is

$$t_{s(max)} = \frac{R_c - R_{min}}{V_t}, \text{ sec } R_c > R_{min} \quad (5-24)$$

Cloud cover data are also often required for airborne and satellite reconnaissance systems in

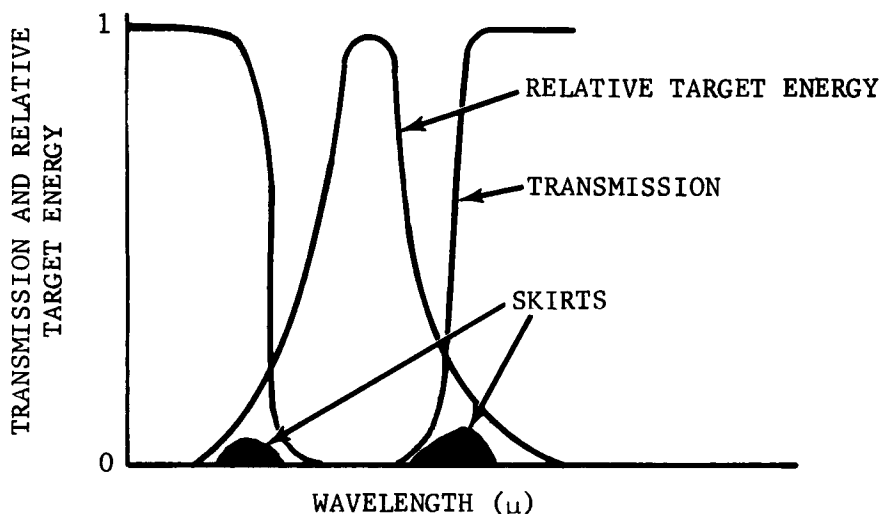


FIGURE 5-4. Relative Target Energy and Transmission vs Wavelength for Plume Emission

determining the percentage of time that ground targets will be visible.

5-2.5 COUNTERMEASURES

The designer of infrared systems must be constantly aware of potential countermeasures that may be used against the system. This knowledge can in some cases permit the inclusion of counter-countermeasures in the initial system design. In almost all cases the details of countermeasure techniques and their performance are highly classified and, as a result, the discussion must be general in nature. IR countermeasures are divided into two general groups representing two functional modes of operation: passive countermeasures and active countermeasures.

5-2.5.1 Passive Countermeasures

Passive countermeasures can be broadly defined as that class of countermeasures which are employed continuously and are not activated as a result of the presence of an attacker. Passive countermeasures exclude the deployment or ejection of physical objects from the defended platform. The most generally employed countermeasure against IR systems is a reduction in target signature. The primary objective of these techniques is to reduce or suppress the level of IR radiation from the defended platform to a level so low that the attacker cannot detect his target until it is too late to mount an attack. The

three dominant suppressing techniques for missile and aircraft targets are shielding, cooling, and additives.

Shielding is a technique whereby the hot engine parts of an aircraft, helicopter, or any other potential target are shielded from all but a very narrow range of aspect angles, usually only a few degrees directly around the exhaust nozzle. *Shielding* and *cooling* are often used simultaneously in order to improve the overall effectiveness. *Fuel additives* are sometimes used in order to reduce plume radiation. These additives can be quenching in nature, such as water, which tends to reduce the temperature and thus the radiation of the plume emission, or they can be inhibiting in nature such as certain chemical additives.

5-2.5.2 Active Countermeasures

Active countermeasures are those countermeasures that either confuse or destroy the attacker's guidance system. Flares, decoys, modulation jammers, and directed energy beams are all considered active countermeasures.

The *infrared flare* is one of the most common countermeasures used to reduce the effectiveness of air-to-air missiles. If the radiant intensity of the ejected flare is slightly greater than that of the intended target and its trajectory is not a too radical departure from that of the intended target, the missile will tend to follow the flare and not the aircraft. The intent is to use a

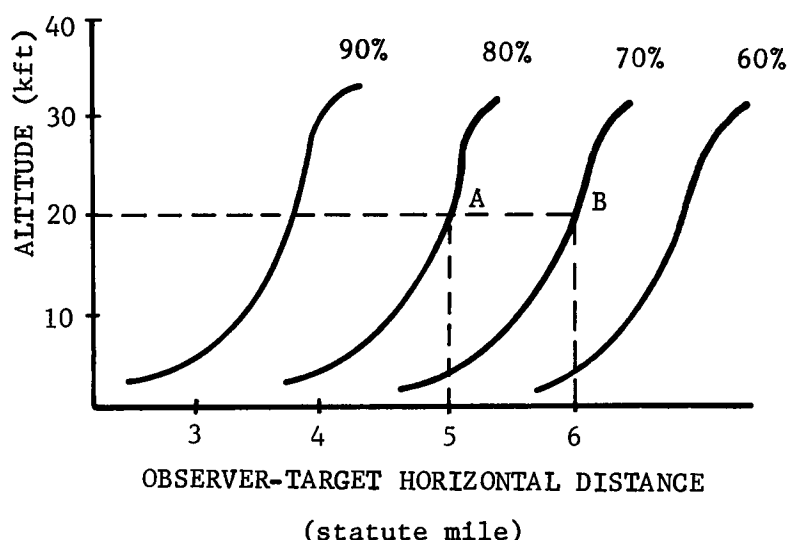


FIGURE 5-5. Estimate of Probability of Cloud-free Line-of-sight from (or to) Surface Level (Washington, D.C.—Summer)

sufficient number of flares deployed at the right time so that when the last flare has burned out, the aircraft is out of the missile's field of view. The missile is then rendered harmless because the remaining time is insufficient for reacquiring the target. It should be realized that since the flare is significantly smaller than the target, it must be substantially hotter in order to emit as much or more energy in any given spectral band. As a result, if the air-to-air missile were to have a two-color tracker (a counter-countermeasure) it could discriminate against the flare and reject it. This, of course, would force the defense into the deployment of a two-color flare (a counter-counter-countermeasure), and so on.

Decoys are objects that simulate the spectral and spatial characteristics of the target but are dispersed in such large numbers that it becomes uneconomical for the attacker to fire at all of them in an attempt to hit the real target(s). As in the case of the flare, the attacker may try to find a discriminant which the decoy does not simulate and use this to reject them in favor of the true target.

Modulation jamming is a technique whereby flashing or blinking lights are used to introduce spurious tracking signals into the missile tracker in an attempt to either completely confuse it or to introduce a significantly large miss-distance so as to render it ineffective.

Potentially, lasers (*directed energy beam*) could be used as a defensive technique to destroy either the optical coatings, filter, or the sensing element of the threatening IR seeker. Achievement of these objectives requires high-power levels not always compatible with airborne platforms. In addition, efficient use of these lasers requires precise pointing mechanisms.

5-3 BASELINE DESIGN CONCEPT

The baseline design concept is a technique used to focus the analysis once a firm set of performance requirements have to be established. The sensor system is then optimized by performing hardware and sensor parametric trade-offs about the baseline design point to determine the most economical way to achieve the performance requirements. It is almost always premature to establish a baseline design

concept prior to the firm delineation of the performance requirements; however, it must be remembered that cost and schedule constraints may require the revision of the performance specifications if the trade-off analyses of the baseline design and the alternative concepts indicate that the specifications cannot be satisfied. Thus, the baseline design is part of the repeated cost effectiveness analysis.

5-3.1 SPECTRAL OPTIMIZATION

The selection of the optimum spectral band and the choice of detector are the most critical decisions made in designing an infrared sensor. The optimum spectral region must be selected in the context of the operational mission, the targets, background, and transmission characteristics; and size, weight, power, and cost constraints imposed on the system. The two dominant factors involved in spectral selection are system sensitivity and background rejection. Both of these factors affect the spectral location and the spectral bandwidth, and are always in opposition. The maximum target-to-background ratio is achieved by selecting an infinitesimally small bandwidth at the spectral location of maximum target-to-background contrast as shown in Fig. 5-6. However, since the bandwidth is infinitesimally small, the signal-to-noise ratio is essentially zero. In order to increase the signal-to-system-noise ratio, the spectral band must be widened which reduces the signal-to-background ratio since the background is increasing faster than the target as the optimum point is the center wavelength. The resolution of this problem is generally found in minimizing the number of detectors required for a series of fixed-aperture diameters, then developing a philosophy of making aperture/detector trade-offs.

5-3.1.1 Trade-offs

The instantaneous field of view and the detector material, in addition to sensitivity requirements, must be considered in selecting the optimum spectral region. The optimum spectral region can be defined as the one that maximizes the signal-to-background-plus-noise ratio ρ_β and simultaneously satisfies the minimum signal-to-noise constraint ρ_N . These can be defined by the following expressions

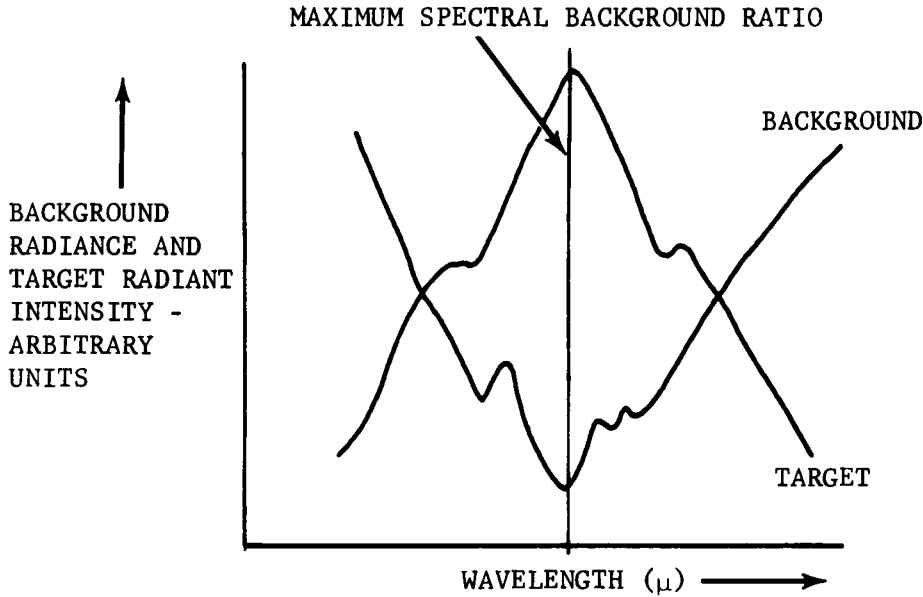


FIGURE 5-6. Example Spectral Background and Target Radiant Intensity

$$\rho_{\beta} = \frac{\frac{1}{R^2} \int_{\lambda_1}^{\lambda_2} J(\lambda) \tau(\lambda) d\lambda}{\left[\left(\alpha \int_{\lambda_1}^{\lambda_2} B(\lambda) \tau_B(\lambda) d\lambda \right)^2 + N^2 \right]^{1/2}} \quad (5-25)$$

and

$$\rho_N \leq \frac{\frac{1}{R^2} \int_{\lambda_1}^{\lambda_2} J(\lambda) \tau(\lambda) d\lambda}{N} \quad (5-26)$$

where

ρ_{β} = signal-to-background plus noise ratio

ρ_N = signal-to-noise ratio $\frac{S}{N}$

$J(\lambda)$ = spectral radiant intensity of target, w sr⁻¹ μ⁻¹

$\tau(\lambda)$ = atmospheric transmission for target

$\tau_B(\lambda)$ = atmospheric transmission for background

R = range, cm

α = instantaneous field of view, sr

$B(\lambda)$ = background spectral radiance, w sr⁻¹ μ⁻¹

N = rms system noise, w cm⁻² [Eq. 5-4]

Eqs. 5-25 and 5-26 are based on the target, background, transmission spectral characteristics, and the detector noise characteristics.

Assume the target and background radiance and the transmission coefficient to be as shown in Figs. 5-7 and 5-8, and a mission detection range of 7 km in a temperate atmosphere. Also assume the field of view of the sensor to be very small so that all backgrounds will be at a range equal to or greater than the target. The apparent target and background (as seen through the atmosphere) will then be as shown in Fig. 5-9. It is apparent that transmission has significantly altered the spectral characteristics of both target and background.

Next, assume an instantaneous field of view of 10⁻⁶ sr selected on the basis of resolution and number of detectors. It should be noted that this is an extremely significant design selection, therefore, several iterations may be required to determine the optimum detector subtense. The cumulative target and background irradiation curves are shown in Fig. 5-10. These curves show the amount of energy up to the long-wavelength cutoff λ_2 on the abscissa. The plateau region is the result of the strong absorption at 4.4 microns. The signal-to-background-plus-noise ratio ρ_{β} is illustrated in Fig. 5-11 for several short-wavelength cutoffs λ_1 . The curves with the

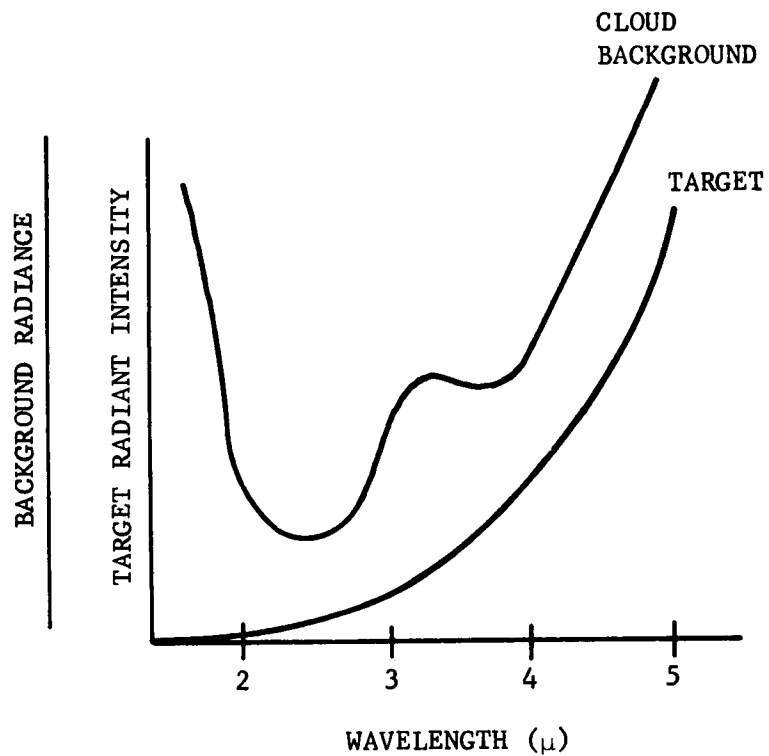


FIGURE 5-7. Sample Spectral Signature of Target and Background

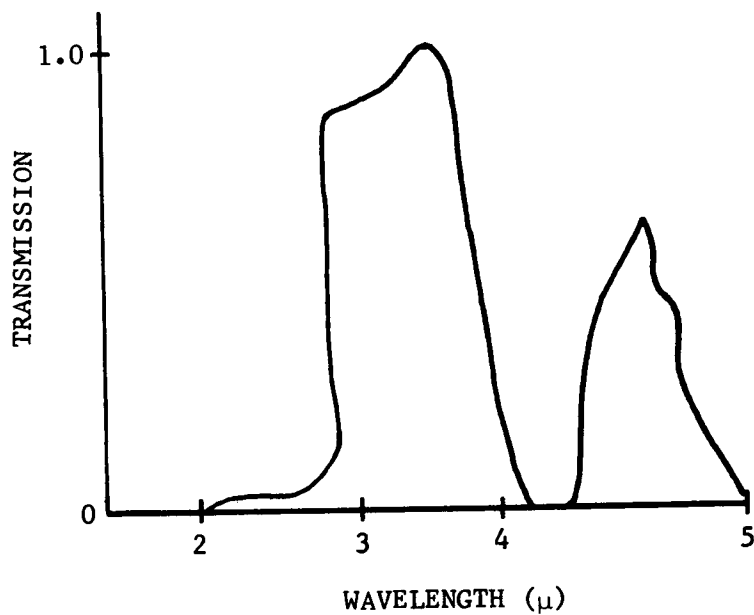


FIGURE 5-8. Spectral Transmission Curves

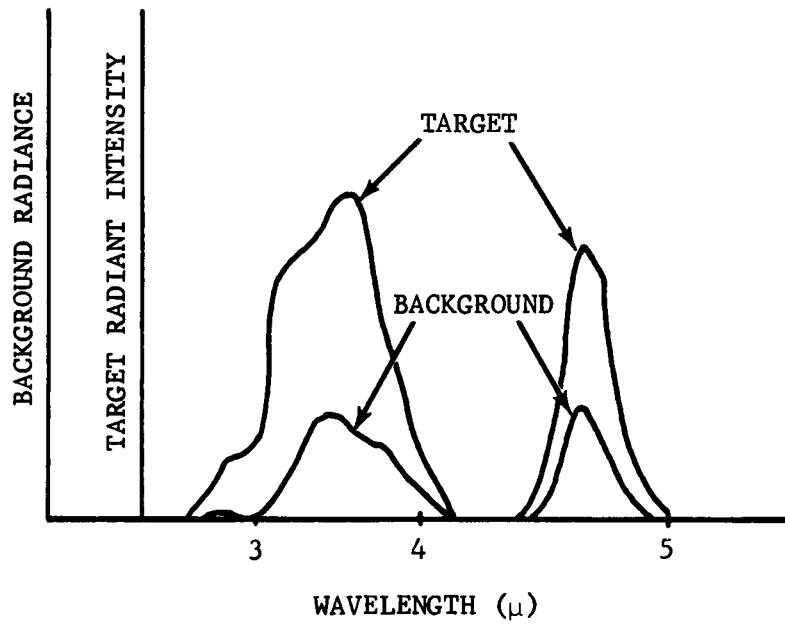


FIGURE 5-9. Apparent Target and Background Signatures

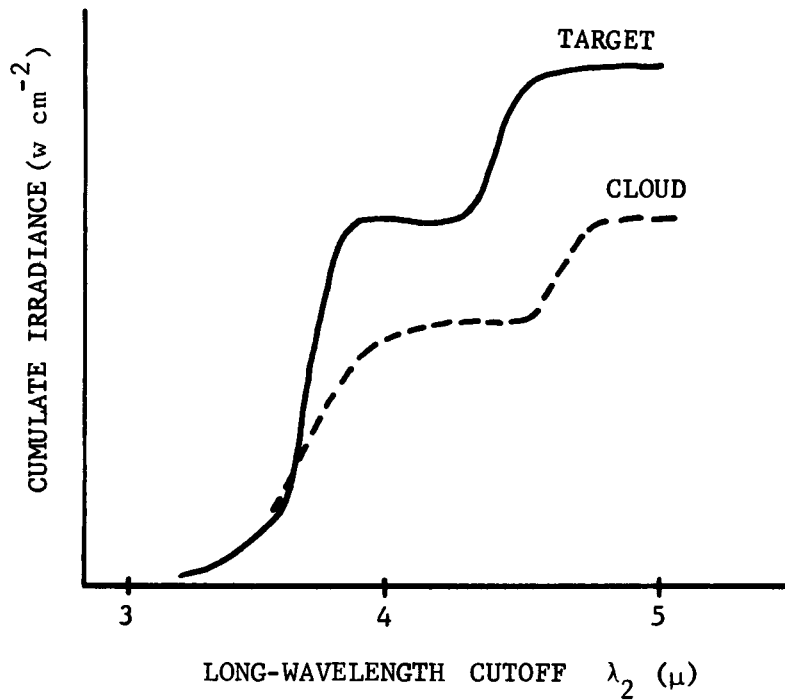


FIGURE 5-10. Target and Background Cumulative Irradiance vs Upper Wavelength Cutoff

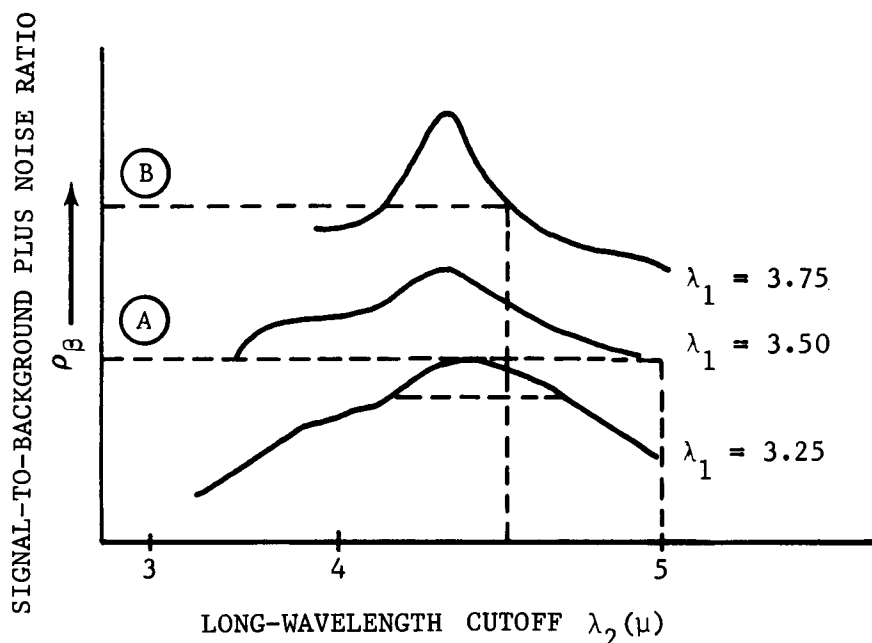


FIGURE 5-11. Signal-to-background Plus Noise Ratio for Various Upper and Lower Wavelength Cutoffs

larger values of ρ_β represent narrow spectral bands.

At this point the signal-to-noise constraint must be invoked. Assume that a minimum S/N ratio of 6 has been determined based on an analysis of Eqs. 5-11 and 5-14. Also keep in mind that size constraints limit the collecting aperture to some fixed maximum. In the spectral region of interest, the two potentially useful detector materials are PbSe and InSb. Fig. 5-12, which illustrates the cumulative S/N ratios ρ_N for these two detector materials, indicates that InSb is more sensitive than PbSe. For any given detector material, the optimum band is the most narrow band that satisfies the constraint of $S/N = 6$. This is found by iteratively selecting different combinations. Since InSb is more sensitive, it can satisfy the requirement with a narrower band than can PbSe (in this example, 3.75 to 4.50 microns vs 3.50 to 5.00 microns). The implications for the signal-to-background ratio are illustrated in Fig. 5-11. The system using PbSe would operate at position A of this graph while the system using InSb would operate at position B. It is apparent then that the most sensitive detector also provides the better background rejection capability. It should be noted that only a few aspects of the spectral region selection problem have been illustrated in

this paragraph. For example, the trade-off of detector instantaneous field of view was not examined. However, even before this paragraph can be completed, a discussion on the final choice between detector materials must be included.

5-3.1.2 Detector Selection

The availability of detector materials for specific spectral regions, their physical properties, sensitivities, and cost are some of the more significant considerations in selecting a spectral region and the design of an infrared sensor. The most significant detector parameters which influence the choice of detector materials are spectral response, detectivity D^* , responsivity, cooling requirements, minimum size constraints, cell-to-cell uniformity, long-term stability, manufacturing tolerances, array technology, and costs.

The spectral response of most detector materials is relatively narrow in that their sensitivities outside of the limiting band are usually not satisfactory for weapon system applications. As a result, there are few examples in which more than two or possibly three detector materials are serious candidates for a specific application. Of these candidates, the second consideration is the

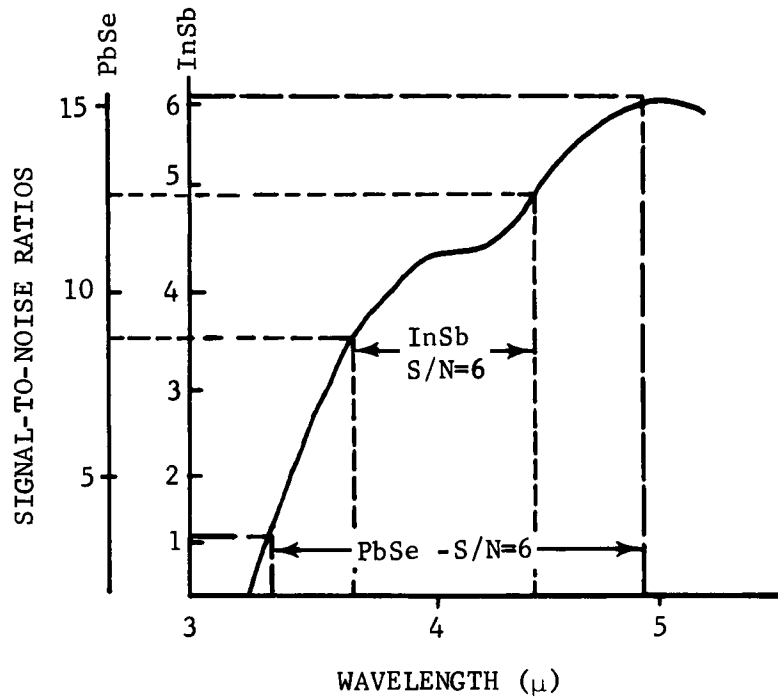


FIGURE 5-12. Cumulative Signal-to-noise Ratios for Two Detector Types

intrinsic sensitivity of the detector material under the system operating conditions. It is clear that detector sensitivity has a significant impact on both system size and system performance.

In order to achieve maximum sensitivity, most detector materials must be cooled to cryogenic temperatures. The electrical power required to provide this cooling is often the most significant portion of the sensor's power budget, and in many applications is often the parameter that determines the choice of detector material. For example, mercury-doped-germanium Ge:Hg can operate in the 3- to 5-micron region, but must be cooled to or below 30°K. On the other hand, indium-antimonide InSb also operates in the 3- to 5-micron region; however, it must be cooled to only 77°K. For equivalent heat inputs, the Ge:Hg system will require approximately three times the input power as will the InSb sensor, consequently, a substantial system trade-off could be made relative to size (due to cooling requirements) before selecting the detector material.

Detector cell size is also an important parameter in the selection of a detector material. It was shown that the instantaneous field of view of a detector was a significant parameter in eliminating background clutter. The detector

area is related to the field of view by Eq. 5-8 and the linear dimensions X and Y are given by

$$X = D_o(f/no.)\theta_x \quad (5-27)$$

$$Y = D_o(f/no.)\theta_y \quad (5-28)$$

$$\alpha \approx \theta_x \theta_y \text{ (sr)} \quad (5-29)$$

where θ_x , θ_y are the detector's angular dimensions. The state-of-the-art usually limits the minimum physical dimension at which a given detector material can be manufactured. For some detectors this may be 0.001 in. while for others it may be 0.004 in. Thus, if very small instantaneous fields of view are required for background rejection, and the optical diameter D_o and optical speed $f/no.$ are limiting the package size, it may not be possible to use a particular detector material due to its size limitations.

When large arrays are required for specific applications, the existence of array technology and the uniformity of the detectors in the array also influence the choice of detector materials. For example, there are only two detector materials (PbS and Ge:Hg) for which large array (greater than 100 detectors) technology currently exists. The long-term stability of detector

sensitivity and responsivity also must be considered in the choice of a detector material.

5-3.2 FRAME-TIME OPTIMIZATION

In many cases the frame time can be derived and optimized based on target geometry and kinematic considerations. For example, consider the problem posed in par. 5-2.1.1 in which detection and acquisition are required by some range R_{min} as defined by Eq. 5-2. The optimum scan rate will be defined as the rate that minimizes the aperture diameter D_o while assuring target detection at a minimum range R_{min} which provides an acceptable signal-to-background-noise ratio S/B . As shown in Eq. 5-9

$$S/B = \frac{J\tau}{\alpha BR^2}$$

The following simplified relationship for atmospheric transmission τ_a is used to arrive at an analytic solution of the optimum frame time:

$$\tau_a = \tau \left(\frac{1}{R^x} \right)^x \geq 0 \quad (5-30)$$

which is an approximation for a negative exponential, where x is determined empirically in the spectral region of interest for the ranges of interest.

For many detector materials (e.g., PbS) the detectivity D^* term in Eq. 5-21 is a function of the frame time t_s as a result of its high-frequency time-constant roll-off past some knee frequency

$$D^* = \hat{D}^* \left(\frac{t_s}{t_o} \right)^Y \quad \begin{matrix} Y \geq 0 \\ t_s \geq t_o \end{matrix} \quad (5-31)$$

where

\hat{D}^* = detectivity of the detector before roll-off[†], w cm^{-2}

t_o = frame time that would produce the roll-off knee frequency (3 dB point) for a given size detector, sec

t_s = frame time, sec

Y = number which is empirically determined

[†] Frequency roll-off is defined as a frequency beyond which the output signal relative to input signal begins to be attenuated.

A linear array of detectors is assumed to cover the elevation field of view. The electrical (filter) bandwidth of the filter $\Delta f'$ is approximated by

$$\Delta f' = \frac{1}{2t_d}$$

where t_d is the time it takes a point image to cross a detector. If the detector is of width θ_x and the system is scanning at a rate ω rad/sec, then

$$t_d = \frac{\theta_x}{\omega} \quad (5-32)$$

and

$$\Delta f' = \frac{\omega}{2\theta_x} \quad (5-33)$$

If the field of view in the direction of scan is ϕ and the frame (scan) time is t_s , then

$$\omega = \frac{\phi}{t_s} \quad (5-34)$$

and

$$\Delta f' = \frac{\phi}{2t_s\theta_x} \quad (5-35)$$

Substituting Eqs. 5-30, 5-31, and 5-35 into NEI Eq. 5-21, and solving for S/N , we obtain

$$S/N = \frac{J\tau}{R^x R^2} \sqrt{\frac{2}{\phi}} \left[\frac{\pi D_o \epsilon_o \epsilon_e \hat{D}^* t_s^Y}{4(f/no.) t_o^Y} \right] \sqrt{\frac{t_s}{\theta_y}} \quad (5-36)$$

If the signal-to-noise ratio for a particular detector is to be constant, independent of range, it is required, therefore, from Eq. 5-9 that

$$\alpha = K_1 R^2 \quad (5-37)$$

where K_1 is a constant multiplier.

For square detectors

$$\theta^2 = \alpha \quad (5-38)$$

$$\theta_y = \theta_x = \sqrt{\alpha} \quad (5-39)$$

By substituting Eq. 5-39 into Eq. 5-36, the following relationship is obtained between D_o and R

BIBLIOGRAPHY

OPTICS

- Stanley S. Ballard and James Steve Browder, "Thermal Expansion and Other Physical Properties of the Newer Infrared-Transmitting Optical Materials", *Appl. Opt.* 5, 1873-6 (1966).
- Gillespie, Olsen and Nichols, "Transmittance of Optical Materials at High Temperatures in the 1μ to 12μ Range", *Appl. Opt.* 4, 1488-93 (1965).
- George Hass, "Filmed Surfaces for Reflecting Optics," *J. Opt. Soc. Am.* 45, 945-53 (1955).
- Jamieson, et al., *Infrared Physics and Engineering*, McGraw-Hill, Inc., N.Y., 1963, pp.234-89.
- Rudolph Kingslake, Ed., *Applied Optics and Optical Engineering, Vol. I*. Academic Press, N. Y., 1965, pp.111-25, 153-200, 285-372.
- Rudolph Kingslake, Ed., *Applied Optics and Optical Engineering, Vol. III*, Academic Press, N. Y., 1965, pp.269-330.
- George Linsteadt, "Infrared Transmittance of Optical Materials at Low Temperature", *Appl. Opt.* 3, 1453-6 (1964).
- Donald E. McCarthy, "The Reflection and Transmission of Infrared Materials: I, Spectra from 2-50 Microns", *Appl. Opt.* 2, 591-5 (1963).
- Donald E. McCarthy, "The Reflection and Transmission of Infrared Materials: III, Spectra from 2μ to 50μ ", *Appl. Opt.* 4, 317-20 (1965).
- Donald E. McCarthy, "The Reflection and Transmission of Infrared Materials: IV, Bibliography", *Appl. Opt.* 4, 507-11 (1965).
- Donald E. McCarthy, "The Transmittance of Optical Materials from 0.17μ to 3.0μ ", *Appl. Opt.* 6, 1896-8 (1967).
- MIL-STD-141, *Optical Design*, 5 October 1962, pp.13-1-52, 17-1-10, 20-1-94, 21-1-77, 22-1.
- The Optical Industry and System Directory*, The Optical Publishing Co., Pittsfield, Mass., 1967.
- Roderic M. Scott, "Optical Engineering", *Appl. Opt.* 1, 387-97 (1962).
- Francis Weston Sears and Mark W. Zemansky, *University Physics*, Addison-Wesley, Reading, Mass., 1955.
- D. G. Fink, Ed., *Television Engineering Handbook*, McGraw-Hill, Inc., N.Y., 1957.
- L. Larmore, *Introduction to Photographic Principles*, Prentice-Hall, Englewood Cliffs, N. J., 1958.
- R. Kingslake, *Lenses In Photography*, Barnes, N. Y., 1963.
- L. J. Bodi, "Electroluminescent Lamp Brightness As a Function of Construction and Excitation Parameters", *Illum. Eng. Vol. LXI*, No. 4, Sec. 1, April 1966.
- W. C. Roberson, *Display Switching Study*, Final Rept. RADC-TR-65-125 Contract AF3-(602)-3264, August 1965.
- Weber, White, and Manning, *College Physics*, 2nd Edition, McGraw-Hill, Inc., N. Y., 1957.
- M. Born and E. Wolf, *Principles of Optics*, 3rd Rev. Edition, Pergamon Press, N. Y., 1965.
- Jenkins and White, *Principles of Optics*, 3rd Edition, McGraw-Hill, Inc., N. Y., 1957.
- R. Winfield, "The Matricon, an Alpha-Numeric Target to Cathode Ray Symbol Tube", in Third National Symposium on Information Display, February 1964, Technical Session Proceedings, Soc. for Info. Display (L. A. 1964).
- E. Leith and J. Upatnieks, "Wavefront Reconstruction With Diffused Illumination and Three Dimensional Objects", *J. Opt. Soc. Am.* 54, No. 11, 1295 (1964).
- E. Leith and J. Upatnieks, "Reconstructed Wavefronts and Communication Theory", *J. Opt. Soc. Amer.* 52, No. 10, 1123 (1962).
- E. Leith and J. Upatnieks, "Wavefront Reconstruction With Continuous-Tone Objects", *J. Opt. Soc. Amer.* 53, No. 12, 1377 (1963).
- W. T. Cathey, Jr., "Three Dimensional Wavefront Reconstruction Using a Phase Hologram", *J. Opt. Soc. Amer.* 55, 457 (1965).
- Three Dimensional Wavefront Reconstruction*, Lecture by E. Leith, Univ. of Rochester (Feb. 3, 1965).
- E. Leith and J. Upatnieks, "Microscopy by Wavefront Reconstruction", *J. Opt. Soc. Amer.* 55, No. 5, 569 (1965).

THERMAL CONTROL

Passive

Radiation Heat Transfer Analysis for Space Vehicles, ASD TR 61-119, Dec. 1961.

Coatings for the Aerospace Environment, WADD TR 60-773, July 1961.

Passive Thermal Control Coatings, AD Report No. 602, 894, Lockheed Missiles and Space Company, May 1963.

The Effects of Extreme Ultraviolet Radiation on the Reflectance of Thermal Control Surface Coatings, AD Report No. 625 442, Air Force Institute of Technology WPAFB, Aug. 1965.

Claude

C. A. Schulte, A. A. Forole, T. P. Neuchling, R. E. Kronauer, "A. Cryogenic Refrigerator for Long-Life Applications in Satellites", Int. Advances in Cryogenic Engineering 10, Sec. A-L, 477-485 (1965).

Insulation

W. H. Sternbentz, J. W. Baxter, *Thermal Protection System for a Cryogenic Spacecraft Propulsion Module*, Lockheed Missile and Space Co., Report A794993, NASA CR-54879, 2, Nov. 15, 1966.

J. M. Bonneville, *Design and Optimization of Space Thermal Protection for Cryogenics — Analytical Techniques and Results*, Report ADL 65958-02-01, NASA CR-54190, A. D. Little, Inc., Dec. 18, 1964.

Advanced Studies on Multi-Layer Insulation Systems, Report ADL 67180-00-04, NASA CR-54929, A. D. Little, Inc., June 1, 1966.

A. P. Schlosinger, E. W. Bentilla, *Research and Development Study on Thermal Control by Use of Fusible Materials*, Interim Report NSL 65-16, Northrop Space Laboratories, Feb. 1965.

Thermophysical Properties of Thermal Insulating Materials, Tech. Doc. Report

ML-TDR-65-5, April 1964, WPAFB, Ohio.

Thermoelectric

A. D. Kraus, *Cooling Electronic Equipment*, Prentice-Hall, Englewood Cliffs, N. J., 1965.

COOLERS

General

C. A. Stochl, E. R. Nolan, *Current Status and Future Trends of Cryogenic Coolers for Electronic Applications*, Tech. Report ECOM-2524, July 1964, U. S. Army Electronics Laboratory, U. S. Army Electronic Command, Fort Monmouth, N. J.

Solid Coolers

U. E. Gross, R. P. Mandal, T. W. Lawson, *Solid-Cryogen Cooler Design Studies and Development of an Experimental Cooler*, Tech. Report AFFDL-TR-65-233, WPAFB, Ohio, July 1967.

Stirling

J. W. L. Kohler, "The Stirling Refrigeration Cycle", Scientific American 212, No. 4, 119-127 (1965).

A. Daniels, F. K. DePre, "Closed Cycle Cryogenic Refrigerators as Integrated Cold Sources for Infrared Detectors", Appl. Opt. 5, No. 9 (Sept. 1966).

K. W. Cowans, P. J. Walsh, "Continuous Cryogenic Refrigeration for Three to Five Micron Infrared Systems", Int. Advances in Cryogenic Engineering 10, Sec. A-L, 468-476 (1965).

Pulse Tube

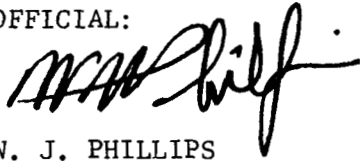
P. Krycak, M. J. Levy, *Pulse Tube Refrigerator Analysis*, ASME Paper 66-WA/PID-3, Nov-Dec 1966.

W. E. Gifford, R. C. Longworth, "Pulse Tube Refrigeration Progress", Int. Advances in Cryogenic Engineering 10, Sec. M-U, 69-79, (1965).

(AMCRD-TV)

FOR THE COMMANDER:

OFFICIAL:

A handwritten signature in black ink, appearing to read "W. J. Phillips", with a period at the end.

W. J. PHILLIPS
Colonel, GS
Chief, HQ Admin Mgt Ofc

CHARLES T. HORNER, JR.
Major General, USA
Chief of Staff

DISTRIBUTION:
Special